Decoding Tie2 Signaling with AI-Based Designed Proteins to Mitigate Vascular Diseases

Yan Ting Zhao

A dissertation submitted in partial fulfillment of the requirements for the degree of
Doctor of Philosophy

University of Washington
2022

Reading Committee
Hannele Ruohola-Baker, PhD – Chair
Richard Presland, PhD
Carol Ware, PhD
Julie Mathieu, PhD

Program Authorized to Offer Degree:
Oral Health Sciences

University of Washington

Abstract

Decoding Tie2 Signaling with AI-Based Designed Proteins to Mitigate Vascular Diseases

Yan Ting Zhao

Chair of the Supervisory Committee:
Hannele Ruohola-Baker
Department of Biochemistry

❖ *Background*

Blood vessels are crucial for tissue regeneration and proper organ functions. Functional endothelial cells display heterogeneity in stability and permeability that facilitate organ function and tissue homeostasis. Tie2 signaling controls vascular remodeling, stability, and permeability. Understanding the angiopoietin-Tie2 pathway will allow the regeneration of stable, functional blood vessels to treat diseases related to vascular dysfunctions in the oral cavity, such as oral cancers[1,2], diabetic oral complications[3], pulpitis[4], periodontitis, and tooth loss[5]. Thus, investigating the Tie2 pathway that regulates angiogenesis is paramount in regenerative dentistry and oral medicine. Angiopoietin-1 (Ang1) and -2 (Ang2) modulate Tie2 signaling via nearly identical receptor-binding domains (F-domain) but elicit opposing vascular outcomes. Ang1 stabilizes blood vessels and reduces permeability while Ang2 does the opposite despite sharing high structural similarity. To date, the mode of Ang-Tie2 activation and downstream molecular events leading to vascular stability is not fully understood.

❖ *Objectives*

This study aims to dissect the molecular basis of the Tie2 pathway and the subsequent molecular events leading to vascular stability using artificial intelligence-based algorithms to computationally designed proteins as scaffolds for probing the mechanism of the Tie2 pathway.

❖ *Methods*

A combination of RoseTTAFold and AlphaFold was employed to computationally design protein scaffolds for conjugating the Ang1 F-domain at various valencies and geometries to produce F-domain scaffolds. These F-domain constructs were used to probe (I) the molecular basis of Tie2 downstream signaling output and (II) the subsequent molecular events leading to tight junction formation. Tie2 signaling was analyzed using quantitative western blot, wound healing assay, tube formation assay, and a tight junction recovery assay in human umbilical vein endothelial cells (HUVEC) and human brain microvascular endothelial cells (HBMECs). Quantitative super-resolution microscopy was used to identify the molecular components that underly the Tie2 interaction upon receptor clustering in HUVECs and HBMECs. Controlled cortical impact to generate traumatic brain injury (CCI-TBI) in murine models was used to evaluate the in vivo effect of vascular repair upon Tie2 activation.

❖ *Results*

Upon screening the designed F-domain scaffolds, two broad phenotypic classes were identified and distinguished by the number of presented F-domains. Scaffolds presenting 3 to 4 F-domains have Ang2-like activity, up-regulating pFAK and pERK, but not pAKT, and failing to induce cell migration and vascular stability. In contrast, scaffolds presenting 6, 8, 12, 30, or 60 F-domains have Ang1-like activity, up-regulating pAKT and inducing FOXO1 nuclear exclusion, cell migration, and vascular stability. When examined *in vivo*, superagonist icosahedral

nanoparticles displaying 60 F-domains significantly improved revascularization in hemorrhagic brains after a controlled cortical impact injury. To further investigate how Tie2 stabilizes blood vessels at the molecular level, F-domains conjugated to two-dimensional protein sheets[6] were employed to identify the molecular interactions that Tie2 makes. We found that clustering Tie2 receptors produces two classes of Tie2 clusters that recruit integrin α5β1, adherens junctions (VE-Cadherin), and tight junctions (ZO1, claudin-5, and occludin). The knockdown of α5 integrin using siRNA demonstrated that tight junction recruitment to Tie2 clusters does not require integrin, while VE-Cadherin is integrin-dependent. Upon detailed examination, super clustering Tie2 forms two functional classes of Tie2 complexes. The Tie2-integrin complex upregulates the pAKT/FOXO1 signaling axis to promote cell survival via transcriptional change and recruits pCAS and VE-cadherin to promote cell migration. The other Tie2 clusters localize at cell-cell junctions and orchestrate the assembly of ZO1, claudin-5, and occludin to form tight junctions. Tie2 activation using agonistic F-domain scaffolds accelerates tight junction (CLDN5 and ZO1) re-assembly after chemical disruptions in 2D endothelial cell culture, reinforcing the notion that Tie2 activation initiates tight junction formation.

❖ *Conclusions*

For the first time, this study illustrates that F-domain valency determines Tie2 signaling and vascular outcome. Tie2 activation generates two functional classes of Tie2 clusters that regulate endothelial cell gene expression and junctional cell-cell adhesion to modulate vascular stability and permeability. In essence, this study utilized protein design as a novel tool for investigating biochemical processes involving receptor tyrosine kinases (RTKs). The Tie2 superagonists and antagonists characterized here hold tremendous therapeutic value for tissue regeneration, wound healing, and cancer therapy.

Table of Contents

List of Figures and Tables

Chapter I - Introduction

Background

Vascular Stability and Permeability are vital for Organ Function

The vascular stability and permeability of different organs exhibit heterogeneity. The brain, heart, and lung blood vessels are continuous with relatively low permeability. In contrast, the kidney, liver, dental pulp, and salivary glands are highly permeable with discontinuous endothelium and fenestration. Endothelial cells of different tissues express a unique combination of adherens junctions (AJs) and tight junctions (TJs) at the paracellular space that determines vascular permeability and function of organs[7]. AJs such as VE-Cadherins and PECAM-1 are expressed on the basal side of the endothelium (Fig. 1). TJs, namely claudins, occludin, and junctional adhesion molecules (JAMs) localize on the apical luminal side. Different isoforms of TJ proteins also determine the tightness and permeability of the endothelium. Claudin isoforms 1-5, 11, 14, and 19 participate in tight sealing between cells via highly conserved cysteine residues on the first extracellular loop[8]. Claudin-2/10b/15 and claudn10a/17 are pore-forming molecules that make beta barrels between claudins of adjacent cells that facilitate cations and anions diffusion, respectively[8–10]. Charged residues, for example, isoleucine of claudin-2, on the first extracellular loop are critical to ion permeability[8]. JAM-C is expressed in all endothelial cells. JAM-A involved in tight sealing is highly expressed in brain endothelium, but JAM-B is expressed in permeable vessels of the liver and lymphatic system[11]. ZO1 and ZO2 are expressed in all endothelial cells, but ZO3 is restricted in the blood-brain barrier (BBB)[11]. Thus, the vasculature of different tissues expresses a unique composition of TJ proteins.

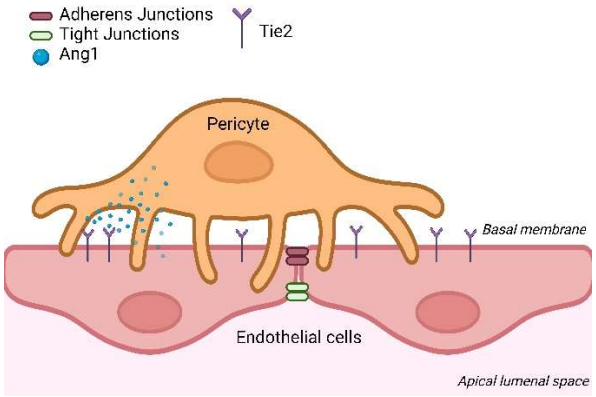

Figure 1. Endothelial cell polarity. Endothelial cells line the vascular wall connected by AJs and tight TJs. Common AJs are VE-Cadherins and PECAM-1 localizing on the basal side of the endothelium facing pericytes. TJs like claudins, occludin, and junctional adhesion molecules (JAMs) localize on the apical luminal side to seal and prevent leakage. Pericytes secrete Ang1 that activate Tie2 receptors on endothelial cells to regulate angiogenesis, vascular stability, and permeability.

The blood-brain barrier (BBB) is a highly selective vasculature that tightly regulates the molecules and cells that enter the brain tissues[7]. Human cerebral microvascular endothelial cells express high levels of claudin-3/5/9/11/12, ZO-1/2/3, JAM-A/C, and occludin to maintain the BBB's tight sealing[11]. Under normal conditions, the BBB is impermeable to most drugs, cytokines, and immune cells. Inflammation and chronic angiogenesis increase BBB permeability leading to degenerative neural diseases like Alzheimer's and Parkinson's disease[12]. Vasculature in the heart needs to be tightly sealed due to the high pressure of blood flow varying from 60-250 mm Hg[13]. Generating heart-specific blood vessels to accommodate the varying blood pressure throughout this organ is extremely challenging but is critical to preventing deleterious vessel ruptures in the heart[13]. Thus, cardiac endothelial cells express a number of TJs such as claudin1/5/9 and ZO-1. However, overexpression of TJs can elevate blood pressure and increase the risk for stroke. The pulmonary vessels of the lung form a dense net-like structure that acts as an air-blood barrier for gas exchange while limiting the exchange of larger molecules. Lung endothelial cells express ZO-

1, claudin5, and occludin[11]. Permeability increase can lead to pulmonary edema, as seen in acute lung injury[14].

Vasculature in human kidneys and liver have high permeability with a discontinuous endothelium that forms fenestration (pores in the endothelium) for efficient diffusion and filtration[7]. These vessels express TJ proteins such as claudin1/5, ZO-1, and Occludin[11]. Interestingly, the liver's endothelial cells double up as antigen-presenting cells providing additional immune detection in the liver. Human salivary glands also have relatively low expression levels of claudin-1/5, ZO1, and occludin to allow efficient diffusion of ions, proteins, and water in/out of the glands[11,15]. TJ abnormality in salivary glands has been implicated in Sjogren's syndrome[15]. Dental blood vessels enter through the root apical openings and travel up to the dental pulp into the crown region. Like kidneys and liver, dental pulp blood vessels are also fenestrated to facilitate diffusion and filtration[4,16]. Blood vessels also serve a vital role in routine tooth maintenance. Dental pulp stem cells (DPSCs) differentiate into odontoblasts to regenerate dentin upon injury[17]. The dental pulp microvasculature provides a unique niche for DPSCs[18]. Co-culturing HUVECs and DPSCs on agarose scaffolds has been demonstrated to form vascularized pulp-like tissue with dentin deposition[19,20]. However, if DPSCs in this model differentiate into odontoblast completely, the vascular network will have lost the niche to support DPSCs[21], which is not ideal for tooth regeneration. In summary, stable tissue-specific vasculature is critical for proper organ functions. It is crucial to understand how blood vessels develop and manipulate the key signaling pathways involved to support the vascular need of specific organs in tissue regeneration and diseases.

Vascular Development

Vascular development is vital in embryogenesis. Blood vessels supply oxygen and nutrients to nourish the growing embryo. Vasculogenesis and angiogenesis are the two main processes that initiate vascular formation and remodeling, respectively (Fig. 2). Vasculogenesis drives mesoderm-derived hemangioblast differentiation to make endothelial cells. Endothelial cells interact and condense to form lumenized primitive vascular networks in the embryo and yolk sac and form the heart[22–24] (Fig. 2A). This process emerges during early gastrulation on embryonic days E6.5-8.5 in the mouse[23,25,26]. Vasculogenesis is orchestrated by FGF, Sonic hedgehog (Shh), VEGF, and TGF-β signaling[23]. FGF signaling induces mesoderm differentiation into angioblasts[27]. Inhibition of the FGF pathway in mice results in numerous vascular defects highlighting its importance in early vascular development[28–30]. Shh signaling regulates vascular maturation via mural cell recruitment such as pericytes and smooth muscle cells[31]. VEGFA and VEGFR1 are highly expressed in the embryonic stage and engage in vasculogenesis. Genetic ablation of VEGFA and VEGFR1 genes is lethal, resulting in early embryonic death[24,32]. TGF-β activation promotes endothelial expression of fibronectin and collagens[33] and cell proliferation in a dose-specific manner. A low dose of TGF-β administration supports angiogenesis, while a high dosage elicits inhibitory effects[23,34]. Knockout of TGF-β components such as ALK1/5, TβRII, and endoglin in mice are also embryonic lethal due to vascular abnormality[35,36]. As tissues and organs thicken, hypoxia initiates angiogenesis for vascular remodeling and branching[35,36].

Angiogenesis is the formation of new blood vessels from existing vasculature at around E9.5 to vascularize organs[23,37] (Fig. 2B). The hypoxic environment in the growing embryo induces the upregulation of HIF-1α[38–41]. HIF1α dimerizes with HIF-1β and binds to DNA to promote gene

expression of pro-angiogenic factors such as VEGFs, angiopoietins, and PDGF[42]. In response to pro-angiogenic factors, vascular endothelial cells self-dissociate and sprout to form tip cells with filopodia that migrate toward the direction of the pro-angiogenic stimuli to start new vessel branching. The VEGF pathway promotes tip cell differentiation to initiate angiogenesis[43–45]. Tip cells produce Dll4 to activate Notch on adjacent cells to form stalk cells[44]. Notch-Dll4 triggers stalk cell proliferation and lumen formation to support the branching of vessels. Notch-Dll4 signaling controls the organization of the vascular tree through downregulating VEGF to reduce excessive proliferation and migration of the growing stalk and tip cells shown in zebrafish and mouse studies[46,47]. Slit2/Robo1 drives endothelial tube formation. FGF up-regulates α5β1 integrin expression to coordinate cell proliferation and migraion[48,49]. PDGF and angiopoietin/Tie2 signaling regulates vascular maturation and stabilization. Proliferating endothelial cells produce PDGF-B as a chemoattractant to signal PDGFβ receptors on mesenchymal cells for pericytes and smooth muscle cells to differentiate and migrate toward the new vessels[50,51]. PDGF has been shown to promote vascular regeneration and stabilization in post-injury brain tissue[50,52]. Ang/Tie2 modulates the paracrine communication between endothelial-mural cells and the autocrine signaling feedback within endothelial-endothelial cells[23,37,53–55]. Mural cells such as pericytes and smooth muscle cells secrete Ang1, which activates Tie2 receptors expressed in endothelial cells to promote vascular stabilization and maturation. In the absence of Ang1, endothelial cells upregulate Ang2 expression that self-activate to induce endothelium destabilization. Ang2 expressed in hypoxic tissues may be another driving force for angiogenesis initiation in addition to VEGF. Among the described pathways, the angiopoietin-Tie2 pathway is essential to vascular stabilization and maturation.

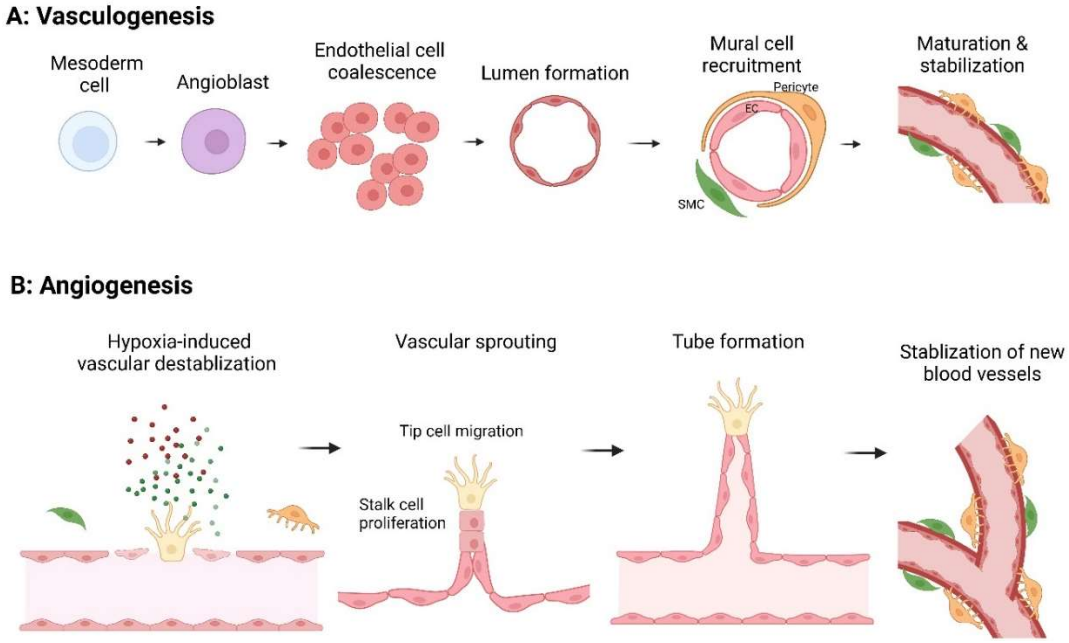

Figure 2: A schematic of blood vessel formation from A) vasculogenesis and B) angiogenesis. Mesoderm-derived angioblasts differentiate into endothelial cells (pink). Endothelial cells aggregate to form lumenized endothelium to form blood vessels. Newly formed blood vessels recruit mural cells, pericytes (orange) and smooth muscle cells (SMC, green), for vascular maturation and stabilization. As the tissue thickens, the hypoxic environment sends signals to activate endothelial cells to initiate angiogenesis. In response to pro-angiogenic factors, the endothelial cells dissociate and mural cells detach from the blood vessel. Vascular sprouting consists of tip cells (yellow) migrating toward the stimuli, and stalk cells (square pink cells) proliferate to follow the lead of tip cells. Tube formation promotes endothelial lumen formation. Mural cells are recruited to the new blood vessels for stabilization.

Angiopoietin-Tie2 Signaling in Angiogenesis

The Angiopoietin-Tie2 (Ang-Tie2) pathway is vital for vascular homeostasis and remodeling in both normal and pathological conditions. Ang-Tie2 signaling also serves a pivotal role in tooth regeneration[56,57] and oral cancer[58,59]. In mice, homozygous knockout of Tie2 or Ang1 results in early embryonic death with severe vascular defects such as vascular underdevelopment, dilation, and rupture[37,60,61]. Mice with the homozygous knockout of Ang2 can survive up to postnatal day 14 but lack ischemia-induced neovascularization[62,63]. These animal studies highlight the crucial role of the Ang-Tie2 pathway in normal vascular development and postnatal vascular remodeling. Angiopoietins bind and cluster Tie2 receptors leading to auto-phosphorylation of the tyrosine residues on the cytosolic domains[64–68]. Upon Tie2 receptor phosphorylation, adaptor proteins are recruited and activate downstream second messengers to regulate angiogenesis. Tie2 activation attracts adaptor proteins such as PI3K, Grb2, Grb7, DOK-R, and ABIN2 to induce phosphorylation of second messengers, namely pAKT, pERK1, pFAK, pPAK1, and IKK/pIκB respectively. Activating second messengers drives endothelial cell proliferation, migration, sprouting, tube formation, and immune response to modulate angiogenesis, vascular stability, and vessel permeability[37]. The binding of Ang1 to Tie2 up-regulates pAKT, pERK1/2, and pFAK, resulting in improved vascular stability and a decrease in permeability. Interestingly, Ang2 is a context-dependent agonist/antagonist of Tie2. Without the Tie2 phosphatase, VE-PTP, Ang2 activates Tie2/pAKT in lymphatic endothelial cells[69,70]. In vascular endothelial cells that express VE-PTP, Ang2 sometimes inhibits pTie2 and pAKT[71,72], while others show Ang2 activation of pAKT[72,73]. Despite the contradicting observations, the general outcome of Ang2 leads to vascular destabilization, increased permeability, and vessel remodeling[37]. The delicate balance between Ang1 and Ang2 regulates Tie2 signaling output for normal blood vessel development and remodeling.

Numerous efforts have investigated the differential Tie2 signaling outcomes mediated by Ang1 and Ang2. Yet, the exact mechanism(s) governing the action of angiopoietins remains unclear. Structurally, the two ligands share 60% homology in their amino acid sequences. Both proteins exhibit a super clustering domain (SCD), a coiled-coil domain (CCD), and a receptor-binding domain known as the fibrinogen-like domain (F-domain) [74–77]. The F-domains on Ang1 and Ang2 have almost identical tertiary structures and comparable affinities to bind Tie2 (K_D ~3 nM)[71,75]. Ang1 and Ang2 are able to self-associate into higher-order multimers via disulfate bonds between the cysteine residues on the SCD and CCD[78]. Ang1 has a higher tendency than Ang2 to form higher-order oligomers. This difference is likely due to an extra cysteine residue on the linker region (between the CCD and F-domain) of Ang1 that Ang2 lacks because when the missing cysteine is introduced to Ang2 in this region more Ang2 aggregation was observed[78]. Studies of angiopoietin oligomerization, as visualized through electrophoresis reducing gels and electron microscopy, illustrate that both Ang1 and Ang2 populate a range of oligomeric states[79,80]. Utilizing natural angiopoietins, fusion proteins (CompAng1 and CompAng2), modified Ang1 (CMPAng1), and anti-Ang1 antibodies (ABTAA) to correlate ligand oligomerization with Tie2 signaling outcomes were inconclusive due to the multiple oligomeric states that these ligands exist in[79,81–84]. Moreover, the relationship between ligand-specific oligomerization and Tie2 downstream pathway activation was not investigated thoroughly.

Conversely, another report argues that the differences between Ang1 and Ang2 lay within

their F-domains[85]. Chimeric angiopoietins generated by swapping the F-domains of Ang1 and Ang2 demonstrated that chimeric Ang2 (with Ang1 F-domain) increases phosphorylation of Tie2, while chimeric Ang1 (with Ang2 F-domain) does not. However, this study only analyzed the general Tie2 phosphorylation while multiple tyrosine sites on Tie2 can be phosphorylated, and different phosphorylation sites produce specific signaling outcomes[37,64–66,86]. The **first aim** of this thesis investigates the molecular basis of the angiopoietin-Tie2 pathway in detail to fully delineate the relationship between angiopoietin oligomeric states and the specific Tie2 signaling output. I **hypothesize** that oligomeric states of angiopoietins regulate Tie2 activation and vascular outcome. Self-assembling computationally designed protein scaffolds at a well-defined oligomeric state were employed to elucidate the mechanism that drives the Ang1 and Ang2 phenotype.

Role of Tie2 in Vascular Permeability

Vascular permeability is controlled by paracellular molecular composition, transcellular passages, and fenestration of the endothelium to modulate organ homeostasis and inflammatory responses[87]. Previous studies suggest Tie2 signaling plays a role in vascular permeability transcriptionally and spatially at the paracellular space. Ang1 strengthens cell-cell junction formation to stabilize blood vessels and reduce permeability, while Ang2 does the opposite. Through the Tie2/PI3K/pAKT signaling axis, Ang1 increases vessel stabilization via the induction of PECAM (AJs) dephosphorylation and translocation to endothelial cell-cell junctions[88]. Super clustering Tie2 receptors demonstrated the recruitment of AJs, PECAM and VE-Cadherin[6], suggesting that Tie2 may be a direct initiator of AJs and TJs formation. Activation of the MAPK/ERK pathway, a downstream target of Tie2, increases permeability due to ZO1 and occludin relocation out of the cell-cell junction[89]. Ang1 stimulation is thought to up-regulate the expression of VE-cadherin, ZO1, and Claudin-5[90–93]. In mice, the expression of ZO1 and Claudin-5 positively correlates with Ang1 and α5 integrin upregulation in brain tissues with induced-ischemic injury suggesting Ang1-Tie2 and α5β1 integrin promotes the recovery of blood brain barrier (BBB) integrity[91]. In cancer, Ang1/Ang2 ratio, measured in serum, is low[94]. An elevated level of Ang2 up-regulates MMP1/2/9 expression; these proteases likely disrupt cell junctions leading to leaky blood vessels and expression of ZO1, occludin, and claudin5 expressions are downregulated[94–98]. Insufficient Ang1 coupled with a high level of Ang2 causes TJ disruption and leaky blood vessels leading to cancer metastasis and invasion of distant tissues. The molecular events that occur upon Tie2 activation and TJ formation have not been thoroughly investigated. The ***second aim*** of this project investigates how Tie2 signaling orchestrates tight junction formation. I **hypothesize** that Tie2-integrin regulates adherens and TJ proteins for strengthening vascular stability and modulating permeability.

Role of α5β1 integrin in Tie2 signaling

Tie2 signaling is highly complex. In addition to angiopoietins, Tie2 signaling can be modulated by co-receptors such as Tie1, VETPP, and integrin. Numerous studies demonstrate α5β1 is essential for Tie2 signaling. α5β1 activation enhances Tie2 signaling output and angiogenesis[99–101]. Integrins are heterodimers composed of α and β subunits expressed by many cell types. The integrins are a family of proteins that regulate focal adhesion complexes for cell-extracellular matrix attachment and migration[102,103]. Integrins αvβ3, αvβ5, and α5β1 are up-regulated in newly formed blood vessels[48]. αvβ3 and αvβ5 inhibit *in vitro* and in vivo angiogenesis[104–106]. Genetic ablation of α5 integrin in mice is lethal to the embryo and

accompanied by vascular leakage in the embryo and extraembryonic vasculature[107]. α5 co-localizes with Ang1, and phosphorylated Tie2 in mouse cerebral vessels post-injury[91,99] and gene expression of TJ, ZO1 and claudin-5 temporally correlate with integrin[91]; suggesting Tie2-integrin interaction encourages vascular repair. Moreover, antibody blockade of α5β1 increases *in vitro* endothelial cell permeablility[108]. β1 promotes endothelial cell sprouting in postnatal vascular remodeling in mice. Deleting β1 destabilizes cell-cell junctions and improper VE-Cadherin internalization in mature blood vessels[109]. α5β1 integrins co-localize with Tie2 upon stimulation with COMP-Ang1[101]. Tie2 association with α5β1 induces FAK recruitment to the cytosolic domains of Tie2 and results in vascular repair[99,100]. Seeding endothelial cells on fibronectin (the natural integrin ligand) enhances ERK1/2 phosphorylation upon Ang1 stimulation[101]. Interestingly, monomeric Ang1 is suggested to bind integrin directly and activate integrin-linked kinase leading to pAKT activation and cell survival in mouse heart tissue[110,111].

Conversely, other studies also argue that α5β1 is inhibitory for Tie2 signaling. The dual action of α5β1 and Ang2 inhibits Tie2 activation[112,113]. Inhibiting α5 and β1 heterodimerization activates Tie2 phosphorylation and enriches VE-Cadherin (CD144) and ZO1 at cell-cell junctions[112,114]. The role of α5β1 integrin in Tie2 signaling is debatable. Collectively, how integrin interacts with Tie2 and influence signaling output is not fully understood. The ***third aim*** of this study is to investigate the mechanistic relationships between angiopoietins, Tie2, and integrin. I **hypothesize** that oligomerization states of angiopoietin influence the mechanistic interplay between integrin and Tie2 to produce differential vascular outcomes.

Significance

The Angiopoietin-Tie2 pathway is an essential regulator for both normal and pathological vascularization, serving a pivotal role in tooth regeneration and oral cancer[58,59], respectively. It is critical to investigate the regulation of the Tie2 pathway to improve overall oral health. Vascular dysfunction is observed in periodontitis and oral cancer. Targeting the Tie2 pathway offers a new therapeutic perspective against these oral diseases. Periodontitis affects more than 40% of adults in the United States and has an 11% prevalence worldwide[21]. Periodontitis is chronic inflammation in the periodontal tissue caused by Gram-negative bacteria such as *Porphyromonas gingivalis*. Smoking, diabetes, and poor oral hygiene are risk factors for periodontitis[115,116]. The periodontium as the supporting structure for the teeth is comprised the gingiva, periodontal ligament (PDL), cementum, and alveolar bone[117]. The PDL is a major periodontal tissue component that maintains tooth stability and function. Periodontal ligament fibroblasts (PLFs) secrete a collagen matrix and signaling factors to maintain PDL integrity[118,119]. Severe periodontitis escalates gum tissue recession, increases tooth mobility, and raises the risk of tooth loss. Receded gum tissue is irreversible. Although surgical periodontal therapy may regenerate lost tissue, outcomes are variable[21,115,116,120]. Post-surgery, patients may experience side effects such as tissue detachment on operated and neighboring sites[121], increased tooth mobility[122], and hypersensivity[122,123]. Pro-inflammatory cytokines stimulate the production of MMPs by fibroblasts and immune cells, resulting in the degradation of the collagen fibers in the PDL[21]. Reduced vascular endothelial function is also strongly associated with peridontitis[124,125]. Chronic inflammation in periodontitis can alter vascular responses and increase the expression of pro-inflammatory cytokines and leukocyte adhesion molecules, resulting in vascular endothelial dysfunction[126]. Tie2 signaling controls immune response via NFκB; Ang1 inhibits NFκB by inducing the translocation of NFκB out of the nucleus, while Ang2 promote nuclear NFκB to upregulate expression of pro-inflammatory genes, namely MMPs, ICAMs, and VCAM-1[37,94,127–129]. Tie2 activation induces PLF differentiation, survival, and proliferation via Akt and MAPK-c-Jun pathways[130]. Tie2 activation also protects periodontal tissues from ligature/LSP-induced inflammatory tissue destruction and stimulates osteoblast differentiation to stimulate bone growth[131,132]. Targeting the Tie2 pathway may improve endothelial functions and anti-inflammation in periodontitis. The Tie2 super agonists characterized in this study have tremendous potential in promoting normal vascular endothelial function, periodontal ligament regeneration, and bone regeneration to reverse periodontal damage.

Tooth decay is another major issue in dentistry[133], and both can lead to tooth loss. Dental caries affects 91% of adults (20 to 26 years old) in the U.S.[134]. Pathogenic attributes from *Streptococcus mutans* and other anaerobic microorganisms cause acidic aberration in the enamel, dentin, and dental pulp[135]. In response to the low pH from the cariogenic acid front, dental pulp stem cells (DPSCs) differentiate into pulp cells and odontoblasts to regenerate the dental pulp and dentin, respectively. Yet, the regenerative capacity of DPSCs diminishes as the age and severity of the damage increases[17,136,137]. Moreover, damaged enamel cannot be regenerated due to the lack of ameloblasts and their progenitors in postnatal humans[138]. The congenital disease, Amelogenesis Imperfecta (AI), causes defective enamel formation during tooth development and affects 1/718 to 1/14,000 people depending on the population; there is no cure for this disease[139–141]. The resulting bacterial infection from the absence of enamel may cause inflammation in the dental pulp, also known as pulpitis[4]. Severe pulpitis can cause tooth loss. Diabetic patients also experience

salivary dysfunction; lower saliva production (xerostomia) and change in saliva composition impact the saliva buffering and cleansing capacity, leading to increased risk for dental caries and tooth lost[3]. The current method to restore defective dentitions is to replace teeth with synthetic material; however, prostheses have limited durability and low biocompatibility. Dental fillings and crowns require replacements leading to the further loss of natural tooth structure[142]. Dental implants can cause tissue trauma and inflammation, or peri-implantitis, resulting in bone[123] and soft tissue loss[143]. Dental implants are not always available to all patients. Patients with insufficient pre-operative bone levels or osteoporosis have poor a dental implant prognosis. Tissue regeneration and induced pluripotent stem cell technologies offer a new gateway to regenerating natural teeth; however, regenerative dentistry is only possible if the cells receive adequate nutrients and oxygen supply from blood vessels. Underneath the mineralized hard tissues, teeth are living organs supported by blood vessels in the dental pulp. The dental pulp is highly vascularized with fenestrated blood vessels to facilitate nutrient diffusion and waste removal in the tooth[39]. The lack of vascularization results in nutrient deficiency and can lead to cell necrosis and poor repair[144,145]. One objective of this study is to dissect the molecular basis of the Angiopoietin-Tie2 pathway and generate Tie2 super agonists for vascularizing the pulp tissue for tooth regeneration and improving tooth organoid implantation for tooth loss.

Furthermore, the Angiopoietin-Tie2 pathway has recently gained attention in oral cancer research. Oral squamous cell carcinoma (OSCC) is the most common head and neck cancer (4/100,00) that kills 145,328 people each year worldwide[146,147]. In the U.S. alone, there were 53,000 new cases and 10,860 deaths in 2019[148]. Tobacco and alcohol use are major risk factors for OSCC[149]. Carcinogens found in tobacco, such as aromatic hydrocarbon benzopyrene and tobacco-specific nitrosamines (TSNs), can cause DNA damage in oral keratinocyte stem cells. The alcohol metabolite, acetaldehyde, accumulates in oral mucosa which will cause DNA damage. Alcohol can increase the permeability of oral epithelium, allowing easier carcinogen penetration. Alcoholic beverages also contain carcinogenic compounds, specifically N-nitroso compounds, mycotoxins, urethane, and inorganic arsenic, further damaging the oral epithelium[149]. Surgical removal of the cancerous tissue remains the gold standard treatment for oral cancers[150]. However, surgery often removes a large area of tissue, and reconstructive surgery, such as bone or skin grafting, is necessary to restore facial features and functions[150]. Sufficient blood vessels are essential to support and promote the integration of the grafted and native tissues.

Radiotherapy is another standard treatment to eradicate cancer cells in oral cancer[151]. Unfortunately, numerous clinical studies have shown a high level of tumor recurrence and metastasis post-radiotherapy due to residual cancer stem cells[151]. Irradiated glioblastoma stem-like cells (GSCs) can transdifferentiate into tumor-derived endothelial cells (TDECs). TDECs up-regulate pTie2 and pAKT to drive tumor angiogenesis, supporting tumor proliferation and recurrence[152]. In *Drosophila melanogaster,* stem cells are protected by dying daughter cells that send an Ang1 homolog, Pvf1, to activate Tie2 signaling post-radiation. The Pvf1 signal inhibits apoptosis in stem cells. These stem cells enter quiescence but re-enter the cell cycle 24 hours later to repopulate the radiation-damaged tissue. Xing et al. hypothesized that "if such property is conserved in cancer, it could explain the tumor recurrence in post-radiotherapy patients[153]." Moreover, radiation activates the epithelial-mesenchymal transition and oncogenic metabolism, making recurrent oral tumors more metastatic via invasion of regional lymph nodes and distant lung tissues[58,151,154]. In various types of cancers, including OSCC, Ang2 is abnormally

upregulated[58,94]. Elevated Ang2 levels encourage tumor angiogenesis, producing low-grade leaky blood vessels, facilitating cancer metastasis[94]. The Tie2 super agonists and antagonists characterized in this study have numerous implications in cancer therapy. The superagonists can enhance vascularization for better wound healing in post reconstructive surgery for oral cancer patients and stabilize Ang2-mediated leaky vessels to prevent cancer metastasis. The Tie2 antagonists can inhibit Tie2/pAKT signaling concurrently with radiotherapy to prevent tumor angiogenesis, survival, and proliferation for eradicating cancer stem cells effectively. Vascular dysfunction is highly prevalent in oral diseases and cancer. Investigating the Tie2 pathway may offer a novel therapeutic approach in oral medicine and regenerative dentistry.

Hypothesis and Specific Aims

The Angiopoietin-Tie2 pathway (Ang/Tie2) is critical in blood vessel remodeling, maturation, and stability[37,67,68]. To date, the regulation of this essential pathway has not been fully elucidated. Tie2 signaling can be modulated by angiopoietins[37,77,155–157]. Angiopoietin-1 (Ang1) is an agonist that binds and activates tyrosine kinase immunoglobin and epidermal homology domain 2 (Tie2) receptors to promote vessel stabilization[37,60,78,158], while Angiopoietin-2 (Ang2) antagonizes Tie2, destabilizes blood vessels, and increases vascular remodeling[37,71,72,159,160]. Despite the structural similarity between Ang1 and Ang2, the underlying mechanism that drives these opposing phenotypes is unclear due to the multiple oligomerization states that both ligands populate[75,76,80,85].

Aim 1: Determine the relationship between F-domain valency/geometry and Tie2 activation to probe the molecular basis of Tie2 signaling output

The ***first aim*** of this thesis project is to fully delineate the molecular basis that governs the Ang-Tie2 interactions and activation. In collaboration with the Institute for Protein Design at the University of Washington, we generated a wide range of protein scaffolds to bind and cluster Tie2 receptors into various configurations. It is **hypothesized** that scaffolds conjugated with the Ang1 receptor-binding domain (F-domain) at various valences and geometries can regulate Tie2 signaling outcome and control angiogenesis in a systematic fashion. *Aim 1* will focus on characterizing F-domain scaffolds in human umbilical vein endothelial cells (HUVECs) to correlate F-domain valency with Tie2 activation.

1.1 Computationally design an array of protein scaffolds covalently linked to the Tie2-binding domain (Ang1 F-domain) at a range of valencies and geometries to manipulate Tie2 receptor clustering.
1.2 Examine the agonism and antagonism of the designed F-domain scaffolds on the Tie2 pathway to elucidate the molecular basis that governs Ang1 vs. Ang2 phenotypes.
1.3 Assess F-domain scaffold functionality to stimulate *in vitro* and *in vivo* angiogenesis.

Aim 2: Delineate the role of Tie2 signaling in junctional stability and integrity of the endothelium.

Ang/Tie2 signaling governs angiogenesis and vascular permeability. Ang1 strengthens cell-cell junction formation to stabilize blood vessels and reduce permeability, while Ang2 induces leaky blood vessels. In addition to the Tie2 agonists and antagonists (Fd scaffolds) characterized in Aim 1, GFP-tagged two-dimensional protein sheets conjugated with F-domains (Fd-sheets) are employed to analyze the molecular components within the activated Tie2 clusters on HUVECs visually in super-resolution microscopy. Super clustering Tie2 receptors demonstrate the recruitment of AJs, PECAM and VE-Cadherin[6] suggesting a direct modulation of AJ assembly. AJ formation is an essential precursor to TJ formation. The ***Second aim*** of this project investigates the molecular events downstream of Tie2 leading to TJ formation. I **hypothesize** that Tie2 activation directly recruits adherens and tight junction proteins that strengthen vascular stability and modulate permeability. In Aim 3, Tie2 super agonists, antagonists, and Fd-sheets treatment will be used to analyze TJ formation upon Tie2 activation in both HUVECs and human brain microvascular endothelial cells (HBMECs).

2.1 Asses the efficacy of Tie2 activation on tight junction recovery in endothelial cells after chemical disruption.
2.2 Evaluate Tie2 co-localization with tight junction molecules upon Fd-sheets treatment in super-resolution immunofluorescence imaging.

Aim 3: Investigate the mechanistic interplay between Tie2-α5β1 integrin and the functional role of this interaction in vascular stability

The TJ markers, ZO1 and CLDN5, correlates with Ang1 and α5 integrin expression spatially and temporally in brain tissues post injury in mice suggesting Tie2 and α5β1 integrin promotes the recovery of blood brain barrier (BBB)[91]. However, the role of α5β1 in Tie2 signaling is controversial. Many suggest that α5β1 integrin association with Tie2 enhances Tie2 activation and upregulates cell migration, while others suggest α5β1 can inhibit Tie2[91,92,99,100,112,161–164]. The ***third aim*** of this study examines Tie2-α5β1 interaction and the functional role of this complex in junctional stability of the endothelium. I **hypothesize** that large clusters of Tie2 molecules will prompt positive regulators such as integrin to co-localize, and that this complex promotes tight junction formation. *Aim 3* will examine the effect of Tie2 recruitment of TJs in wild type vs α5β1 knockdown mutant endothelial cells.

3.1 Evaluate Tie2 co-localization with integrin upon Fd-sheets treatment in super-resolution immunofluorescence imaging.
3.2 Examine the change in Tie2 activity and tight junction recruitment when α5β1 is reduced using siRNA knockdown.
3.3 Determine F-domain engagement in Tie2-α5β1 association using *de novo* designed Tie2 and integrin mini binders.

Chapter II – Methodology

Materials & Methods

Computationally Designed F-domain scaffolds

Since the Ang1 and Ang2 F-domains are nearly identical, we hypothesized that the differences in Ang1 and Ang2 signaling stem from differences in the valency and geometry of Tie2 receptor engagement. Because the range of oligomerization states of Ang1 and Ang2 have been difficult to determine, particularly when engaging Tie2 receptors, we set out to determine the molecular basis for the signaling differences by generating a series of synthetic computationally designed ligands displaying F-domains with a wide range of possible valences (3, 4, 6, 8, 12, 30, and 60 copies) and geometries (cyclic, tetrahedral, and icosahedral). The designed oligomeric proteins were expressed in E. coli as fusions to the SpyCatcher protein domain[165], and the Ang1 F-domain (E280-F498) was secreted from 293F cells using a human siderocalin secretion tag, a hexahistidine purification tag and the SpyTag sequence at the N-terminus. Following cleavage of the secretion and purification tags, the F-domain was conjugated *in vitro* to the designed assemblies through spontaneous intramolecular amide bonds formed between SpyCatcher–SpyTag via the Lys and Asp residue side chains[165] (Fig 1A and Appendix 1A). Protein sequences and details on protein production, purification, and conjugation are available in the methods and supporting information (Appendix 4 and Appendix Table 1).

We developed three classes of designed symmetric proteins to serve as scaffolds to control the presentation of the F-domain: helical bundles, homo-oligomers, and protein nanoparticles (Fig 1A). The first class, the helical bundles, are parametrically generated de novo proteins that exhibit cyclic symmetry and are stabilized by hydrogen-bond networks across multiple chains[166] (B. In this study, we used trimeric, hexameric, and octameric helical bundles[167] with an N-terminal fusion to the SpyCatcher protein to allow for conjugation with the F-domain. These designs are annotated as H3, H6, and H8. The second class, homo-oligomers, are designed helical repeat proteins docked into cyclic configurations and contain computationally designed protein–protein interfaces that drive their association in solution. The two proteins in this category, tpr0C3F (Tet1-A) and tpr1C4F (C4)[168], are composed of three or four identical copies of an idealized tetratricopeptide (tpr) repeat protein, respectively, and contain a C-terminal fusion to the SpyCatcher protein to allow for conjugation with the F-domain. The tpr0C3_r4 (Tet1-A.2) construct is composed of three identical copies of tpr repeat protein with two additional repeating monomers. We also included a tetrameric protein comprised of four copies of idealized ankyrin repeats (AkC4, pdb id 5HS0). The third class, co-assembling protein nanoparticles that exhibit tetrahedral or icosahedral symmetry, are able to display twelve or sixty copies of the F-domain, respectively. T33_dn2 is a tetrahedral nanocage consisting of two trimeric proteins based on idealized tpr sequences (pdb id and 5HRZ) and contains a fusion to the N-terminus of the A component to the SpyCatcher protein to allow for conjugation with the F-domain, and we refer to this construct as Tet1. T33_dn10 is a tetrahedral nanocage consisting of two trimeric proteins: one based on an idealized tpr sequence (pdb id 6V8E) and a de novo helical repeat protein (pdb id 5K7V). It contains a fusion to the C-terminus of the de novo helical repeat protein to the SpyCatcher protein to allow for conjugation with the F-domain, and we refer to this construct as Tet2. I53-50 is an icosahedral protein nanoparticle, which we refer to as Icos1, composed of a pentameric subunit consisting of 12 copies of pentameric Lumazine synthase RibH2 from Mesorhizobium loti (PDB ID 2obx) and 20 copies of trimeric 2-keto-3-deoxy- 6-phosphogluconate (KDPG) aldolase from Thermotoga Maritima (PDB ID 1wa3). The version of KDPG aldolase used utilizes a fusion with SpyCatcher protein to allow for covalent

conjugation with the SpyTagged F-domain. The trimeric component of Icos1 with three copies of F-domains was also tested, annotated as Icos1A. A version of the pentameric component containing SpyCatcher was also used, allowing for conjugation and display of an additional 60 copies of F-domain, this construct was designated as Icos1-200%. I53-47 is an icosahedral protein nanoparticle composed of 12 copies of pentameric Lumazine synthase (PDB ID 2obx) and 20 copies of the trimeric macrophage migration inhibitory factor from Trichinella Spiralis (PDB ID 1hf0)[169]. It contains a fusion to the SpyCatcher protein to the pentameric component to allow for conjugation with the F-domain, and it is annotated as Icos2.

Synthetic genes encoding each of the SpyCatcher-designed protein fusions were built in a vector with a standard T7 promoter system and (His)6 tag. The proteins were expressed in E. coli and purified by immobilized nickel-affinity chromatography (Ni2+ IMAC) and size-exclusion chromatography (SEC). SpyTag Fdomain was secreted from HEK293F cells as a human siderocalin (hSCN) fusion with a (His)6 tag at the N-terminus of the fusion construct (10.1093/nar/gkr706) and purified by immobilized nickel-affinity chromatography (Ni2+ IMAC). The SpyTag F-domain was obtained by cleavage of the fusion construct using a TEV site engineered at the C-terminus of the hSCN partner which was captured by a secondary Ni2+ IMAC purification. The cleaved SpyTag F-domain was further purified using SEC.

F-domain Conjugation

F-domain fused with SpyTag and scaffold fused with SpyCatcher were mixed at 1:1.2 molar ratio. The mixture is incubated at room temperature for 4 hours or overnight at 4º C at nutation. The mixture was purified by SEC, and SDS–PAGE gels were used to quantify the efficiency of the reaction (Appendix S4).

Cell culture

Human Umbilical Vein Endothelial Cells (HUVECs) were acquired from Lonza (C2519AS). Cells were grown on 0.1% gelatin-coated (Sigma, G1890-100G) 35-mm cell culture dishes in EGM2 medium. Briefly, EGM2 consists of 20% fetal bovine serum (BioWest, S1620), 1% penicillin–streptomycin (Gibco, 15140122), 1% GlutaMAX (Gibco, 35050061), 1% ECGS (endothelial cell growth factor), 1 mM sodium pyruvate (Gibco, 11360070), 7.5 mM HEPES (Gibco, 15630130), 0.08 mg/ml heparin (Fisher BioReagents, 904108-1), 0.01% amphotericin B (Gibco, 15290018), a mixture of 1x RPMI 1640 (Gibco, 1875093) with and without glucose (Gibco, 11879020) to reach a 5.6 mM glucose concentration in the final volume. Media were filtered through a 0.2-µm filter. HUVECs were expanded and serially passaged to reach passage 4 before cryopreservation.

ECGS was extracted from 25 mature whole bovine pituitary glands from Pel-Freeze biologicals (Lonza, 57133-2). Pituitary glands were homogenized with 187.5 ml of ice-cold 0.15 M NaCl (Fisher Chemical, CAS7647-14-5) and adjusted to pH 4.5 with HCl (Sigma-Aldrich, 320331). The solution was stirred at 4°C for 2 hours and then centrifuged at 4,000 RPM for 1 hour at 4°C. The supernatant (wine colored) was collected and adjusted to pH 7.6 followed by addition of 0.5 g/100 ml streptomycin sulfate (Sigma, S9137) and stirred at 4°C overnight. Next day, the supernatant was centrifuged at 4,000 RPM for 1 h at 4°C. The supernatant was sterile filtered using a 0.45-µm filter and stored at -20°C.

MCF10A and MCF10A-CAS-mscarlet cells were obtained from the Cooper lab, FredHutch and cultured in media described previously[170]. The medium consist of DMEM/F12 (Gibco, 11330032), 5% horse serum (Gibco, 16050130), 20ng/ml EGF (Sigma-Aldrich, SRP3027), 0.5mg/ml hydrocortisone (Sigma-Aldrich, H4001), 100ng/ml cholera toxin (Millipore, C8052), 10ug/ml insulin (Sigma-Aldrich,11070-73-8) and 1% penicillin–streptomycin (Gibco, 15140122). MCF10A cells were starved in the same media without EGF and contain 2% horse serum as assay media.

Phosphorylation analysis of HUVECs stimulated with designed proteins

One straw of passage 4 HUVECs was thawed in a 35-mm dish and cultured in EGM2 medium until almost 80% confluence was reached. Cells were then passaged 1:4 (passage 6) into four 35-mm plates followed by another 1:2 passage (passage 7) at 80–90% confluence into a total of eight plates. Once cells reached 80% confluence, and EGM2 was aspirated and cells rinsed with 1× PBS (Gibco, 10010023) twice. The cells were then starved by adding 2 ml of DMEM low glucose 1 g/l (Gibco, 11885-084) serum-free media per plate for 16 h. At 16-h timepoint, the media was aspirated. Ang1 (R&D system, 923-AN-025), Ang2 (R&D system, 623-AN-025), or scaffolds were suspended in starvation media at 18 nM F-domain concentration and added to the cells for a 15- or 30-min incubation at 37°C. After treatment, the medium was aspirated, and cells were washed once with 1× PBS before harvesting total protein for analysis.

Total protein isolation

After scaffold treatment, the medium was aspirated, and the cells were gently rinsed with 1x phosphate-buffered saline. Cells were lysed with 130 µl of lysis buffer containing 20 mM Tris–HCl (Sigma-Aldrich, 1185-53-1) (pH 7.5), 150 mM NaCl, 15% glycerol (Sigma-Aldrich, G5516), 1% triton (Sigma-Aldrich, 9002-93-1), 3% SDS (SigmaAldrich, 151-21-3), 25 mM β-glycerophosphate (Sigma-Aldrich, 50020100G), 50 mM NaF (Sigma-Aldrich, 7681-49-4), 10 mM sodium pyrophosphate (Sigma-Aldrich, 13472-36-1), 0.5% orthovanadate (Sigma-Aldrich, 13721-39-6), 1% PMSF (Roche Life Sciences, 329-986), 25 U benzonase nuclease (EMD, 70664-10KUN), protease inhibitor cocktail (PierceTM Protease Inhibitor Mini Tablets, Thermo Scientific, A32963), and phosphatase inhibitor cocktail 2 (Sigma-Aldrich, P5726), respectively, in a tube. Cell lysate was collected in a fresh Eppendorf tube. 43.33 µl of 4× Laemmle Sample buffer (Bio-Rad, 1610747) containing 10% beta-mercaptoethanol (Sigma-Aldrich, M7522-100) was added to the cell lysate and then heated at 95°C for 10 min. For pTie2 Y992 analysis, cells were lysed with 70 µl of lysis buffer and 23 µl of sample buffer was added before boiling. The boiled samples were either used for Western blot analysis or stored at -80°C.

Western blotting

The protein samples were thawed and boiled at 95°C for 10 minutes. 30 µL of protein sample per well was loaded and separated on a 4-10% SDS-PAGE gel for 30 minutes at 250 Volt. The proteins were then transferred onto a nitrocellulose membrane for 12 minutes using the semidry turbo transfer Western blot apparatus (Bio-Rad, USA). Post-transfer, the membrane was blocked in 5% bovine serum albumin for 1 hour. After 1 hour, the membrane was probed with the respective antibodies: pAkt-S473 (Cell Signaling, 9271S) at 1:2,000 dilution; pERK1/2 p44/42 (Cell signaling, 4370S) at 1:1,000 dilution; pFAKY379 (Cell signaling, 8556S) at 1:5,000 dilution; Tie2 (Cell Signaling, 4224S) at 1:1,000 dilution; pTie2 Y992 (R&D sys., AF2720) at 1:500

dilution; α5 integrin (Millipore, AB1928) at 1:1,000; and β-Actin (Cell Signaling, 3700S), S6 (Cell Signaling, 2217S), and β-Tubulin (Cell Signaling, 2146S) at 1:10,000 dilution. Membranes with primary antibodies were incubated at 4°C, overnight on a rocker. Next day, the membranes were washed with 1X TBST (3 times, 10 minutes interval). For pFAK, pERK1/2, ERK, Tie2, α5 integrin, β-Actin, S6, and β-Tubulin, the respective HRP-conjugated secondary antibody (Bio-Rad, USA) at 1:10,000 dilution was added and incubated at room temperature for 1 hour. For pTie2 (Y992), 1:1,000 secondary antibodies were added for 1-hour incubation at room temperature. For pAKT(S473), following washes, the membrane was blocked in 5% milk at room temperature for 1 hour and then incubated in the respective HRP-conjugated secondary antibody (1:2,000) prepared in 5% milk for 1 hour. All the membranes were washed with 1× TBST (3 times, 10 minutes of interval) after secondary antibody incubation and developed using Chemiluminescence developer and imaged using Thermo Scientific CL-Xposure Film or Bio-Rad ChemiDoc Imager.

Data were quantified using the ImageJ software to analyze band intensity. Quantifications were done by calculating the peak area for each band using ImageJ. The peak area of the target proteins was divided by the peak area of housekeeping proteins. All signaling levels are normalized to Icos-cage levels as an internal positive control.

Competition assay

HUVECs were cultured and starved as mentioned in the protocol above. At the 16-hour timepoint the medium was aspirated and replaced with fresh DMEM low glucose pre-mixed with 9 nM of Ang1 and scaffolds at 27 or 45 nM F-domains[71]. The cells were stimulated with treatment for 15 min. After 15 min, the medium was aspirated, the cells were washed once with 1× PBS and total protein was harvested for analysis. All experiments were performed with F-domain scaffolds at 90% conjugation. Tie2 or a5 integrin Knockdown Passage 7 HUVECs at 100,000 cells per 35-mm plate cell density were transfected with 40 nM of siRNA (SMARTpool, Dharmacon, Inc.) targeting *TEK* (siRNA: M-003178-03-0005) or *ITGA5* (siRNA: L-00800300-0005) mRNA using a Lipofectamine Transfection Kit (Invitrogen, 13778-075) in EGM2 medium. After 24 hours of siRNA incubation, media were changed with fresh EGM2 to allow cell recovery for 24 hours before 16 hours of serum starvation with low glucose DMEM. Starved HUVECs were treated with scaffolds at 18 nM of F-domain concentrations or PBS for 15 minutes before protein lysate collection for analysis.

Tube formation assay

Tube formation was done according to a previously described protocol with modifications[171]. Briefly, passage 6 HUVECs were seeded onto 24-well plates precoated (30 min prior to seeding) with 150 µl of 100% cold Matrigel (Corning, 356231) at 1.5 × 105 cells/well density. Wells of HUVECs were treated with different scaffolds at 90 nM F-domain concentrations or PBS in low glucose DMEM medium supplemented with 0.5% FBS for 24 hours in which old media was aspirated and replaced with fresh media without scaffolds. The cells continue to be incubated up to 72 hours. Capillary-like structures were observed, and 20 randomly selected microscopic fields were photographed under Nikon Eclipse Ti scope. Thereafter, these tubular formations were quantified by calculating the number of nodes, meshes, and tubes using angiogenesis analyzer in ImageJ software at the terminal time point. Data were normalized to the PBS vehicle as a log2 fold change.

Scratch assay

Scratch assay was done according to a previously published protocol with modifications[172]. Briefly, HUVECs were seeded onto 35 mm, 0.1% gelatin-coated plates and cultured in EGM2. Once a monolayer of cells was established, a scratch was made on the cell layer using a 200-µl pipette tip. Media were changed to DMEM low glucose supplemented with 2% fetal bovine serum. Scaffolds were added into the media at 18 nM F-domain concentrations, and PBS was used as a negative control. The imaging was performed under phase-contrast microscopy at 0 and 12 hours. The images were quantified using ImageJ software to calculate the change in wound area for the 12-hour time interval. The change in area was then divided by the original wound area to obtain the ratio of wound healing. The ratios were normalized to PBS vehicle as log2 fold change.

Cell viability assay

Cell viability assay was performed according to a previously published protocol with the following modifications[73]. HUVECs were seeded onto a 96-well plate precoated with 0.1% gelatin at 2×10^4 cells/well. The following day, HUVECs were serum starved using low glucose DMEM with PBS or F-domain scaffolds at 18 nM of F-domain for 16 hours. Cells that were not starved were supplemented with 20% FBS as a positive control. Cell viability was examined using the CellTiter-Glo Luminescent Cell Viability Assay according to product protocol (Promega, G7570). Luminescent signal was measured using Wallac EnVision multiplate reader. Relative luminescence unit (RLU) was calculated by subtracting the average background signal (wells containing the reagent and media only) from sample wells.

Animals

Prior to beginning all animal studies, the University of Washington Institutional Animal Care and Use Committee (IACUC) evaluated and approved all procedures and power analysis for comparing independent samples (with and alpha 0.05 and 85% confidence) to ensure the ethical use and treatment of animals. For all TBI experiments, six-month-old C57Bl/6 male and female mice were purchased from the Jackson Laboratory.

Controlled cortical impact (TBI model)

Prior to CCI-TBI, animals were anesthetized and placed in a stereotactic frame. After a midline incision, the scalp was opened to expose the cranium. A small burr hole was drilled (~ 1 mm diameter) ~ 1.0– 1.8 mm caudal to the bregma (1.0 mm medial-lateral) to allow placement of an injury probe over the cortex. A fourth-generation Ohio State University impactor was placed on the dura to a touch force of 2–4 kDyn. To impart a controlled cortical impact, a hit was performed as the probe accelerated 4.3 m/s with a displacement of -0.8 mm and 15 ms dwell[173]. After injury, the probe was retracted, the bone deficit was repaired with bone wax, the scalp was closed, and the animal was allowed to recover with fluid and analgesic administration in a heated environment. Mixed sex cohorts were used to account for neuroprotective effects of estrogen and progesterone after TBI[174–176]. Moreover, estrus cycle effects within the female cohort were controlled for with mixed housing and study completion within one estrus cycle (i.e., $\leq$ 7 days). Synthetic nanocage drugs were administered by retro-orbital i.v. injection on anesthetized animals at 6, 24, 48, and 72 hours post-injury (1.0 mg/ kg/day). Animal studies were performed in a manner to randomize injury and cohort selection for each treatment to ensure the study was performed in a double-blinded fashion throughout all data collection and tissue analysis.

Histology and immunofluorescence

Tissue was harvested from euthanized animals exsanguinated by transcardiac perfusion with saline and fixed with 4% paraformaldehyde for histological analysis. Tissues were then cryoprotected by equilibration to 30% sucrose (Fisher, S5-500) and embedded in OCT medium (Tissue Tek, Inc., 4583) and cryosectioned. All immunofluorescent stains and tissue processing were performed on serial sections (1:6; 30 lm). Tris-buffered saline (TBS, Sigma, 901235) equilibrated tissues were permeabilized (0.3% Triton X100) and blocked (3% bovine serum albumin, BSA). Primary antibodies diluted in blocking solution were incubated at 4°C overnight: Iba1 (1:500, WAKO, NC9288364), CD31 (1:500, R&D system, AF3628), mouse albumin (1:500, ICL, Inc., GAL-90A), GFAP (1:1,000, Millipore, AB5541M1), NG2 (1:100, Millipore, MAB5384), pAKT S473 (1:200, Cell Signaling, 9271S), and DAPI (Thermo Fisher, 62248). Tissues were washed in 0.1% Tween-20 TBS. Fluorescent secondary antibodies diluted (1:500) in Tween-TBS 2% donkey serum (Jackson Immuno, 017-000-121) were incubated with tissues 2–12 hours.

For immunofluorescence imaging of HUVECs, passage 7 cells were seeded on glass coverslips coated with 0.1% gelatin and cultured until confluency. Once confluent, cells were starved for 16 hours in low glucose DMEM (1 g/l D-glucose). Then, cells were stimulated with angiopoietins or F-domain scaffolds at 100 nM of F-domain concentration for 15 minutes before fixing with 4% PFA (EMS, 15710) for 13 minutes. For F-domain sheet experiments, 20 nM of F-domain was added to the cells for 30 min before fixation. The fixed cells were washed three times at 5 min each before blocking for 1 hour with 3% BSA (VWR, 0332-500G) and 0.1% Triton X-100 (Sigma, T9284-500ML) in PBS while on nutation. The cells were incubated with primary antibody diluted at 1:100 in blocking agent over night: Tie2 (Cell Signaling, catalog #4224S), FOXO1 (Cell Signaling, 2880), and α5 integrin (Millipore, 1928). After the primary antibody, the cells were washed three times at 5 min each with PBS while on nutation. The cells were then incubated with secondary antibodies (1:200 and 1:100 for Tie2) and phalloidin (1:100, Invitrogen, A12380) diluted in blocking agent for 1 hour and 20 min at 37°C. Secondary antibodies were then removed, and cells were washed three times at 10 minutes each with PBS on nutation. Coverslips were sealed using VECTASHIELD (Vector laboratories, H-2000-2) upside-down on glass slides for analysis on confocal (Leica) or super-resolution (Delta vision OMX SR) microscopy. Selected OMX images were constructed with Imaris 9.7 to create 3D visualizations.

Evans blue extravasation

To quantify vascular and blood–brain barrier repair, Evans blue (Sigma-Aldrich, 314-13-6) was injected retro-orbitally (2% w/v in saline, sterile filtered). Tissue was harvested after euthanasia and imaged to visualize topical Evans Blue extravasation. Each brain was divided along the midline to separate the left and right hemi- spheres and incubated in 500 µL formamide at 55°C. After 24 hours, tissue debris was cleared by centrifugation (≥ 13,000 rcf, 15 minutes). Evans Blue fluorescence was quantified by a TECAN infinite 200Pro plate-reader (excitation: 620 nm, emission: 680 nm). To account for gender differences, Evans blue fluorescence was normalized to express values as a function of body mass (n = 6; 50:50 gender representation). Similarly, brain tissue was imaged on a Xenogen imager to qualitatively examine Evans Blue epifluorescence in serial sections.

Albumin extravasation

Tissue stained with goat antibodies against serum albumin (Immunology Consultant Lab; 1:500) and imaged by a donkey anti- goat antibody conjugated with AlexaFluor-647 (1:500, Jackson Immuno, 715-605-151). Floating sections were counterstained with 40,6-diamidino-2-phenylindole (DAPI) and mounted on slides. After tissue immunofluorescence was scanned by an Olympus VS120 slide-scanner, serum albumin immunofluorescence was quantified with OlyVIA analysis software (Olympus Life Sciences). Briefly, the areas of the ipsi- and contralateral hemispheres were traced in serial section at the TBI lesion epicenter and 180 lm rostral and caudal serial sections. Next, albumin immunofluorescence was set to a minimum intensity-threshold, which remained consistent across all animals to ensure the data were unbiased for each mask-area quan- tification.

CD31+ vessel quantification and analysis

Immunofluorescence of CD31+ vasculature was quantified across serial (1:6) CCI-TBI brain sections (30 μm). Vascular endothelium was stained with a goat antibody against CD31 (R&D Systems, Inc., diluted 1:500) and visualized via a donkey anti-goat antibody conjugated with AlexaFluor-488 (Invitrogen, 1:500). Images of CD31+- vessels were used to quantify vasculature within the CCI-TBI lesion. A grid was overlaid on images to quantify vessels within 100 μm of the lesion surface and then normalized as a function of the surface area (mm2) to account for variations in lesion size among males and females. ImageJ software (NIH) was used to measure lesion surface and volume as a function of tissue loss by tracing the lesion face and interpolating the cortical surface. Similarly, vessel diameter was measured on 3–5 sections. The cross-sectional distance between the outer margins of CD31+-vessels was measured to report microvascular diameter within 300 μm of the lesion surface (ImageJ software) on a 1:6 series, and data were reported as the mean for each animal (n = 4).

Tight junction recovery assay

To evaluate the effect of Tie2 activation on TJ assembly, endothelial cells were treated with an action inhibitor Latrunculin-A (LatA) to disturb TJ proteins[177] before F-domain scaffold administration. Briefly, confluent HUVECs or HBMECs on coverslips were treated with 0.25μM of LatA diluted in growth medium for 30 minutes. After 30 minutes, LatA were washed with PBS before adding F-domain scaffolds at 100 or 200 nM diluted in LG DMEM + 10% FBS for 30 minutes or 2 hours. Post treatment, cells were fixed with 4% PFA for immunofluorescence staining with antibodies (detailed protocol in Histology and immunofluorescence section) to visualize ZO1 (Invitrogen, 1:100) or Claudin-5 (Abcam, 1:100).

Statistical analysis

All quantifications show the mean, and error bars are ± SEM. Ordinary one-way ANOVA with post hoc test, Bonferroni, or Dunnett test was used for multiple comparisons, and a two-tailed, unpaired t-test was used for comparing groups of two using GraphPad Prism. *P*-values < 0.05, 0.01, 0.001, 0.0001 are indicated with *, **, *** and ****, respectively.

Chapter III - Results

Part I: Probing the molecular basis of angiopoietins-Tie2

INTRODUCTION

Angiopoietins regulates Tie2 signaling and vascular function. Ang1 and Ang2 both contain a Tie2-binding fibrinogen-like domain (F-domain), a coiled-coil domain, and an amino-terminal super clustering domain (SCD) for multimerization[80]. Ang1 and Ang2 interact with Tie2 through very similar binding modes[75,76] via nearly identical F-domain structures[75] with similar affinity for Tie2 (K_D3 nM)[71]. Thus, many previous studies postulated that the differences in Ang/Tie2 signaling outputs produced by Ang1 and Ang2 are due to differences in their oligomerization state. Electron microscopy characterization of the Ang1 and Ang2 suggests Ang1 has a greater tendency to self-associate into higher-order oligomers[78–80], which has been proposed to stem from two cysteine residues (41 and 54) in the SCD of Ang1 that is not present in Ang2[78]. When multivalent angiopoietins bind to Tie2, angiopoietins clusters a different number of Tie2 receptors due to their oligomeric state. Constructs displaying multiple F-domains, such as Comp-Ang[79,81] and Ang1 surrogates[80] have been demonstrated to produce Ang1-like activity but correlating ligand-receptor valency with signaling output is not straightforward since both Ang1 and Ang2[78], Ang1 surrogates[80], and Comp-Ang[79,81] can occupy a range of oligomeric states. Similarly, antibodies against Ang2 (ABTAA)[84] or Tie2 (hTAAB)[178] produce Ang1-like signaling outcome, but the oligomerization state of the active signaling complexes is unclear. Moreover, work with chimeric mouse angiopoietins generated by swapping the F-domains of Ang1 and Ang2 suggested the F-domain is the determinant for Tie2 activation, not the oligomeric state[85]. Here we generate and characterize computationally designed protein scaffolds presenting the Ang1 F-domain in a wide range of valences and geometries to probe the mode of Tie2 activation.

RESULTS

Aim 1.1 Generation of F-domain scaffolds

To investigate the molecular basis of the Ang1 and Ang2 signaling differences systematically, we generated a series of computationally designed ligands which display F-domains in a wide range of valencies (2, 3, 4, 6, 8, 12, 30, and 60 copies of F-domain) and symmetries (cyclic, tetrahedral, and icosahedral) (Fig 1A). We employed previously designed dimeric (Fc-Fd), trimeric (H3, Tet1-A, Tet1-A.2, and Icos1-A), tetrameric (C4 and AkC4), hexameric (H6), octameric (H8) cyclic oligomers with 3, 4, 6, and 8 subunits, and tetrahedral (Tet1 and Tet2) and icosahedral (Icos1 and Icos2) with 12 and 60 copies of F-domains, respectively[167–169,179]. All other scaffolds were produced by genetically fusing the F-domain with SpyTag and covalently conjugated to SpyCatcher fused to the N- or C-terminus of the designed scaffold subunits[165] (Fig. 1A and Appendix 1A) . To analyze the dependency of F-domain distance on Tie2 activity, trimeric configurations wherein F-domain attachment points ranged from 2.2 nm to 8.0 nm were designed. The SpyTag–SpyCatcher conjugation efficiency was ~80% for the tetrameric

scaffolds and 90% or greater for all the remaining scaffolds (Fig. 1B). The negative stain electron micrographs show spherical particles of the expected size (~30nm) and shape with small spikes corresponding to the SpyCatcher domain displayed on the particle surface (Fig. 1C). A dimeric F-domain scaffold were genetically fused with the human IgG Fc domain to present two copies of F-domains, Ang1-Fc (Appendix 1U)[179]. Ang1-Fc were further assembled into higher order oligomers by combining with O4 and I5 designs described in Divine et al[179] that presents 24 and 60 copies of F-domains, respectively (Appendix 1U). This set of scaffolds was to confirm that activity of different F-domain valency could be repeated in systems without SpyCatcher-SpyTag.

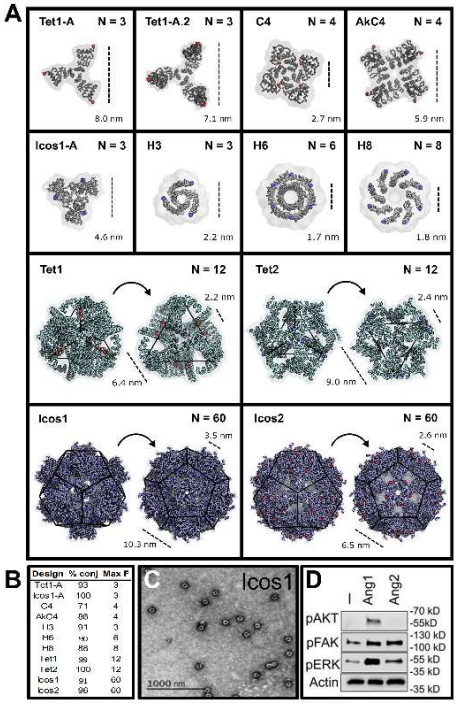

Figure 1. Computationally designed scaffolds with tunable F-domain valencies and geometries. A) Designed F-domain scaffold structures. Red and purple dots indicate N- and C-terminal sites of F-domain conjugation, respectively. N is the maximum number of conjugated F-domains. Dashed lines - distance between F-domain conjugation sites. Cyclic homo-oligomers series: trimeric scaffolds (Icos1-A, Tet1-A, and Tet1-A.2), tetrameric scaffolds (C4 and AkC4), and helical bundles (H3, H6, and H8). Nanocages: tetrahedral scaffolds (Tet1 and Tet2) and icosahedral scaffolds (Icos1 and Icos2 present sixty copies of the F-domain on the trimer and pentamer subunits, respectively). **B**) The average F-domain to scaffold conjugation efficiency. **C**) Negative stain electron micrograph of Icos1 scaffold with 60 F-domain conjugation sites. Scale bar is 1,000 nm. **D**) Serum-starved HUVECs were stimulated with 18 nM of angiopoietins.

Aim 1.2 Correlating Tie2 signaling output with F-domain valency and geometry

F-domain valency regulates Tie2 activity

We evaluated the activity of F-domain scaffolds by determining their signaling profiles in Human Umbilical Vein Endothelial Cells (HUVECs). Serum-starved HUVECs were treated with angiopoietins or F-domain scaffolds at 18nM for 15 minutes, and the activation of downstream signaling pathways were analyzed by Western blot for AKT (S473), ERK1/2 (T202/Y204), FAK (Y397), and Tie2 (Y992) phosphorylations using immunoblotting. Consistent with previous studies, Ang1 treatment increased phosphorylation of AKT (S473), FAK (Y397), and ERK1/2 (T202, Y204), whereas we found Ang2 only activated FAK and ERK (Fig. 1D).

Upon analyzing AKT phosphorylation, the effect of F-domain valency has on pAKT activation is remarkable. Scaffolds presenting 3-4 copies of F-domains, regardless of their geometries and F-domain distances all failed to activate pAKT. (Fig. 2A, D, E, H, I, L, and Appendix 1C and D). In contrast, all the scaffolds displaying six or more F-domains strongly

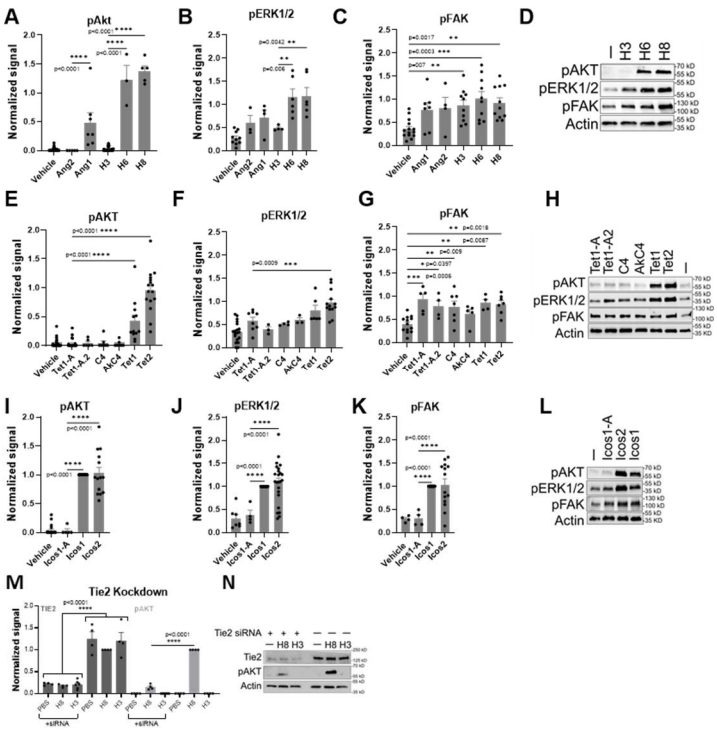

Figure 2. F-domain valency determines Tie2 signaling output. Serum starved HUVECs were stimulated with designed scaffolds normalized to 18 nM of F-domains for 15 min and analyzed by immunoblotting. **(A, E, I)** pAKT, **(B, F, J)** pERK1/2, and **(C, G, K)** pFAK phosphorylation levels were quantified and normalized to Icos1 signaling levels. Representative immunoblot gels of HUVECs treated with **(D)** helical bundles, **(H)** trimeric and tetrameric homo‐oligomers and tetrahedral nanocages, (L) Icosahedral nanocages and trimeric subunit. Bars represent the mean ± SEM. One‐way ANOVA with Bonferroni test was used for multiple comparisons to calculate P‐values. (****) indicates $P < 0.0001$.

activated AKT. The use of different geometric series of scaffolds with overlapping F-domain valency highlights the importance of F-domain valency. Cyclic helical bundles: H3, H6, and H8 which have nearly identical geometry though only hexameric H6 and octameric H8 strongly activate pAKT while the trimeric H3 failed to induce AKT phosphorylation (Fig. 2A and D). We also observed a significant increase in Tie2 phosphorylation in both H8 and H3 scaffolds treated samples, suggesting that the synthetic ligands act through a similar pathway as angiopoietins (Appendix 5A and B). To confirm that the F-domain scaffolds regulating pAKT work through Tie2 receptors, we knocked down Tie2 expression in HUVECs using siRNA. This significantly reduced H8-dependent pAKT levels compared with wildtype cells stimulated with H8 (Fig. 2M-N), indicating that the multivalent F-domain scaffold is acting on pAKT through the Tie2 receptor. The nano-scale tetrahedral and icosahedral cages are comprised of two self-assembling components, one of which is conjugated to the F-domain. The dimeric (Ang1-Fc) and trimeric (Tet1-A and Icos1-A) subunits presenting F-domains failed to activate pAKT on their own (Fig. 2E, I, and Appendix 1U-W). However, when combined with the partner nanoparticle component which assemble into a tetrahedral (Tet1 and Tet2), Octahedral (O42.1), or icosahedral (Icos1, Icos2, I52.3) cage, respectively, all nanocages strongly activate pAKT.

All scaffolds, except dimeric scaffold (Fd-Fc) induced ERK phosphorylation (Fig. 2B, F, J, and Appendix 1V, X). There was little effect of F-domain valency have on FAK phosphorylation. All scaffolds presenting 2 to 60 copies of F-domains upregulated pFAK (Fig. 2C, G, K and Appendix 1V, Y). FAK phosphorylation appears to be somewhat sensitive to geometry as Tet1-A activated the highest level of FAK phosphorylation relative to the other trimeric constructs (Fig. 2G). These results suggest that the induction of Tie2 clusters by two F-domains are sufficient to upregulate phosphorylation of FAK, three F-domains are needed for phosphorylation of ERK1/2, and the phosphorylation of AKT requires six or more F-domains.

F-domain scaffolds are Tie2 super agonists

To compare the potency of the synthetic ligands and assess the effect of multivalency on cell binding affinity/avidity, we investigated the concentration dependence of AKT and ERK1/2 activation for a subset of scaffolds alongside Ang1 and Ang2 for comparison. Serum starved HUVECs were treated with F-domain scaffolds or angiopoietins for AKT and ERK1/2 analysis using immunoblotting (Fig. 3 and Appendix 1F–L). All scaffolds with six or more copies of F-domains activated pAKT more efficiently than Ang1 when comparing their lower half-maximal (EC_{50}) for AKT activation (Fig 3A-B). Impressively, the EC_{50} of H8 scaffold (1.4 nM F-domain) is 19-fold lower than Ang1 EC_{50} (27 nM F-domain). Moreover, AKT activation produced by the tested F-domain scaffolds was less variable than Ang1. No AKT phosphorylation was observed in H3 and Ang2 titrations, even at high concentrations.

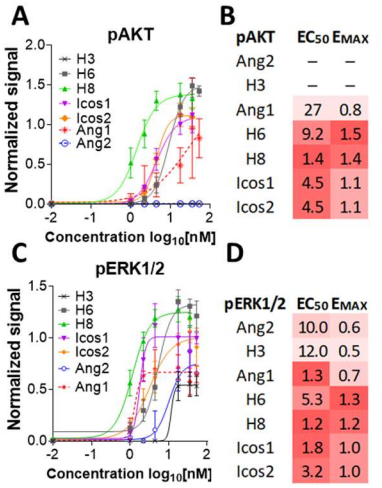

Figure 3. F-domain scaffolds are Tie2 super agonists. Dose-response curves, EC50, and EMAX for **A-B)** pAKT and **C-D)** pERK1/2 activation. Heatmap color scale: darker red color indicates lower EC_{50} and higher E_{MAX} values. The curves, EC_{50} and E_{MAX} values are calculated using Prism, GraphPad.

The high valency F-domain scaffolds produced a higher level of pERK1/2 (higher E_{MAX}) on average compared to Ang1 and Ang2 (Fig. 3C-D). Notably, H8 is again the most active agonist (E_{MAX} = 1.2) compared with Ang1 (E_{MAX} = 0.7) and Ang2 (E_{MAX} = 0.6). H8 also had the lowest EC50 (1.2 nM F-domain). The efficiency and maximum signaling level of H3 and Ang2 to activate pERK1/2 were very similar with E_{MAX} = 0.5 and 0.6, respectively, and EC_{50} = 12 and 10 nM F-domain, respectively. Overall, high valency F-domain scaffolds behave as Tie2 super-agonists that produced a more robust signaling output than Ang1 (for pAKT and pERK activations) or Ang2 (for pERK activation).

Ang1, but not Ang2, activates pAKT which phosphorylates FOXO1 and induces translocation out of the nucleus in endothelial cells, the expectation is that modulating endothelial cell gene expression will promote cell survival[84,180–182]. We found that both Ang1 and H8 induced FOXO1 nuclear exclusion while H3 and Ang2 did not (Fig. 4A-D and Appendix 5C-D). Moreover, H8 is significantly better than Ang1 for FOXO1 inhibition (Fig. 4D). In cell survival assay, H8 promoted a higher level of cell survival compared to PBS control in 16-hour serum deprivation (Appendix 2E).

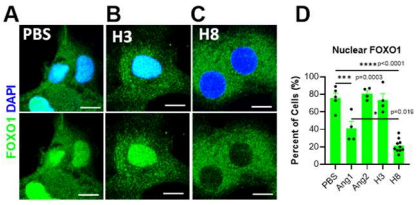

Figure 4. Tie2 super agonists induce FOXO nuclear exclusion. Serum starved HUVECs were treated with 100 nM of Ang1, Ang2, F-domain scaffolds or PBS. **A-C)** Representative images of FOXO1 localization upon angiopoietins or Fd-scaffold administration in **D)** Quantification of nuclear FOXO1 shown as percent of cells with nuclear FOXO1 stain. 100 cells were counted per sample. Scale bars are 10 μm.

Trimeric F-domain scaffolds are Tie2 super antagonists.

Ang2 is known as a partial agonist/antagonist, depending on cellular context. Ang2 inhibits Ang1-dependent pTie2[71] and pAKT[72], but in the absences of Ang1, Ang2 upregulate pAKT[73]. To explore the Ang2 antagonism, we utilized trimeric F-domain scaffolds that do not activate pAKT to compete with Ang1-induced pAKT in HUVECs. Consistent with previous observation[72], Ang2 significantly attenuated Ang1-dependent pAKT signaling at 45 nM (Fig. 5A). We found that the trimeric scaffolds, H3, Tet1-A, and Icos1-A also reduced Ang1-induced pAKT level (Fig. 5B and Appendix 1M-O). H3 was the most effective pAKT antagonist when compared to Ang2 at 45 nM F-domain. Interestingly, we observed large variations in Ang2 activity. Commercial Ang2 suspended in carrier protein, BSA, did not activate pAKT. In other batches of Ang2 without BSA, pAKT was up-regulated. When BSA (50 µg/ml BSA) was added back to these batches, it reduced Ang2 capacity to activate pAKT (Appendix 1Z). BSA prevents protein aggregation or misfolding[183] thus it could play a role in maintaining Ang1 and Ang2 physiological oligomerization states. We propose that Ang2 can aggregate into higher order ligand clusters in the absence of physiological amounts of carrier proteins. This may explain the contradicting Ang2 activity in different studies and resonates with our hypothesis that low F-domain valency acts like Ang2 while high F-domain valency acts like Ang1. In conclusion, we found Ang2 antagonism is F-domain valency dependent. Trimeric scaffolds are Ang2-like and cannot activate pAKT but can compete with Ang1 for Tie2 binding thus downregulating Ang1-dependent pAKT activation.

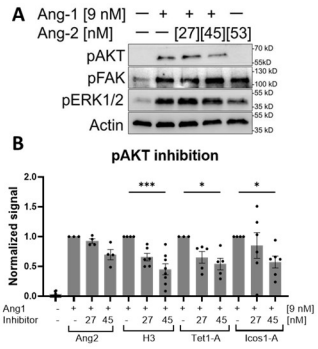

Figure 5. F-domain scaffolds are Tie2 super antagonists. Serum starved HUVECs were treated with 9 nM of Ang1 +/- Ang2 or trimeric scaffolds at 27 or 45 nM of F-domain. **A)** representative immunoblot for inhibition of Ang1-dependent pAKT signaling by Ang2. **B)** quantifications of pAKT inhibitions by Ang2, H3, Tet1-A, and Icos1-A. pAKT band intensity were normalized to Ang1-dependent pAKT level.

Aim 1.3 - Analyzing the *in vitro* and *in vivo* angiogenesis capacity of F-domain scaffolds

Tie2 super agonists promote cell migration via actin rearrangement

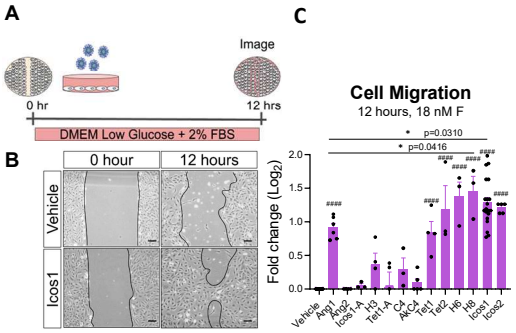

Figure 6. Tie2 super agonists accelerate cell migration. A) Schematic representation of the *in vitro* scratch cell migration/ wound healing assay. **B)** Icos1 at 18 nM F-domain stimulates cell migration relative to PBS/vehicle control. Scale bars are 100 µm. **C)** Comparison of cell migration induced by Ang1, Ang2, and designed F-domain scaffolds after 12 hours of treatment. The change in wound area is normalized to vehicle control. All experiments have at least 3 biological replicates. (*) is the comparison between F-domain scaffolds vs Ang1, and (#) is the comparison between F-domain scaffolds vs Vehicle. (####) indicated p<0.0001.

Angiogenesis requires sprouting, proliferation, tube formation, and migration of endothelial cells[184], and activation of Tie2 by Ang1 promotes cell migration[185–187]. To evaluate the capacity of the F-domain scaffolds to promote cell migration and wound healing, F-domain scaffolds were tested in an *in vitro* cell migration assay[172]. Confluent HUVECs were scratched in the center of

the dish to model a wound. The wound was treated with or without F-domain scaffolds at 18 nM of F-domain for 12 hours to evaluate the change in the wound area as a measure for cell migration (Fig. 6A-B). High F-domain valency scaffolds: H6, H8, Icos1, and Icos2 increased cell migration (2- to 3-fold) compared with the vehicle ($P < 0.0001$). H8 and Icos1 induced more migration than Ang1 ($P < 0.05$). In contrast, low F-domain valency scaffolds: H3, Tet1-A, C4, and Icos1-A, like Ang2[73], did not increase cell migration (Fig. 6C and Appendix 2A).

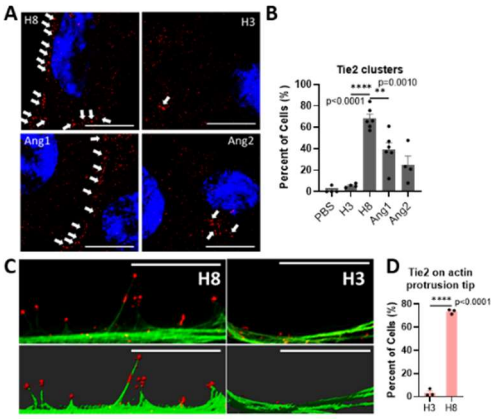

Figure 7. Super clustering Tie2 induces actin rearrangement. Starved HUVECs were stimulated with scaffolds or angiopoietins and stained with **A)** Tie2 antibodies for analyzing plasma membrane Tie2 clusters. Scale bars are 10 µm. **B)** Quantification shows the percent % of total cells that exhibit large Tie2 clusters on the plasma membrane. **C)** Top panels shows H8 or H3 treated cells analyzed under super-resolution microscopy shows actin protrusions with Tie2 clusters at the tip. Lower panels are Imaris reconstructed 3D model of the super-resolution images. Scale bars are 5 µm. **D)** Quantification of percent of cells exhibited actin protrusions with Tie2 clusters at the tip. 100 cells were counted per sample.

Ang1 is suggested to induce Tie2 receptor super clustering[79,80,84,186], thus we studied the effect of the F-domain scaffolds on Tie2 clustering on the plasma membrane using confocal and super-resolution microscopy. H8-treated cells produced a considerably higher percent of cells expressing large Tie2 clusters on the plasma membrane than Ang1-treated cells, while Ang2- and H3-treated cells were comparable to PBS controls (Fig. 7A-B). Upon analyzing the Tie2 clusters using super-resolution microscopy (OMX) and Tie2 super clusters were associated with dramatic cytoskeletal rearrangements. Cells treated with H8 showed actin protrusions with Tie2 clusters at the leading tip of the extensions; such morphology was absent in H3-treated cells (Fig. 7C-D). One hypothesis to explain these actin protrusions is that H8 induces HUVEC cell cytoskeletal rearrangements that mimic the cytoskeletal changes observed previously in endothelial cell sprouting and cell migration[188–190]. This could explain the mechanism for the elevated cell migration capacity of Ang1-like F-domain scaffolds (Fig. 6C).

Tie2 super agonists enhance in vitro vascular stability

We also investigated the effect of the F-domain scaffolds on the stability of HUVEC-derived capillary-like structure as described previously[171]. HUVECs were plated on 100% Matrigel and incubated with or without F-domain

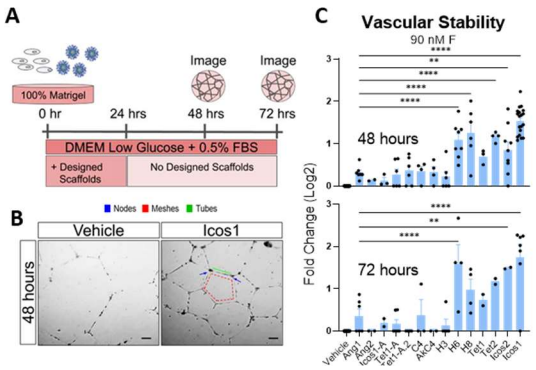

Figure 8. Tie2 super agonists promote vascular stability. A) Schematic of in vitro tube formation assay; F-domain scaffolds (designed scaffolds) were added at 90 nM F-domain and removed at 24h; vascular stability was analyzed at 48h and 72h timepoints. **B)** Representative increase in vascular stability by Icos1. The number of nodes (blue) meshes (red), and tubes (green) were quantified using angiogenesis analyzer plugin in ImageJ. Scale bar is100 µm. **C)** Effect of F-domain scaffolds on the vascular stability at 48- and 72-hour timepoint were assessed by taking the average of the number of nodes, meshes, and tubes and normalized to vehicle as log2 fold change.

scaffolds at 90 nM of F-domain for 24 hours. The scaffolds were removed, and the stability of the formed tubules were followed up to 72 hours thereafter (Fig. 8A). Images of the tubule structures were imaged at 48- and 72-hour timepoints and quantified to evaluate vascular stability (Fig. 8B and Appendix 2B, D). The higher valency scaffolds H6, H8, Tet2, Icos1, Icos2, O42.1, and I52.3 enhanced vascular stability considerably compared with Ang1 at the 48-hour timepoint (Fig. 8C top). H6, Icos1, and Icos2 were significantly better than Ang1 at the 72-hour timepoint (Fig. 8C bottom). H8, O42.1, and I52.3 were better than PBS at the 72-hour timepoint (Appendix 2C). Icos1 stabilized vascular tubules 2.4-fold and 3-fold better than Ang1 at 48- and 72-hour timepoints, respectively (Fig. 8C). Scaffolds 2-4 F-domain—Icos1-A, H3, Tet1-A, Tet1-A.2, C4, and AkC4—stabilized the tubules at levels between Ang1 and Ang2.

F-domain valency dictates angiopoietin activity

The phenotypes produced by the different F-domain scaffolds in the assays described thus far are summarized in Fig 3G along with those of Ang1 and Ang2. The scaffolds fall into two broad groups. The first group, like Ang1, induces AKT phosphorylation and tube formation (top of Fig. 9), while the second group, like Ang2, induces FAK and ERK phosphorylation but not Akt phosphorylation and tube formation (bottom part of Fig. 9). The first group contains all of the scaffolds presenting six or more SpyCatcher domains, and the second group contains all of the scaffolds with four or fewer domains. This suggests that there are two primary modes of signaling through the Tie2 receptor and that the signaling output produced by a Tie2 agonist depends primarily on its F-domain valency: High valency F-domains lead to an Ang1-like phenotype, while 3–4 F-domains produce an Ang2-like phenotype (Appendix 3). While valency is the dominant determinant of signaling output, the geometry of Tie2 clustering also appears to play a role; for example, the lower valency scaffolds differ somewhat in the induction of FAK phosphorylation, ERK phosphorylation, and vascular stability.

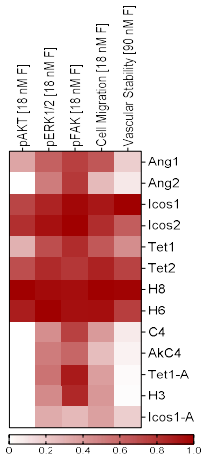

Figure 9. Designed F‐domain scaffolds fall into Ang1‐ and Ang2‐like classes. Color indicates highest (1) to lowest (0) pAKT, pERK1/2, and pFAK levels which were column normalized. Cell migration level and vascular stability (48‐h timepoint) were also column normalized from highest to lowest.

Icosahedral F-domain nanocage accelerated wound healing in mouse after TBI

Icosahedral scaffold housing 60 copies of F-domains, Icos1 demonstrated super agonistic property over other Ang1-like scaffolds. Icos1 produced the most stable signaling output and longest lasting effect on vascular stability. To determine whether the super agonist behavior of Icos1 carries over to the *in vivo* situation, Icos1 is selected for vascular repair in mouse after traumatic brain injury. The Ang/ Tie2 pathway has been shown to play a critical role in the loss of neuronal survival and function after TBI in aged animals[191–193]. We investigated the effect of Icos1 super-agonist administration after a controlled cortical impact injury (CCI-TBI) in adult mice (6

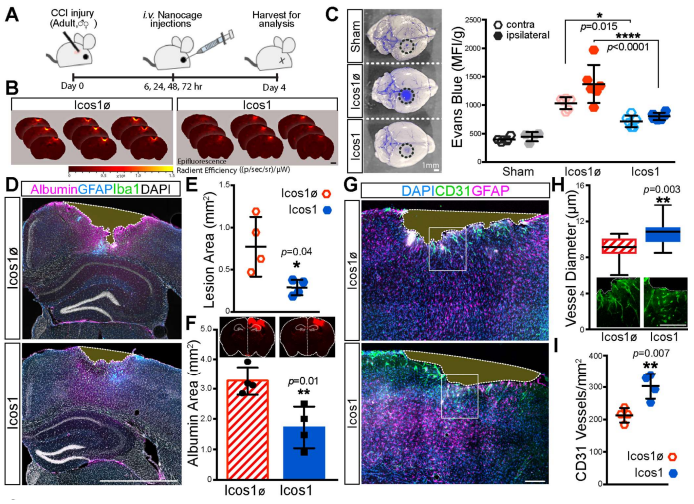

Figure 10. Icosahedral F-domain scaffold restores BBB function and enhances angiogenesis after injury. **A)** Schematic of CCI-TBI experiments. Injured animals were injected with Icos1ø (control) or Icos1 injection at 6, 24, 48, and 72 hours post-injury followed by Evans blue (5% in saline) injection before brain tissues were harvested on 4 days post-injury. **B**) Evans Blue epifluorescence was imaged in serial sections (30 µm) through the CCI-TBI lesion to visualize tissue penetrance and lesion spread, scale bar is 1 mm. **C**) Evans blue extravasation in brain tissue (black dotted circle indicates lesion site) was quantified by fluorescence intensity in tissue extracts from hemispheres contra- and ipsilateral to the injury. Intensity measurement from female and male mice was normalized against body mass to report changes in BBB permeability in Icos1ø- and Icos1-treated animals (n = 6). Scale bar is 1 mm. **D-E)** CCI-TBI brain sections were stained for reactive astrocytes (GFAP, blue), microglia (Iba1, green), and serum albumin (magenta) to highlight tissue margins (dotted white line) and quantify secondary damage as a function of lesion area (E: bar, 1 mm. **F**) Cumulative blood extravasation into brain tissue (white outline) was imaged by albumin immunofluorescence to establish an unbiased intensity-threshold mask (red) and quantify the area of blood serum extravasation (mm2), bar is 500 µm. **G–I**) Brain tissues stained by GFAP (magenta) and CD31 immunofluorescence (green) were imaged by confocal microscopy to measure angiogenesis as a function of vessel diameter (H: n = 4, the boxes show 25th to 75th percentiles, and whiskers represent the min and max values.) and quantify the number of CD31 vessels (I: n = 4) at the site of injury of animals 4 days post-injury, bars in G and H are 100 µm.

months old). After a mild CCI-TBI, Icos1 or Icos1 cage without F-domains (Icos1ø) were administered by bolus i.v. injections (1.0 mg/kg) at 6, 24, 48, and 72 h post-injury (Fig. 10A). On day 4, animals were injected (i.v.) with Evans blue to quantify BBB dysfunction and vascular leakage [193,194]. Remarkably, animals treated with Icos1 showed reduced Evans blue tissue penetrance and lesion expansion (Fig. 10A-B); Icos1-treated animals showed a significant, 1.7-fold reduction of Evans blue fluorescence (mean fluorescence intensity, MFI) in brain extracts derived from both ipsi- and contralateral hemispheres compared with Icos1ø controls (Fig. 10C; ipsilateral: 805 vs. 1,375 MFI/g; contralateral: 719 vs. 1,036 MFI/g; respectively, n = 6).

Secondary neurodegeneration and lesion expansion after CCI-TBI has been attributed to significant loss of microvasculature, chronic microbleeds, and BBB dysfunction that spreads from the primary injury[195–198]. Histological analysis of tissues on the second cohort of CCI-TBI animals to visualize reactive astrocytes (GFAP stain), microglia (Iba1 stain), and albumin to visualize tissue margins, and brain tissue loss was quantified as a function of lesion surface area between albumin highlighted tissue margins within serial sections of the CCI lesion (Fig. 10D, highlighted with white-dotted outline). As before, male and female animals were normalized against body mass to account for animal size-based differences. We observed a 3.5-fold increase in lesion expansion (i.e., tissue loss) in Icos1ø versus Icos1 nanoparticle treatment (Fig. 10E). Vascular leakiness was further quantified by albumin extravasation into the brain parenchyma. An unbiased threshold intensity mask overlay analysis on serial tissue sections centered at the CCI lesion and quantified cumulative postinjury neurovascular breakdown as a function of the area stained by serum albumin extravasation within the ipsilateral hemisphere (Fig. 10F, image insets). Control-treated (Icos1ø) animals showed extensive serum albumin extravasation throughout the injured brain, whereas albumin levels in the parenchyma of Icos1-treated animals were attenuated by 50% (Fig. 10F). Thus, Icos1 super-agonist treatment reduced secondary tissue loss and albumin accumulation after CCI-TBI, which is consistent with the observed increase in BBB integrity.

Notably, Icos1-treated tissues show enhanced Tie2 activation throughout the injury along CD31 vessels compared to in comparison to Icos1ø-treated (Appendix 6A-E). Moreover, Icos1-treated tissue showed prevalent phospho-Tie2 colocalization on pericytes with processes that extended along vascular elements (Appendix 6C-F: elongated NG2+pTie2+ processes CD31 vessels). Importantly, Tie2 activation with super-agonist treatment was only noted in tissue proximal to the site of injury, whereas pTie2/pAKT immunostaining in contralateral brain tissue was similar in Icos1 and Icos1ø controls (Appendix 7A–D). Thus, drug delivery to the brain was a function of injury-dependent vascular permeability and not a result of delivery across an intact BBB. Tie2 super-agonists activated Tie2 signaling and phospho-Akt in NG2+-pericytes to form a critical barrier and cluster around vasculature (Fig 8I, Icos1, inset), which could provide a much needed therapeutic to stabilize BBB function and reduce the side effects of neurovascular dysfunction and traumatic injury to the CNS.

Results in Aim 1 are now published in EMBO Report[199]

Part II: ***Dissecting molecular events upon Tie2 activation for vascular stability***

INTRODUCTION

The angiopoietin-Tie2 pathway regulates blood vessel stability, remodeling, and permeability. Part I of this study illustrated Tie2 activation using a designed super agonist, Icos1 expedited vascular repair and wound healing in injured mouse brains. To further investigate the molecular basis in Tie2-mediate vascular repair, this section will dive into the molecular events upon Tie2 activation that led to vascular stability. The mechanistic interplay in the Tie2 pathway is complicated due to co-receptors such as integrins, Tie1, and VE-PTP that can influence Tie2 signaling outcome. VE-PTP and Tie1 are suggested as Tie2 inhibitors. The role of α5β1 integrin is controversial; it can enhance or inhibit Tie2. Induced ischemic brain injury in mice showed upregulation of Ang1, α5 subunit, and TJ (CLDN5 and ZO1) expression at the same vascular rupture site 72 hours post injury suggesting that Tie2 and integrin promoted vascular repair in the BBB post injury[91,92,99]. However, it is not known if these proteins are upregulated in the same cell or cell types and the potential mechanistic interplay between Tie2-angiopoietins and α5β1 is not fully understood. The role of α5β1 in vascular stability and permeability remains ambiguous. α5β1 integrin is proposed by many to enhance Tie2 signaling[91,99–101] while others also have argued α5β1 association inhibits Tie2[112,113]. The interactions of Tie2 with angiopoietins and α5β1 integrin at the plasma membrane may be essential for regulating the subsequential signaling required for vascular stability and permeability.

Vascular permeability and stability are controlled by AJ and TJ molecules. We previously demonstrated superclustering Tie2 receptors recruited the AJ components, PECAM and VE-Cadherin[6], suggesting that Tie2 may be an initiator for the assembly of AJs and TJs at endothelial cell-cell junctions. However, to date, the Tie2 mechanism of function in TJ assembly has not been dissected. This section of my study investigated the mechanistic interplay between angiopoietins, Tie2, and α5β1 integrin that orchestrate TJ formation in endothelial cells. I **hypothesize** that high F-domain valency ligands induce Tie2-α5β1 association to promote TJ formation for vascular stability.

RESULTS

Aim 2.1 Tie2 activation accelerate tight junction recovery after chemical disruption

In part I of my project, Tie2 superagonist, Icos1 demonstrated remarkable vascular repair and wound healing capacities (Fig. 10). Since TJ formation between endothelial cells can promote vascular stability, we evaluated whether or not Tie2 signaling can regulate TJ formation. We used chemical inhibition of actin polymerization in HUVECs and HBMECs (Latrunculin A, LatA) to study the recovery process after the disruption of TJs[177,200]. In particular, we tested the capacity of Tie2 signaling to accelerate the TJ recovery process. Briefly, a

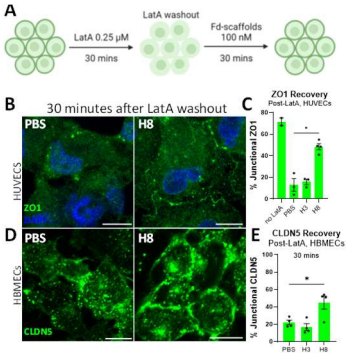

Figure 11. Tie2 activation accelerated tight junction recovery after chemical disruption. **A)** HBMECs or HUVECs were treated with LatA for 30 minutes before Tie2 activation. Images of accelerated junctional **B)** ZO1 and **D)** CLDN5 recovery upon H8 treatment for 30 minutes, bar = 10 μm. Quantifications showing the percent of cells showing junctional **C)** CLDN5 and **E)** ZO1 after 30 minutes in H8, H3 or PBS treated cells.

confluent monolayer of HUVECs or HBMECs were treated with LatA for 30 minutes, then LatA was washed out (Fig. 11A). Angl-like ligand (H8, Fig.9), Ang2-like ligand (H3, Fig. 9), or PBS control was added for another 30 minutes before PFA fixation for immunofluorescence staining to visualize junctional ZO1 and CLDN-5 (Fig. 11B&D). Impressively, H8 significantly accelerated the recovery of junctional ZO1 (3.7-fold) and CLDN-5 (2.5-fold) compared to PBS and H3 (Fig. 11C&E). This result illustrated that Tie2 activation enhances TJ assembly in the paracellular space of endothelial cells to regulate vascular stability and permeability. Although Tie2 activation can induce the expression of TJ proteins, this is a short 30-minute assay, suggesting that the function of Tie2 in this recovery process may be independent of transcription. We will confirm the action of Tie2 in H8-treated cells with or without α-amanitin (transcription inhibitor)[201] to evaluate TJ recovery independent of transcription.

Aim 2.2 Clustering Tie2 forms two Tie2 complexes

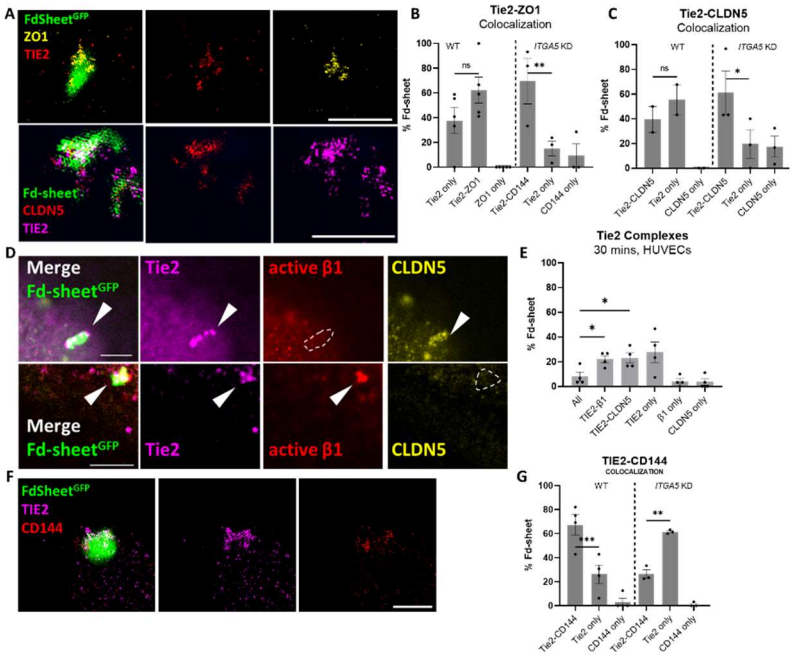

Figure 12. Two classes of Tie2 complexes. A) Super-resolution OMX images showing Tie2 clusters under Fd-sheeet colocalized with **A)** ZO1, CLDN5, and **F)** CD144. Bars = 5 μM. Quantification showing percentage of Fd-sheets colocalizing Tie2 +/- **B)** ZO1, **C)** CLDN5, or **G)** CD144 in wild-type cells (WT) vs. siRNA-treated cells to knockdown α5 expression (*ITGA5 KD*). **D)** Confocal images of cell stained with antibodies to visualize Tie2, active β1, and CLDN5. **E)** Quantification showing percentage of Fd-sheets with Tie2 colocalizing CLDN5, active β1, or both. At least 30 sheets were counted in each sample.

As discussed above, Ang1, α5β1, and TJs (CLDN5 and ZO1) expression were all upregulated at the lesion site post injury in mice suggesting that Tie2 and integrin promoted vascular repair in the blood-brain barrier post injury[91,92,99]. However, it was unclear how Tie2, α5β1, and TJs relate to each other. To probe these interactions, micrometer-scale 2-dimensional protein sheets presenting F-domains were used to analyze the association partners upon clustering of Tie2 receptors. Fd-sheets were fabricated as described previously[6] by combining two self-assembling subunits, A and B to form hexagonal layers. A subunit was fused with SpyCatcher and conjugated to GFP-SpyTag and F-domain-SpyTag (Fd-sheets). To assemble the sheets A-GFP, A-Fd, and B are mixed at 1:4:5 molar ratio, respectively. Upon Fd-sheets treatment in HUVECs, the TJ proteins: ZO1, claudin-5 (CLDN-5), and occludin (OCLN) colocalized with Tie2 under the Fd-sheets (Fig. 12A-C and appendix 8A-B). Surprisingly, quantitative analysis of the Tie2 clusters

revealed two types of Tie2 complexes in wild-type HUVECs: Tie2-TJs and Tie2-only (Fig. 12B-C). To evaluate whether α5β1 is needed for the recruitment of TJs, HUVECs were pre-treated with siRNA against *ITGA5* mRNA to knockdown α5 before Fd-sheets administration. Our results showed eliminating α5 did not inhibit ZO1 and CLDN-5 recruitment to Tie2 clusters (Fig. 12B-C), suggesting that integrin α5β1 was not required for TJ formation. Interestingly, the proportions of Tie2-ZO1 or -CLDN5 were upregulated, while the Tie2-only group showed a significant reduction in the knockdown compared to the wild-type cells (Fig. 12B-C). We also observed clustering Tie2 produced two classes of Tie2 clusters (Fig. 12D). Data revealed two types of Tie2 clusters: Tie2-TJ and Tie2-α5β1 clusters (Fig. 12E). Surprisingly, the data demonstrated α5β1-Tie2 is not responsible for TJ recruitment, thus we further investigated the function of the Tie2-α5β1 complex. AJs formation is required for cell-cell attachment to facilitate TJ formation, and indeed our data show Tie2 clusters did recruit AJ, CD144 under the Fd-sheets (Fig. 12F-G). We also performed knockdown experiments of α5 to test whether or no CD144 recruitment is inhibited. Our data show that the knockdown of α5 significantly reduced the level of Tie2-CD144 colocalization compared to the wild-type cells (Fig. 12G). The Tie2- α5β1 complex is needed for the recruitment of AJ.

Aim 3.1 α5β1-Tie2 complex regulates focal adhesion complex

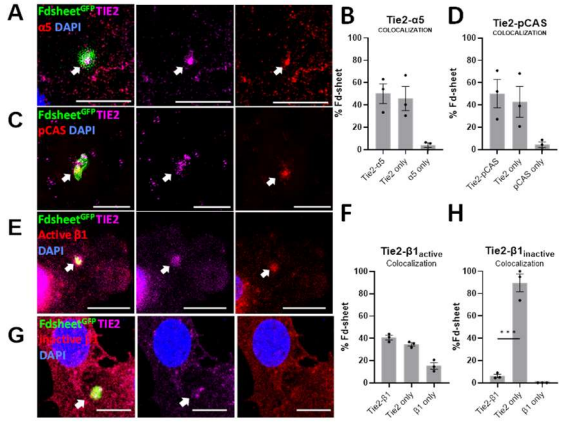

Figure 13. Tie2 clusters recruit and activate α5β1 integrin. Serum starved HUVECs treated with Fd-sheets at 20 nM F-domain concentration for 30 minutes before fixation for immunofluorescence staining. Confocal images of Tie2 colocalizing with **A)** α5, **C)** pCAS, **E)** active β1, but not **G)** β1 inactive under the GFP-tagged Fd-sheets. **B,D,F,H)** Quantifications show the frequency of Tie2 colocalizing with α5, pCAS, active β1, and inactive β1 per Fd-sheets. At least 30 Fd-sheets were counted in each sample.

α5β1 integrin association with Tie2 enhance angiogenesis upon Ang1 stimulation while others argue α5β1 also inhibits Tie2 and TJ formation[99–101,112,114,202]. Our data show α5β1 integrin was not involved in TJ recruitment to Tie2. Thus, we further explored the role of the α5β1-Tie2 complex in endothelial cells. Serum-starved HUVECs were treated with Fd-sheets to visualize Tie2 supercluster and the association with α5β1 integrin and its downstream target, pCAS[203,204]. Upon super clustering Tie2 receptors, α5β1 integrin but not α3 integrin colocalize with Tie2. α5 and active β1 integrin domains were found with Tie2 under the Fd-sheets while inactive β1 and α3 were not (Fig 13A-B, E-H and Appendix 8C). The recruitment of α5β1 to Tie2 clusters was rapid; half of the Tie2 clusters colocalized with α5 already at 10 minutes timepoint while longer incubation did not show significant changes (Appendix 8D-E).

Integrin regulates focal adhesion (FA) complex assembly and recruits pCAS to promote cell-to-extracellular matrix adhesion and migration[203,204]. Activation of α5β1 by seeding

endothelial cells on fibronectin enhanced Ang1-dependent cell migration[99,101]. α5β1 interaction with Tie2 clusters may play a role in the enhancement of migration that was observed with the high valency F-domain scaffolds (Fig. 6C). To evaluate whether α5β1 regulates Tie2-mediated cell migration, we analyzed the components of the focal adhesion complex, pCAS upon super clustering Tie2. As expected, pCAS was also observed accumulating under the Fd-sheets (Fig. 13C&D). Data suggest super clustering Tie2 using Fd-sheets (Ang1-like) recruited α5β1 integrin and induced pCAS activation. pCAS is a component of the focal adhesion complex that promotes cell migration[203–205], which likely explains our findings that Ang1-like super agonists accelerate cell migration in aim 1 via the integrin/pCAS pathway (Fig. 6C)

Aim 3. 2 F-domains bind and bring α5β1 and Tie2 into a complex

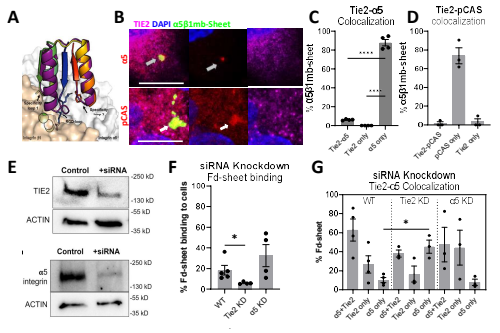

Figure 14. F-domain binds integrin. A) *de novo* designed α5β1 mini binder structural model. **B)** Confocal images of α5 integrin clusters under α5β1mb-sheets. Quantification of pCAS and α5 but not Tie2 under the α5β1mb-sheets. **C-D)** HUVECs were treated with siRNA against α5 or Tie2 before starvation and Fd-sheets administration. **E)** Representative western blots confirm the efficiency of α5 or Tie2 knockdown. **F)** Quantification of Fd-sheet binding to cells in wild type, Tie2 knockdown, α5 knockdown, 100 cells were counted in each sample. **G)** Quantifications of Tie2-α5 under the bounded Fd-sheets. Bars = 10 μM.

Previous studies suggested that the F-domain could activate integrin in cell lines that do not express Tie2[110,111], thus, it is not clear whether Tie2-α5β1 complexes are formed via a receptor-receptor interaction or shared ligand. To investigate the mode of interaction between Tie2 and α5β1, *de novo* designed mini binder (mb) with high specificity and affinity to bind the α5β1 heterodimer was used to cluster α5β1[206] (Fig. 14A). The α5β1-specific mini-binders (α5β1mb) were designed to mimic the binding interface between α5β1 and Fibronectin (FN) via FN's RGD sequence loop which is presented on the mb (Fig. 14A). In addition to the RGD loop, two specificity loops were designed to increase binding affinity and specificity toward the α5β1 heterodimer complex. The α5β1mb structure was predicted by Alphafold2, and this prediction aligned well with the Rosetta-designed structure (Fig. 14A). In BLI *in vitro* binding experiments, α5β1mb bound to α5β1 at nanomolar affinity and the binding was specific for α5β1 integrin since no binding was observed with other analyzed RGD-binding integrins ($\alpha_v\beta3$ and α8β1; Appendix 8F). The α5β1mb was then genetically fused with SpyTag (mb-st) to allow conjugation to the A domain of the sheets presenting SpyCatcher to make α5β1mb-sheets^{GFP} for testing whether integrin clusters recruit Tie2 in HUVECs. Upon α5β1mb-sheets^{GFP} treatment, α5 and pCAS were found clustering under the α5β1mb-sheets^{GFP} while Tie2 was not which suggests that Tie2 or the F-domain was likely responsible for integrin recruitment (Fig. 14B-D). To test whether F-domain was critical for forming the Tie2-α5β1 complex, cells were treated with siRNA against *TEK* or *ITGA5* before Fd-sheets administration (Fig. 14E-G). As expected, the knockdown of Tie2, significantly reduced the amount of Fd-sheets binding to cells compared to wildtype (Fig. 14F). Interestingly, while the knockdown of α5 did not affect the binding of the Fd-sheets (Fig. 14F), the proportion of Fd-sheets bound to α5 only group increased significantly compared to wildtype (Fig. 14G). In summary, clustering α5β1 using α5β1 specific mb-sheets cannot recruit Tie2. The knockdown of Tie2 show Fd-sheets colocalized with α5-only group suggesting that the Tie2-α5β1 hetero-complex likely formed via F-domain binding to both receptors.

F-domains activate α5β1 integrin for cell attachment

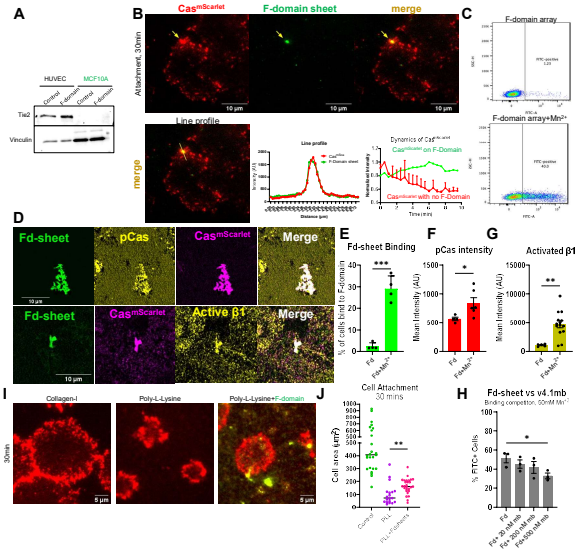

Figure 15. F-domain activates α5β1 integrin in MCF10A cells without Tie2. A) Western blot staining of Tie2 protein expressions in MCF10A and HUVECs cell lysate. **B)** Representative images of live-cell TIRF microscopy of Fd-sheets bound to MCF10A cells expressing CAS-tagged with mscarlet (Cooper Lab, FredHutch). Line prolife analysis of GFP (green, bounded Fd-sheets) and mScarlet (red, CAS) intensities in one timepoint. Line profile analysis of mScarlet intensity over 10 minutes in sites with or without Fd-sheets. **C)** FACS analysis of MCF10A cells treated with Fd-sheets +/- Mn^{+2}. TIRF images of starved MCF10A cells with Fd-sheets bound and colocalizing with **D)** pCAS and active β1. **E)** Quantifications show percent of Fd-sheets binding to cells +/- Mn^{+2} by counting fixed cells. Quantification of **F)** pCAS or **G)** active β1 mean intensities under the Fd-sheets +/- Mn^{+2}. **H)** FACS analysis of cells treated with Fd-sheets -/+ varying concentrations of α5β1mb to evaluate binding competition**. I)** Images of cells adhesion when seeded on collagen or Poly-L-Lysine -/+ Fd-sheets. **J)** Quantification of cell area after 30 minutes of seeding.

To validate whether F-domains truly bind integrin (as seen in Figure 14) and investigate the biological significance of the F-domain-integrin interaction, Fd-sheets were introduced to MCF10A cells that do not express Tie2 (Fig. 15A). Genetically modified MCF10A expressing $CAS^{mScarlet}$ were starved and dissociated into suspension prior to Fd-sheets administration for live-cell TIRF microscopy. Fd-sheets did bind to MCF10A cells. Line profiler analysis of the TIRF images showed Fd-sheets binding to MCF10A cells and colocalizing with $CAS^{mScarlet}$ (Fig. 15B). Dynamic analysis showed the bound Fd-sheets recruited $CAS^{mScarlet}$ near the binding site while other $CAS^{mScarlet}$ that was not bound with the sheets rapidly diffused between the plasma membrane and cytoplasm (Fig. 15B, lower right). Mn^{+2} ion promotes the open conformation of integrin and increases its ligand binding affinity[162]. FACS analysis demonstrated a 40-fold increase in the amount of cell binding to the Fd-sheets (FITC+ cells) with the addition of $Mn^{+2,}$ which further confirmed that Fd-sheets was binding to MCF10A cells via integrin (Fig. 15C). Under the bounded Fd-sheets, pCAS and active β1 were colocalizing under the Fd-sheets (Fig. 15D). The addition of Mn^{+2} also significantly increased the intensities of pCAS and active β1 stain under the Fd-sheets (Fig. 15E-G).

Our data is consistent with previous observations that Ang1 F-domain activated integrin in the absence of Tie2[110,111], but the binding site of the F-domain on integrin has yet to be explored. To find the binding site of the F-domain on integrin, binding competition experiments were performed using MCF10A cells treated with 20 nM $Fd\text{-}sheet^{GFP}$ +/- α5β1mb (20, 200, 500 nM). When Fd-sheets and α5β1mb were presented to the cells, α5β1mb competed with Fd-sheets for integrin binding (Fig. 15H). At 500nM of α5β1mb significantly reduced the amount of FITC+ cells (Fd-sheets) in FACS suggesting that the F-domains and α5β1mb are likely binding integrin at the fibronectin-RGD binding site that prompted integrin activation. Activated integrin assembles the

focal adhesion complex for cell-ECM attachment and migration [48,103,203]. To examine the cellular outcome of Fd-sheets binding to integrin, cell culture dishes were pre-treated using Poly-L-Lysine (PLL) to inhibit cell attachment, then cells seeded with or without Fd-sheets (Fig. 15I). Cells seeded on Fd-sheets + PLL surface attached and spread faster than on the PLL only surface (Fig. 15J). Collectively, we demonstrated that the F-domain could bind to integrin in two different cell lines: HUVECs and MCF10A. F-domains are likely binding to integrin via the RGD-binding sites. Upon F-domain binding, integrin is activated and recruits pCAS (Fig. 13 and 15) to regulate focal adhesion complexes for cell-matrix attachment (Fig. 15J-K) and migration (Fig. 6C).

Aim 3. 3 α5β1-Tie2 complex regulates cell survival via pAKT/FOXO1 pathway

To determine the role of α5β1 integrin in Tie2 signaling, siRNA against *ITGA5* was used to knockdown α5β1 in HUVECs. The knockdown of α5β1 significantly attenuated pAKT activity in H8-treated cells compared to H8-treated wild-type cells (Fig. 16A-B)[199]. pAKT activation drives FOXO1 translocation out of the nucleus[93,182,207–209]. Eliminating α5 before H8 treatment, FOXO1 was restricted in the nucleus compared to the wildtype (Fig. 16C-D). α5β1mb monomer could bind and prevent α5β1-Tie2 complex formation, thus we observed pAKT signal is downregulated in mb+H8 (Appendix 8G). Treating cells with α5β1mb monomer also showed a high percentage of cells that were positive for nuclear FOXO1 stain, similar to the results for siRNA + H8 treated (Fig. 15D). It has been reported that activation of pAKT/FOXO1 pathway promoted cell survival[180,181]; thus we performed RNA sequencing of HUVECs treated with H8 or PBS for 2 hours. Differential gene expression analysis showed 505 genes were differentially expressed in H8 vs PBS-treated cells (Appendix 8H-I). 288 out of 505 genes are downregulated in H8-treated samples. GO-term analysis of the 288 genes shows genes related to apoptosis and cell death were downregulated in H8-treated samples (Appendix 8J). 73/288 genes downregulated in H8-treated cells are FOXO1 targets based on ChEA3 search, but common FOXO1 targets such as Angpt2, BCL-2, and CCR5 were not found. Perhaps 2-hour treatment time or 20 nM of H8 was insufficient to repress their expression significantly (Appendix table 2G). In summary, our data suggested that the α5β1-Tie2 complex promoted cell survival via the pAKT/FOXO1 signaling axis. In addition, genes related to cell-cell and cell-matrix adhesions, cell migration, tube formation, wound healing, and proliferation were upregulated in H8-treated samples, which was consistent with previous observations in Ang1-Tie2 signaling[37] (Appendix 8K).

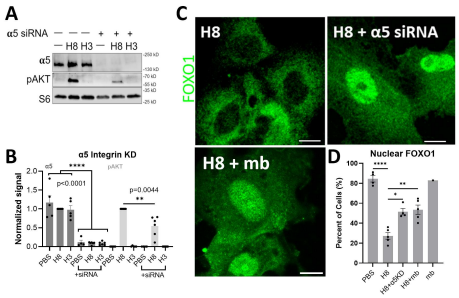

Figure 16. Integrin-Tie2 complex regulate pAKT/FOXO1 signaling to promote cell survival. Serum starved HUVECs were treated with α5β1mb to inhibit α5β1 before H8 administration or HUVECs were pre-treated with siRNA against *ITGA5* to knockdown α5 before starvation and H8 treatment. **A)** Western blot images showing pAKT inhibition upon α5 knockdown in H8-treated cells. **B)** Quantification of pAKT level normalized to H8-treated wild-type cells. **C)** Representative images of FOXO1 localization in wild-type vs siRNA-treated cells. **D**) Quantification of nuclear FOXO1 shown as percent of cells with nuclear FOXO1 stain. 100 cells were counted per sample. Scale bars are 10 μm.

Two functional distinct Tie2 clusters

To summarize our observations, clustering Tie2 receptors using designed proteins revealed two functionally distinct Tie2 complexes. The Tie2-α5β1 clusters activate downstream pAKT/FOXO1 signaling to regulate gene expression in endothelial cells and recruit VE-Cadherin to promote endothelial cell-cell attachment. Stabilized cell-cell attachment is thought to be a prerequisite for formation of TJs between endothelial cells[11]. Tie2-ZO1 clusters are likely localizing at the paracellular space of the endothelium to orchestrate the assembly of TJ molecules, namely CLDN-5 and OCLN, to form the seal between endothelial cells to modulate vascular stability and permeability.

Chapter IV - Discussion & Conclusions

Part I: Probing the molecular basis of angiopoietins-Tie2

Aim 1 discussion

For a long time, the mechanism behind the opposing vascular outcome produced by Ang1 vs. Ang2 was unclear. Many studies postulated these differences were due to angiopoietin oligomeric states, while Procopio et al. (1999) argued the differences lay within the difference in their F-domains. The oligomeric states that agonize Tie2 were also debatable. Oh et al. (2015) demonstrated dimeric Ang1 was enough to activate Tie2, but Davis et al. (2003) argued tetrameric Ang1 is the minimum requirement for activating Tie2. Studies using modified angiopoietins with non-specific oligomeric states resulting in inconsistent conclusions, which further complicated the analysis of the Ang-Tie2 pathway. Furthermore, one study also argued that the different F-domains of Ang1 and Ang2 were the main driver for their activity. Clearly, the regulation of Tie2 signaling is controversial and requires further investigation.

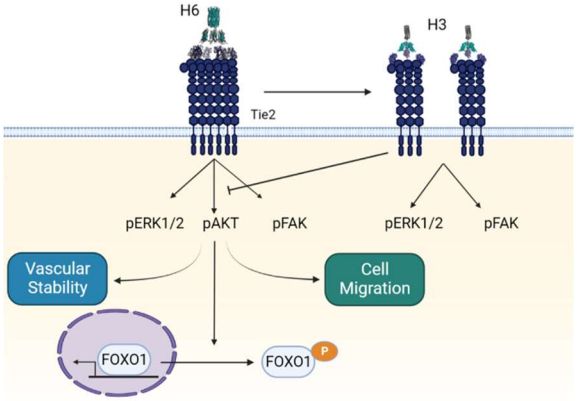

Figure 1. F-domain valency determines Tie2 signaling outcome. Ligands presenting in 6 or more F-domains behaved like Ang1, while ligands housing 3-4 F-domains behaved like Ang2.

In aim 1, we utilized computationally designed proteins that self-assembled into well-defined higher-order oligomers as scaffolds. These scaffolds were conjugated with Ang1 F-domain at well-defined valences and geometries to precisely control Tie2 receptor clustering and have uncovered the molecular basis that governs angiopoietin activity. For the first time, we correlated Ang1 F-domain valency with Tie2 downstream signaling output, namely via pAKT, pERK1/2, and pFAK. Extensive screening of these F-domain constructs revealed two broad classes of F-domain scaffolds distinguished by the number of F-domains (Fig. 1). Scaffolds presenting six or more copies of F-domains have Ang1-like properties, inducing FAK, ERK1/2, and AKT phosphorylation. These Ang1-like agonists accelerated cell migration, enhanced vascular stability, induced FOXO1 nuclear exclusion, and generated Tie2 superclusters at the plasma membrane. The second group of scaffolds housing three to four F-domains behaved like Ang2, upregulating FAK and ERK phosphorylation but not Akt phosphorylation. Like Ang2, these low valency scaffolds failed to induce cellular functions seen in our Ang1-like ligands. Low valency scaffolds inhibited Ang1-dependent AKT phosphorylation similar to Ang2. pAKT activation binds and phosphorylates FOXO (pFOXO) as demonstrated in co-immunoprecipitation experiments previously[180]. 14-3-3 proteins bind pFOXO and mask the nuclear localization signal sequence leading to FOXO nucleus exclusion[180,208–210]. Previous studies show that FOXO localizing in the

nucleus upregulates pro-apoptotic gene expression such as BCL2, FABP4, EGR1, CLEC2, CCL2, BAX, CRCR4, ANGPT2, TRAIL, and CCR5; in contrast, genes that promote proliferation and survival BIRC5 (survivin), CCND1 (Cyclin-D1) are downregulated[182,211–214]. Thus, Ang1-like scaffolds promote cell survival via the pAKT/FOXO1 signaling axis.

Using the F-domain of Ang1, we were able to recapitulate Ang1 and Ang2 phenotypes. Our results suggested the modes of Tie2 receptor signaling depend primarily on F-domain valency. Ang1 activity requires at least six F-domains, while 3–4 F-domains produce an Ang2-like phenotype. Dose-dependent titration experiments of selected F-domain scaffolds demonstrated that Ang1-like F-domain scaffolds are Tie2 super agonists. The antagonistic action of Ang2 also depends on F-domain valency. Low F-domain valency ligands compete with high F-domain valency ligands for Tie2-binding to produce smaller clusters of Tie2 that do not activate pAKT, thus reducing overall pAKT activity. The tested trimeric F-domain scaffolds were demonstrated to be better Tie2 inhibitors than Ang2; they are Tie2 super antagonists. Upon analysis of Tie2 clusters produced by agonistic F-domain scaffolds under super-resolution microscopy, it was seen that these Tie2 super clusters induced actin protrusion with Tie2 at the leading tip. This observation may be the mechanism for Tie2-orcheastrated cell migration and sprouting; both are processes essential to early angiogenesis. This study also demonstrated the efficacy of the Tie2 super agonist, Icos1 to promote wound healing *in vivo* in mice after traumatic brain injury. Icos1 dramatically reduced vascular leakage and reduced lesion area in the injured animals after four days of treatment. Further analysis of long-term effects from Icos1 administration is necessary to evaluate side effects and brain function recovery. In addition, mechanistic regulation of Tie2 for vascular repair and stabilization has not yet been thoroughly dissected.

Part II: Dissecting molecular events upon Tie2 activation for vascular integrity

Aim 2 Discussion

In part 1, we found that Ang1 with six or more F-domains drove vascular integrity, while Ang2 existed in 3-4 F-domains and induced leaky vasculature. We demonstrated *in vivo* Tie2 activation using superagonist, Icos1 accelerated the repair of hemorrhagic vessels after injury in mouse brains, but it was unclear how Tie2 regulated this process. In Aim 2, we follow up this question to dissect the role of Tie2 in vascular stability. Vascular stability and permeability are regulated by AJs and TJs. Tie2 activation upregulates gene expression of the junctional molecules: VE-Cadherin, PECAM1, ZO1, and CLDN5 to promote vascular stability and regulate permeability[90–93]. However, it is unclear whether Tie2 also plays a part in the formation TJs. We further investigated the capacity of Tie2 activation to recover TJs in cell culture after chemical disruption using LatA. Notably, Tie2 activation using the Tie2 agonist, H8, indeed accelerated TJ (ZO1 and CLDN5) re-assembly. To validate that Tie2 directly orchestrated the assembly of TJs, we took advantage of micro-scale protein sheets conjugated with GFP and F-domains to super cluster Tie2 and visualize the interacting components at high resolution. We observed TJ markers

such as ZO1, CLDN-5, and occludin colocalized with Tie2 receptors under the Fd-sheets. Interestingly, quantitative analysis of these Tie2 clusters revealed two types of Tie2 complexes: Tie2-TJ and Tie2-α5β1 (Fig. 2). Eliminating *ITGA5* using siRNA enriched Tie2-TJ association suggesting Tie2-mediated TJ formation is independent of α5β1 integrin, which aligns with previous study showing α5β1 inhibition enriches junctional ZO1[112].

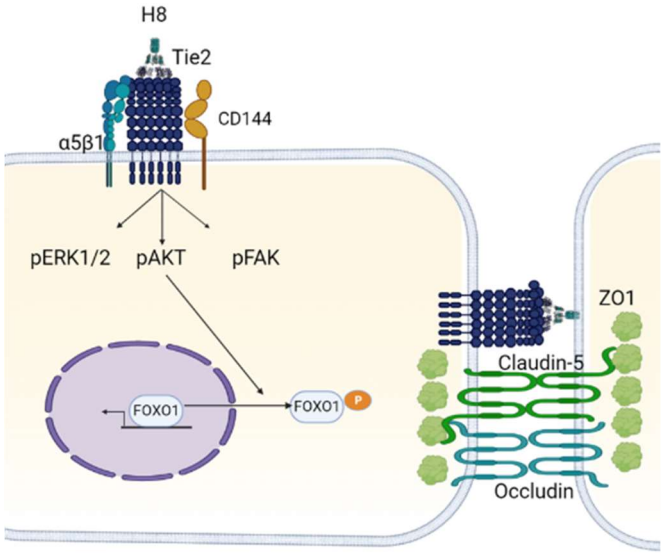

Figure 2. Tie2 super clusters forms two types of Tie2 complexes. Tie2-α5β1 complex recruits CD144 and upregulates pAKT/FOXO1 signaling axis. Tie2-TJ complex localizes at cell-cell junction to stabilize endothelial integrity.

Although α5 knockdown did not affect ZO1 and CLDN5 recruitment to Tie2, but AJ molecule, CD144, recruitment to Tie2 was inhibited. I originally hypothesized that "high F-domain valency ligands induce Tie2-α5β1 association to promote TJ formation for vascular stability", but surprisingly our data suggested otherwise. Interestingly, we found that the Tie2-α5β1 complex regulates CD144 recruitment to Tie2 clusters, which is consistent with previous studies showing that α5β1 integrin modulated CD144 localization in endothelial cells[109,163,215]. However, it is still unclear how this relates to blood vessel stability *in vivo*. First, AJ formation is a known prerequisite for TJ formation, however, we saw that downregulated Tie2-CD144 complexes did not affect TJ recruitment to Tie2 when α5β1 was knockdown. One possible explanation for this is that AJs and TJs are being recruited to Tie2 via different plasma membrane co-factor(s) or downstream molecule(s), and our data illustrated that α5β1 is the co-factor that helps Tie2 to recruit CD144. The molecule(s) that helps Tie2 to recruit TJs remains to be determined. I hypothesize that Tie2 may have assembled AJs and TJs via independent pathways to promote vascular stability, and further investigation is needed to delineate the full mechanism fully. Interestingly, some studies showed transient α5β1 inhibition produced opposing outcomes compared to genetic knockout of α5β1; one led to the accumulation of TJs to the endothelial paracellular space[112,216], while the other induced dramatic vascular leakage[107], respectively. These conflicting results might be due to the fact that many of these transient α5β1 inhibition studies were done using integrin inhibitors (AXT107, ANT161, and mAb13) that were not specific to α5β1. AXT107 and ANT161 targets α5β1 and αvβ3[112,216,217]. mAb13 is a β1-integrin antibody that binds and inactivates β1[218], but this will broadly inactivate many integrin isoforms because the β1 subunit can dimerize with multiple α subunits (α1,2,4,5,6, or v) [48]. In this study, we used siRNA to knockdown *ITGA5,* which would only inhibit α5β1 formation on the cell membrane, and therefore our approach was more specific. We indeed observed α5β1 inhibition resulted in more TJ formation; therefore, the vascular leakage

observed in α5β1 knockout mice was likely due to a different pathway that also regulates permeability. A recent study showed that binding of pericytes-secreted vitronectin to α5β1 on the endothelial cell surface is needed for maintaining blood-brain-barrier functions by inhibiting transcytosis across the endothelium[219], and this might explain the vascular leakage observed in α5 knockout mice [107].

Aim 3 Discussion

Ang1 was previously shown to promote Tie2 and α5β1 association via overexpression of modified Tie2 and α5β1 receptors in cancer cells for fluorescence resonance energy transfer (FRET) or co-immunoprecipitation (with or without chemical crosslink) experiments[99–101], but structural analysis of the Tie2-α5β1 complex has not yet been fully investigated. To explore the endogenous Tie2-α5β1 interaction and the resulting function, Fd-sheets were used to probe the α5β1-Tie2 interaction under a super-resolution microscope. Our data demonstrated that clustering Tie2 recruited active α5β1, and the Tie2-α5β1 complex activated AKT phosphorylation and induced FOXO1 to translocate out of the nucleus in endothelial cells. Using siRNA against *ITGA5* or α5β1mb to reduce Tie2-α5β1 complex formation, we saw that both conditions resulted in pAKT inhibition and FOXO1 nuclear confinement. FOXO1 nuclear exclusion promotes gene expression for cell proliferation and survival[182,211–213]. Indeed, RNA sequencing of HUVECs treated with Ang1-like scaffolds, H8, showed FOXO target genes that promote apoptosis were downregulated, and genes related to cell-cell adhesions were upregulated. Although we did not observe CLDN5, ZO1, and OCLN gene expressions being upregulated in H8-treated samples, Ang1 is known to upregulate these genes[90–93]. Therefore, our treatment conditions need further optimization: higher H8 concentration or longer incubation time. We also found the Tie2-α5β1 complex recruited pCAS and VE-Cadherin indicating the formation of focal adhesion complexes and the reduction of cell-cell adhesion, respectively, which may result in the upregulation of cell migration. The dual functions of the Tie2-α5β1 complex may be the driver for Ang1-dependent cell migration and vascular stability.

To explore the structural basis of the Tie2-α5β1 complex, siRNA targeting *TEK* or *ITGA5* were used to knockdown Tie2 or α5 in HUVECs, respectively. Although the knockdown of Tie2 reduced the amount of Fd-sheets binding to cells, it enabled more Fd-sheets binding to α5 only under the bounded sheets, which suggested that the F-domain was likely binding to integrin directly. We validated this hypothesis in MCF10A cells that lack Tie2 expression. Indeed, Fd-sheets binding to MCF10A via α5β1 integrin was also observed. Our results resonate with previous studies that suggested the Ang1 F-domain binds and activates integrin[110,111]. We propose that the Tie2-α5β1 complex was stabilized through F-domain binding to both Tie2 and α5β1 receptors. Using *de novo* designed α5β1mb (contained RGD) in competition experiments with Fd-sheets in MCF10A cells, α5β1mb were able to compete with F-domain, which suggested that F-domain was likely bound to integrin via the similar RGD-binding site. Fibronectin is the natural ligand for integrin that binds integrin via the RGD sequence on the FN-III_{10} domain[220]. However, F-domain

does not contain RGD, and so Dallabrida et al. (2005) speculated that the QHREDGS sequence on Ang1 F-domain may have facilitated the interaction with integrin because the QHREDGS sequence resembles the REDV motif in fibronectin that bind α4β1[111,221]. Yet, it is unknown whether this motif also participates in α5β1 binding. The structural basis of Ang1-Tie2-intergrin interaction still requires further investigation.

In summary, our data illustrated that Tie2 regulates TJ formation via two Tie2 complexes. The Tie2-α5β1 complex upregulated TJ gene expression via pAKT/FOXO1 signaling, while Tie2 clusters at endothelial cell-cell junctions directly recruited and assembled TJ molecules (Fig 2). Pericyte-to-endothelial cell interaction is essential to maintaining vascular stability and permeability[23,37,53–55]. Pericytes secrete Ang1 in the basal side of the endothelium that binds and activates Tie2. It is likely that the Tie2-α5β1 complex observed in my study would form between pericytes and endothelial cells *in vivo* to inhibit transcytosis and regulate vascular permeability[219].

Conclusion and Future Directions

This study showed that the F-domain valency of angiopoietins is the determining factor for Tie2 signaling output. Ang2 at trimer or tetramer oligomeric states induced smaller Tie2 clusters, which resulted in leaky vasculature, while Ang1 existing at a hexameric state (or higher) produces large Tie2 clusters, which can stabilize blood vessels. High F-domain valency ligands induced two functional classes of Tie2 complexes that worked in parallel to support TJ formation for modulating vascular stability and permeability; the Tie2-TJ complex promotes cell-cell interaction, while the Tie2-α5β1 complex regulates pAKT/FOXO. Tie2 can also be regulated by many other co-factors, namely Tie1 and VE-PTP, which generally inhibit Tie2 activation. How F-domain valency influences the interaction between Tie2 and Tie1 or VE-PTP structurally still requires further exploration. We demonstrated that F-domains cluster α5β1 integrin, with or without Tie2 contribution, which suggests F-domain can interact directly with α5β1 integrin and α5β1 inhibition attenuated Tie2/pAKT activation, which raises some follow-up questions. Does the engagement of integrin affect Tie2 signaling at the extracellular or cytoplasmic domains? Is F-domain essential to the formation of the Tie2-integrin clusters and signaling activation? To answer these questions, we plan to design a high-affinity Tie2-specific mini-binder (Tie2mb) for analyzing the function of the Tie2 clusters independent of α5β1. Using this novel approach, we expect to identify the primary drivers of Tie2 activation and the interplay between Tie2 and integrin. If Tie2mb activates Tie2 in scaffolds at a valency of six or higher, we can conclude that clustering Tie2 receptors are sufficient. If that fails to activate Tie2, we will generate mosaic scaffolds presenting Tie2mb and α5β1mb. If the combination of Tie2mb and α5β1mb leads to Tie2 activation, we can infer that F-domain does not play a role in activation other than bringing the receptors together; otherwise, F-domain may be interacting with other co-factors as well or inducing conformational changes in the receptors to enable proper signaling transduction. Despite the powerful design algorithms at the Institute for Protein Design, our previous attempts to design Tie2mb were unsuccessful. The interface between Tie2 and F-domain is a very flat surface; thus, designing anchoring residues on a flat surface is difficult. One possibility is to make bigger binders to allow more interaction with Tie2. Our effort to design high-affinity Tie2 mini-binders is still underway. Tie2mb is critical for dissecting the Tie2 pathway thoroughly. Tie2mb can also be utilized in therapeutic applications to control angiogenesis for tissue regeneration, cancer therapy, and wound healing.

Proper activation of Tie2 signaling is critical for blood vessel development and normal angiogenesis. Understanding the regulation of the Tie2 pathway using our synthetic angiopoietin-like agonists and antagonists provide a potential tool to stimulate or inhibit angiogenesis, which might be used to treat neurovascular diseases, traumatic brain injury, sepsis, cancers, and various oral diseases that feature vascular dysfunction. They might also be used to promote tooth regeneration, which requires angiogenesis. For example, Tie2 super agonists are also applicable in periodontitis and pulpitis treatment for stabilizing the leaky vasculatures that may relieve tissue inflammation and promote wound healing. The Tie2 super agonists are potentially applicable to promote tooth organoid vascularization for supporting organoid survival and improving

implantation outcomes for tooth regeneration. Conversely, the super antagonists and α5β1mb can be used to inhibit unwanted vascular growth and Tie2/pAKT signaling concurrently. This is relevant to radiotherapy to eradicate vasculogenesis in cancer, including oral squamous cell carcinoma. More generally, our computationally designed protein approach to investigate the role of ligand valency and receptor engagement is broadly applicable to a wide variety of receptor tyrosine kinase signaling.

References

1. Sasahira, T., Kurihara-Shimomura, M., Shimomura, H. & Kirita, T. SERPINE2 is an oral cancer-promoting factor that induces angiogenesis and lymphangiogenesis. *Int J Clin Oncol* 26, 1831–1839 (2021).

2. Shivamallappa, S. M., Venkatraman, N. T., Shreedhar, B., Mohanty, L. & Shenoy, S. Role of angiogenesis in oral squamous cell carcinoma development and metastasis: an immunohistochemical study. *Int J Oral Sci* 3, 216–224 (2011).

3. Rohani, B. Oral manifestations in patients with diabetes mellitus. *World J Diabetes* 10, 485–489 (2019).

4. BERGGREEN, E., BLETSA, A. & HEYERAAS, K. J. Circulation in normal and inflamed dental pulp. *Endod Top* 17, 2–11 (2010).

5. Almoosawy, S. A. *et al.* The oral health status of patients with peripheral vascular disorders: A systematic review. *Vascular* 29, 556–566 (2021).

6. Ben-Sasson, A. J. *et al.* Design of biologically active binary protein 2D materials. *Nature* 589, 468–473 (2021).

7. Herron, L. A., Hansen, C. S. & Abaci, H. E. Engineering tissue-specific blood vessels. *Bioeng Transl Medicine* 4, e10139 (2019).

8. Zihni, C., Mills, C., Matter, K. & Balda, M. S. Tight junctions: from simple barriers to multifunctional molecular gates. *Nat Rev Mol Cell Bio* 17, 564–580 (2016).

9. Vermette, D. *et al.* Tight junction structure, function, and assessment in the critically ill: a systematic review. *Intensive Care Medicine Exp* 6, 37 (2018).

10. Günzel, D. & Yu, A. S. L. Claudins and the Modulation of Tight Junction Permeability. *Physiol Rev* 93, 525–569 (2013).

11. Cong, X. & Kong, W. Endothelial tight junctions and their regulatory signaling pathways in vascular homeostasis and disease. *Cell Signal* 66, 109485 (2020).

12. Sweeney, M. D., Sagare, A. P. & Zlokovic, B. V. Blood–brain barrier breakdown in Alzheimer disease and other neurodegenerative disorders. *Nat Rev Neurol* 14, 133–150 (2018).

13. Kumar, V. A., Brewster, L. P., Caves, J. M. & Chaikof, E. L. Tissue Engineering of Blood Vessels: Functional Requirements, Progress, and Future Challenges. *Cardiovascular Engineering and Technology* 2, 137–148 (2011).

14. Parker, J. C. Acute lung injury and pulmonary vascular permeability: use of transgenic models. *Compr Physiol* 1, 835–882 (2013).

15. Baker, O. J. Current trends in salivary gland tight junctions. *Tissue Barriers* 4, e1162348 (2016).

16. Bentley, D. R. *et al.* Accurate whole human genome sequencing using reversible terminator chemistry. *Nature* 456, 53–59 (2008).

17. Gronthos, S., Mankani, M., Brahim, J., Robey, P. G. & Shi, S. Postnatal human dental pulp stem cells (DPSCs) in vitro and in vivo. *Proc National Acad Sci* 97, 13625–13630 (2000).

18. Shi, S. & Gronthos, S. Perivascular Niche of Postnatal Mesenchymal Stem Cells in Human Bone Marrow and Dental Pulp. *J Bone Miner Res* 18, 696–704 (2003).

19. Dissanayaka, W. L., Zhu, L., Hargreaves, K. M., Jin, L. & Zhang, C. Scaffold-free Prevascularized Microtissue Spheroids for Pulp Regeneration. *J Dent Res* 93, 1296–1303 (2014).

20. Dissanayaka, W. L., Zhu, L., Hargreaves, K. M., Jin, L. & Zhang, C. In Vitro Analysis of Scaffold-free Prevascularized Microtissue Spheroids Containing Human Dental Pulp Cells and Endothelial Cells. *J Endodont* 41, 663–670 (2015).

21. Kwon, T., Lamster, I. B. & Levin, L. Current Concepts in the Management of Periodontitis. *Int Dent J* 71, 462–476 (2021).

22. Vailhé, B., Vittet, D. & Feige, J.-J. In Vitro Models of Vasculogenesis and Angiogenesis. *Lab Invest* 81, 439–452 (2001).

23. D'Amore, P. A. & Patel-Hett, S. Signal transduction in vasculogenesis and developmental angiogenesis. *Int J Dev Biol* 55, 353–363 (2011).

24. Patan, S. Vasculogenesis and Angiogenesis as Mechanisms of Vascular Network Formation, Growth and Remodeling. *J Neuro-oncol* 50, 1–15 (2000).

25. Reagan, F. P. Vascularization phenomena in fragments of embryonic bodies completely isolated from yolk-sac blastoderm. *Anat Rec* 9, 329–341 (1915).

26. Caprioli, A. *et al.* Hemangioblast Commitment in the Avian Allantois: Cellular and Molecular Aspects. *Dev Biol* 238, 64–78 (2001).

27. Cox, C. M. & Poole, T. J. Angioblast differentiation is influenced by the local environment: FGF-2 induces angioblasts and patterns vessel formation in the quail embryo. *Dev. Dyn.* 218, 371–382 (2000).

28. Harding, A. *et al.* Highly Efficient Differentiation of Endothelial Cells from Pluripotent Stem Cells Requires the MAPK and the PI3K Pathways. *Stem Cells* 35, 909–919 (2017).

29. Mullane, E. M. *et al.* Effects of VEGF and FGF2 on the Revascularization of Severed Human Dental Pulps. *J Dent Res* 87, 1144–1148 (2008).

30. Cross, M. J. & Claesson-Welsh, L. FGF and VEGF function in angiogenesis: signalling pathways, biological responses and therapeutic inhibition. *Trends Pharmacol Sci* 22, 201–207 (2001).

31. Chapouly, C., Guimbal, S., Hollier, P.-L. & Renault, M.-A. Role of Hedgehog Signaling in Vasculature Development, Differentiation, and Maintenance. *Int J Mol Sci* 20, 3076 (2019).

32. Fong, G.-H., Rossant, J., Gertsenstein, M. & Breitman, M. L. Role of the Flt-1 receptor tyrosine kinase in regulating the assembly of vascular endothelium. *Nature* 376, 66–70 (1995).

33. Rossant, J. & Howard, L. SIGNALING PATHWAYS IN VASCULAR DEVELOPMENT. *Annu Rev Cell Dev Bi* 18, 541–573 (2002).

34. Hofer, E. & Schweighofer, B. Signal transduction induced in endothelial cells by growth factor receptors involved in angiogenesis. *Thromb Haemostasis* 97, 355–363 (2007).

35. Goumans, M.-J., Liu, Z. & Dijke, P. ten. TGF-β signaling in vascular biology and dysfunction. *Cell Res* 19, 116–127 (2009).

36. Guerrero, P. A. & McCarty, J. H. *Physiologic and Pathologic Angiogenesis - Signaling Mechanisms and Targeted Therapy*. (IntechOpen, 2017). doi:10.5772/66405.

37. Brindle, N. P. J., Saharinen, P. & Alitalo, K. Signaling and Functions of Angiopoietin-1 in Vascular Protection. *Circ Res* 98, 1014–1023 (2006).

38. Karar, J. & Maity, A. PI3K/AKT/mTOR Pathway in Angiogenesis. *Front Mol Neurosci* 4, 51 (2011).

39. Rombouts, C., Giraud, T., Jeanneau, C. & About, I. Pulp Vascularization during Tooth Development, Regeneration, and Therapy. *J Dent Res* 96, 137–144 (2017).

40. Hashimoto, T. & Shibasaki, F. Hypoxia-Inducible Factor as an Angiogenic Master Switch. *Frontiers Pediatrics* 3, 33 (2015).

41. Chen, L., Endler, A. & Shibasaki, F. Hypoxia and angiogenesis: regulation of hypoxia-inducible factors via novel binding factors. *Exp Mol Medicine* 41, 849–857 (2009).

42. Kelly, B. D. *et al.* Cell Type–Specific Regulation of Angiogenic Growth Factor Gene Expression and Induction of Angiogenesis in Nonischemic Tissue by a Constitutively Active Form of Hypoxia-Inducible Factor 1. *Circulation Res J Am Hear Assoc* 93, 1074–1081 (2003).

43. Gerhardt, H. *et al.* VEGF guides angiogenic sprouting utilizing endothelial tip cell filopodia. *J Cell Biology* 161, 1163–1177 (2003).

44. Smet, F. D., Segura, I., Bock, K. D., Hohensinner, P. J. & Carmeliet, P. Mechanisms of Vessel Branching. *Arteriosclerosis Thrombosis Vasc Biology* 29, 639–649 (2009).

45. Shibuya, M. Vascular Endothelial Growth Factor (VEGF) and Its Receptor (VEGFR) Signaling in Angiogenesis. *Genes Cancer* 2, 1097–1105 (2011).

46. Siekmann, A. F. & Lawson, N. D. Notch Signalling and the Regulation of Angiogenesis. *Cell Adhes Migr* 1, 104–105 (2007).

47. Fassbender, J. M., Myers, S. A. & Whittemore, S. R. Activating Notch signaling post-SCI modulates angiogenesis in penumbral vascular beds but does not improve hindlimb locomotor recovery. *Exp Neurol.* 227, 302–313 (2012).

48. Avraamides, C. J., Garmy-Susini, B. & Varner, J. A. Integrins in angiogenesis and lymphangiogenesis. *Nat Rev Cancer* 8, 604–617 (2008).

49. Boudreau, N. J. & Varner, J. A. The Homeobox Transcription Factor Hox D3 Promotes Integrin α5β1 Expression and Function during Angiogenesis*. *J Biol Chem* 279, 4862–4868 (2004).

50. Abramsson, A., Lindblom, P. & Betsholtz, C. Endothelial and nonendothelial sources of PDGF-B regulate pericyte recruitment and influence vascular pattern formation in tumors. *J Clin Invest* 112, 1142–1151 (2003).

51. Jain, R. K. & Booth, M. F. What brings pericytes to tumor vessels? *J Clin Invest* 112, 1134–1136 (2003).

52. Koh, B. I. *et al.* VEGFR2 signaling drives meningeal vascular regeneration upon head injury. *Nat Commun* 11, 3866 (2020).

53. Teichert, M. *et al.* Pericyte-expressed Tie2 controls angiogenesis and vessel maturation. *Nat Commun* 8, 16106 (2017).

54. Peters, K. G. *et al.* Functional Significance of Tie2 Signaling in the Adult Vasculature. *Recent Prog Horm Res* 59, 51–71 (2004).

55. Suri, C. *et al.* Increased Vascularization in Mice Overexpressing Angiopoietin-1. *Science* 282, 468–471 (1998).

56. Nakajima, K. *et al.* Coexpression of Ang1 and Tie2 in Odontoblasts of Mouse Developing and Mature Teeth—A New Insight into Dentinogenesis. *Acta Histochem Cytoc* 47, 19–25 (2014).

57. Zhang, Y. *et al.* DPSCs treated by TGF-β1 regulate angiogenic sprouting of three-dimensionally co-cultured HUVECs and DPSCs through VEGF-Ang-Tie2 signaling. *Stem Cell Res Ther* 12, 281 (2021).

58. Li, C. *et al.* Overexpression of angiopoietin 2 promotes the formation of oral squamous cell carcinoma by increasing epithelial–mesenchymal transition-induced angiogenesis. *Cancer Gene Ther* 23, 295–302 (2016).

59. Kitajima, D. *et al.* Evidence for critical role of Tie2/Ang1 interaction in metastatic oral cancer. *Oncol Lett* 15, 7237–7242 (2018).

60. Suri, C. *et al.* Requisite Role of Angiopoietin-1, a Ligand for the TIE2 Receptor, during Embryonic Angiogenesis. *Cell* 87, 1171–1180 (1996).

61. Dumont, D. J. *et al.* Dominant-negative and targeted null mutations in the endothelial receptor tyrosine kinase, tek, reveal a critical role in vasculogenesis of the embryo. *Gene Dev* 8, 1897–1909 (1994).

62. Gale, N. W. *et al.* Angiopoietin-2 Is Required for Postnatal Angiogenesis and Lymphatic Patterning, and Only the Latter Role Is Rescued by Angiopoietin-1. *Dev Cell* 3, 411–423 (2002).

63. Hackett, S. F., Wiegand, S., Yancopoulos, G. & Campochiaro, P. A. Angiopoietin-2 plays an important role in retinal angiogenesis. *J. Cell. Physiol.* 192, 182–187 (2002).

64. Jones, N. *et al.* A Unique Autophosphorylation Site on Tie2/Tek Mediates Dok-R Phosphotyrosine Binding Domain Binding and Function. *Mol Cell Biol* 23, 2658–2668 (2003).

65. Kontos, C. D. *et al.* Tyrosine 1101 of Tie2 Is the Major Site of Association of p85 and Is Required for Activation of Phosphatidylinositol 3-Kinase and Akt Downloaded from. *Mol Cell Biol* 18, 4131–4140 (1998).

66. Jones, N. & Dumont, D. J. The Tek/Tie2 receptor signals through a novel Dok-related docking protein, Dok-R. *Oncogene* 17, 1097–1108 (1998).

67. Partanen, J. *et al.* A novel endothelial cell surface receptor tyrosine kinase with extracellular epidermal growth factor homology domains. *Mol Cell Biol* 12, 1698–1707 (1992).

68. Puri, M. C., Rossant, J., Alitalo, K., Bernstein, A. & Partanen, J. The receptor tyrosine kinase TIE is required for integrity and survival of vascular endothelial cells. *Embo J* 14, 5884–5891 (1995).

69. Souma, T. *et al.* Context-dependent functions of angiopoietin 2 are determined by the endothelial phosphatase VEPTP. *Proc National Acad Sci* 115, 1298–1303 (2018).

70. Carota, I. A. *et al.* Targeting VE-PTP phosphatase protects the kidney from diabetic injury. *J Exp Med* 216, 936–949 (2019).

71. Maisonpierre, P. C. *et al.* Angiopoietin-2, a Natural Antagonist for Tie2 That Disrupts in vivo Angiogenesis. *Science* 277, 55–60 (1997).

72. Yuan, H. T., Khankin, E. V., Karumanchi, S. A. & Parikh, S. M. Angiopoietin 2 Is a Partial Agonist/Antagonist of Tie2 Signaling in the Endothelium. *Mol Cell Biol* 29, 2011–2022 (2009).

73. Harfouche, R. & Hussain, S. N. A. Signaling and regulation of endothelial cell survival by angiopoietin-2. *Am J Physiol-heart C* 291, H1635–H1645 (2006).

74. Akwii, R. G., Sajib, M. S., Zahra, F. T. & Mikelis, C. M. Role of Angiopoietin-2 in Vascular Physiology and Pathophysiology. *Cells* 8, 471 (2019).

75. Yu, X. *et al.* Structural basis for angiopoietin-1–mediated signaling initiation. *Proc National Acad Sci* 110, 7205–7210 (2013).

76. Barton, W. A. *et al.* Crystal structures of the Tie2 receptor ectodomain and the angiopoietin-2–Tie2 complex. *Nat Struct Mol Biol* 13, 524–532 (2006).

77. Davis, S. *et al.* Isolation of Angiopoietin-1, a Ligand for the TIE2 Receptor, by Secretion-Trap Expression Cloning. *Cell* 87, 1161–1169 (1996).

78. Kim, K.-T. *et al.* Oligomerization and Multimerization Are Critical for Angiopoietin-1 to Bind and Phosphorylate Tie2*. *J Biol Chem* 280, 20126–20131 (2005).

79. Cho, C.-H. *et al.* COMP-Ang1: A designed angiopoietin-1 variant with nonleaky angiogenic activity. *Proc National Acad Sci* 101, 5547–5552 (2004).

80. Davis, S. *et al.* Angiopoietins have distinct modular domains essential for receptor binding, dimerization and superclustering. *Nat Struct Biol* 10, 38–44 (2003).

81. Kim, H.-Z., Jung, K., Kim, H. M., Cheng, Y. & Koh, G. Y. A designed angiopoietin-2 variant, pentameric COMP-Ang2, strongly activates Tie2 receptor and stimulates angiogenesis. *Biochimica Et Biophysica Acta Bba - Mol Cell Res* 1793, 772–780 (2009).

82. Cho, C.-H. *et al.* Long-Term and Sustained COMP-Ang1 Induces Long-Lasting Vascular Enlargement and Enhanced Blood Flow. *Circ Res* 97, 86–94 (2005).

83. Oh, N. *et al.* A Designed Angiopoietin-1 Variant, Dimeric CMP-Ang1 Activates Tie2 and Stimulates Angiogenesis and Vascular Stabilization in N-glycan Dependent Manner. *Sci Rep-uk* 5, 15291 (2015).

84. Han, S. *et al.* Amelioration of sepsis by TIE2 activation–induced vascular protection. *Sci Transl Med* 8, 335ra55 (2016).

85. Procopio, W. N., Pelavin, P. I., Lee, W. M. F. & Yeilding, N. M. Angiopoietin-1 and -2 Coiled Coil Domains Mediate Distinct Homo-oligomerization Patterns, but Fibrinogen-like Domains Mediate Ligand Activity*. *J Biol Chem* 274, 30196–30201 (1999).

86. Souma, T. *et al.* Angiopoietin receptor TEK mutations underlie primary congenital glaucoma with variable expressivity. *J Clin Invest* 126, 2575–2587 (2016).

87. Ono, S., Egawa, G. & Kabashima, K. Regulation of blood vascular permeability in the skin. *Inflamm Regen* 37, 11 (2017).

88. Gamble, J. R. *et al.* Angiopoietin-1 Is an Antipermeability and Anti-Inflammatory Agent In Vitro and Targets Cell Junctions. *Circ Res* 87, 603–607 (2000).

89. Fischer, S., Wiesnet, M., Renz, D. & Schaper, W. H2O2 induces paracellular permeability of porcine brain-derived microvascular endothelial cells by activation of the p44/42 MAP kinase pathway. *Eur J Cell Biol* 84, 687–697 (2005).

90. Lee, J. *et al.* Angiopoietin-1 Suppresses Choroidal Neovascularization and Vascular Leakage. *Investigative Opthalmology Vis Sci* 55, 2191 (2014).

91. Sun, J. *et al.* Vascular expression of angiopoietin1, α5β1 integrin and tight junction proteins is tightly regulated during vascular remodeling in the post-ischemic brain. *Neuroscience* 362, 248–256 (2017).

92. Li, L. *et al.* An angiogenic role for the α5β1 integrin in promoting endothelial cell proliferation during cerebral hypoxia. *Exp Neurol* 237, 46–54 (2012).

93. Gao, F. *et al.* Akt1 promotes stimuli-induced endothelial-barrier protection through FoxO-mediated tight-junction protein turnover. *Cell Mol Life Sci* 73, 3917–3933 (2016).

94. Yu, X. & Ye, F. Role of Angiopoietins in Development of Cancer and Neoplasia Associated with Viral Infection. *Cells* 9, 457 (2020).

95. Hu, B. *et al.* Angiopoietin-2 induces human glioma invasion through the activation of matrix metalloprotease-2. *Proc National Acad Sci* 100, 8904–8909 (2003).

96. Hu, B. *et al.* Angiopoietin 2 Induces Glioma Cell Invasion by Stimulating Matrix Metalloprotease 2 Expression through the αvβ1 Integrin and Focal Adhesion Kinase Signaling Pathway. *Cancer Res* 66, 775–783 (2006).

97. Etoh, T. *et al.* Angiopoietin-2 is related to tumor angiogenesis in gastric carcinoma: possible in vivo regulation via induction of proteases. *Cancer Res* 61, 2145–53 (2001).

98. Das, A. *et al.* Angiopoietin/Tek Interactions Regulate MMP-9 Expression and Retinal Neovascularization. *Lab Invest* 83, 1637–1645 (2003).

99. Pang, D. *et al.* Integrin α5β1-Ang1/Tie2 receptor cross-talk regulates brain endothelial cell responses following cerebral ischemia. *Exp Mol Medicine* 50, 1–12 (2018).

100. Cascone, I., Napione, L., Maniero, F., Serini, G. & Bussolino, F. Stable interaction between α5β1 integrin and Tie2 tyrosine kinase receptor regulates endothelial cell response to Ang-1. *J Cell Biology* 170, 993–1004 (2005).

101. Dalton, A. C., Shlamkovitch, T., Papo, N. & Barton, W. A. Constitutive Association of Tie1 and Tie2 with Endothelial Integrins is Functionally Modulated by Angiopoietin-1 and Fibronectin. *Plos One* 11, e0163732 (2016).

102. Silva, R., D'Amico, G., Hodivala-Dilke, K. M. & Reynolds, L. E. Integrins. *Arteriosclerosis Thrombosis Vasc Biology* 28, 1703–1713 (2008).

103. Mezu-Ndubuisi, O. J. & Maheshwari, A. The role of integrins in inflammation and angiogenesis. *Pediatr Res* 89, 1619–1626 (2021).

104. Drake, C. J., Cheresh, D. A. & Little, C. D. An antagonist of integrin alpha v beta 3 prevents maturation of blood vessels during embryonic neovascularization. *J Cell Sci* 108, 2655–2661 (1995).

105. Hammes, H.-P., Brownlee, M., Jonczyk, A., Sutter, A. & Preissner, K. T. Subcutaneous injection of a cyclic peptide antagonist of vitronectin receptor–type integrins inhibits retinal neovascularization. *Nat Med* 2, 529–533 (1996).

106. Brooks, P. C. *et al.* Antiintegrin alpha v beta 3 blocks human breast cancer growth and angiogenesis in human skin. *J Clin Invest* 96, 1815–1822 (1995).

107. Yang, J. T., Rayburn, H. & Hynes, R. O. Embryonic mesodermal defects in alpha 5 integrin-deficient mice. *Development* 119, 1093–1105 (1993).

108. Lampugnani, M. G., Resnati, M., Dejana, E. & Marchisio, P. C. The role of integrins in the maintenance of endothelial monolayer integrity. *J Cell Biology* 112, 479–490 (1991).

109. Yamamoto, H. *et al.* Integrin β1 controls VE-cadherin localization and blood vessel stability. *Nat Commun* 6, 6429 (2015).

110. Dallabrida, S. M. *et al.* Integrin binding angiopoietin-1 monomers reduce cardiac hypertrophy. *Faseb J* 22, 3010–3023 (2008).

111. Dallabrida, S. M., Ismail, N., Oberle, J. R., Himes, B. E. & Rupnick, M. A. Angiopoietin-1 Promotes Cardiac and Skeletal Myocyte Survival Through Integrins. *Circ Res* 96, e8–e24 (2005).

112. Mirando, A. C. *et al.* A collagen IV-derived peptide disrupts α5β1 integrin and potentiates Ang2-Tie2 signaling. *Jci Insight* 4, (2019).

113. Hakanpaa, L. *et al.* Endothelial destabilization by angiopoietin-2 via integrin β1 activation. *Nat Commun* 6, 5962 (2015).

114. Mirando, A. C. *et al.* Suppression of Ocular Vascular Inflammation through Peptide-Mediated Activation of Angiopoietin-Tie2 Signaling. *Int J Mol Sci* 21, 5142 (2020).

115. Shaddox, L. M. & Walker, C. B. Treating chronic periodontitis: current status, challenges, and future directions. *Clin Cosmet Investigational Dent* 2, 79–91 (2010).

116. Parenti, A., Paccosi, S., Cairo, F. & Defraia, E. Treatment of Periodontitis for the Prevention of Endothelial Dysfunction: A Narrative Review. *Curr Vasc Pharmacol* 13, 749–758 (2015).

117. Staszyk, C., Suske, A. & Pöschke, A. Dental and periodontal anatomy. *Equine Vet Educ* 27, 474–481 (2015).

118. Nagatomo, K. *et al.* Stem cell properties of human periodontal ligament cells. *J Periodontal Res* 41, 303–310 (2006).

119. McCulloch, C. A. G. & Bordin, S. Role of fibroblast subpopulations in periodontal physiology and pathology. *J Periodontal Res* 26, 144–154 (1991).

120. Nascimento, G. G., Leite, F. R. M., Vestergaard, P., Scheutz, F. & López, R. Does diabetes increase the risk of periodontitis? A systematic review and meta-regression analysis of longitudinal prospective studies. *Acta Diabetol* 55, 653–667 (2018).

121. CARNEVALE, G. & KALDAHL, W. B. Osseous resective surgery. *Periodontol 2000* 22, 59–87 (2000).

122. Feller, L. & Lemmer, J. Tooth mobility after periodontal surgery. *Sadj J South Afr Dent Assoc Tydskrif Van Die Suid-afrikaanse Tandheelkundige Vereniging* 59, 407, 409–11 (2004).

123. Clark, D. & Levin, L. Non-surgical management of tooth hypersensitivity. *Int Dent J* 66, 249–256 (2016).

124. Fujitani, T., Aoyama, N., Hirata, F. & Minabe, M. Association between periodontitis and vascular endothelial function using noninvasive medical device—A pilot study. *Clin Exp Dent Res* 6, 576–582 (2020).

125. Amar, S. *et al.* Periodontal Disease Is Associated With Brachial Artery Endothelial Dysfunction and Systemic Inflammation. *Arteriosclerosis Thrombosis Vasc Biology* 23, 1245–1249 (2003).

126. Gurav, A. N. The implication of periodontitis in vascular endothelial dysfunction. *Eur J Clin Invest* 44, 1000–1009 (2014).

127. Parikh, S. M. Dysregulation of the angiopoietin–Tie-2 axis in sepsis and ARDS. *Virulence* 4, 517–524 (2013).

128. Leligdowicz, A., Richard-Greenblatt, M., Wright, J., Crowley, V. M. & Kain, K. C. Endothelial Activation: The Ang/Tie Axis in Sepsis. *Front Immunol* 9, 838 (2018).

129. Milam, K. E. & Parikh, S. M. The angiopoietin-Tie2 signaling axis in the vascular leakage of systemic inflammation. *Tissue Barriers* 3, e957508 (2015).

130. Lim, S.-S., Kook, S.-H. & Lee, J.-C. COMP-Ang1 enhances DNA synthesis and cell cycle progression in human periodontal ligament cells via Tie2-mediated phosphorylation of PI3K/Akt and MAPKs. *Mol Cell Biochem* 416, 157–168 (2016).

131. Bhattarai, G. *et al.* COMP-Ang1 prevents periodontitic damages and enhances mandible bone growth in an experimental animal model. *Bone* 92, 168–179 (2016).

132. Bhattarai, G. *et al.* Functional improvement of collagen-based bioscaffold to enhance periodontal-defect healing via combination with dietary antioxidant and COMP-angiopoietin 1. *Biomaterials Adv* 135, 112673 (2022).

133. Beltrán-Aguilar, E. D. *et al. Surveillance for dental caries, dental sealants, tooth retention, edentulism, and enamel fluorosis--United States, 1988-1994 and 1999-2002.* 1–43 www.cdc.gov/oralhealth (1999).

134. Dye, B., Thornton-Evans, G., Li, X. & Iafolla, T. Dental caries and tooth loss in adults in the United States, 2011-2012. *Nchs Data Brief* 197 (2015).

135. Loesche, W. J. Role of Streptococcus mutans in human dental decay. *Microbiol Rev* 50, 353–380 (1986).

136. Hirose, Y. *et al.* Effects of Extracellular pH on Dental Pulp Cells In Vitro. *J Endodont* 42, 735–741 (2016).

137. Macrin, D. *et al.* Metabolism as an early predictor of DPSCs aging. *Sci Rep-uk* 9, 2195 (2019).

138. Park, S.-J. *et al.* Apoptosis of the reduced enamel epithelium and its implications for bone resorption during tooth eruption. *J Mol Histol* 44, 65–73 (2013).

139. Bäckman, B. & Holm, A. Amelogenesis imperfecta: prevalence and incidence in a northern Swedish county. *Community Dent Oral* 14, 43–47 (1986).

140. Witkop, C. J. Amelogenesis imperfecta, dentinogenesis imperfecta and dentin dysplasia revisited: problems in classification. *J Oral Pathol Med* 17, 547–553 (1988).

141. Smith, C. E. L. *et al.* Amelogenesis Imperfecta; Genes, Proteins, and Pathways. *Front Physiol* 8, 435 (2017).

142. Hu, L., Liu, Y. & Wang, S. Stem cell-based tooth and periodontal regeneration. *Oral Dis* 24, 696–705 (2018).

143. Smeets, R. *et al.* Definition, etiology, prevention and treatment of peri-implantitis – a review. *Head Face Med* 10, 34 (2014).

144. Griffith, L. G. & Swartz, M. A. Capturing complex 3D tissue physiology in vitro. *Nat Rev Mol Cell Bio* 7, 211–224 (2006).

145. Malda, J. *et al.* Oxygen gradients in tissue-engineered Pegt/Pbt cartilaginous constructs: Measurement and modeling. *Biotechnol. Bioeng.* 86, 9–18 (2004).

146. Ghantous, Y. & Elnaaj, I. A. [GLOBAL INCIDENCE AND RISK FACTORS OF ORAL CANCER]. *Harefuah* 156, 645–649 (2017).

147. Inchingolo, F. *et al.* Oral Cancer: A Historical Review. *Int J Environ Res Pu* 17, 3168 (2020).

148. Siegel, R. L., Miller, K. D. & Jemal, A. Cancer statistics, 2019. *Ca Cancer J Clin* 69, 7–34 (2019).

149. Kumar, M., Nanavati, R., Modi, T. & Dobariya, C. Oral cancer: Etiology and risk factors: A review. *J Canc Res Ther* 12, 458 (2016).

150. Valdez, J. A. & Brennan, M. T. Impact of Oral Cancer on Quality of Life. *Dent Clin N Am* 62, 143–154 (2018).

151. Liu, Y., Yang, M., Luo, J. & Zhou, H. Radiotherapy targeting cancer stem cells "awakens" them to induce tumour relapse and metastasis in oral cancer. *Int J Oral Sci* 12, 19 (2020).

152. Deshors, P. *et al.* Ionizing radiation induces endothelial transdifferentiation of glioblastoma stem-like cells through the Tie2 signaling pathway. *Cell Death Dis* 10, 816 (2019).

153. Xing, Y., Su, T. T. & Ruohola-Baker, H. Tie-mediated signal from apoptotic cells protects stem cells in Drosophila melanogaster. *Nat Commun* 6, 7058 (2015).

154. Lee, S. Y. *et al.* Induction of metastasis, cancer stem cell phenotype, and oncogenic metabolism in cancer cells by ionizing radiation. *Mol Cancer* 16, 10 (2017).

155. Lee, H. J. *et al.* Biological characterization of angiopoietin-3 and angiopoietin-4. *Faseb J* 18, 1200–1208 (2004).

156. Saharinen, P., Eklund, L. & Alitalo, K. Therapeutic targeting of the angiopoietin–TIE pathway. *Nat Rev Drug Discov* 16, 635–661 (2017).

157. Bilimoria, J. & Singh, H. The Angiopoietin ligands and Tie receptors: potential diagnostic biomarkers of vascular disease. *J Recept Sig Transd* 39, 187–193 (2019).

158. Moore, J. O., Lemmon, M. A. & Ferguson, K. M. Dimerization of Tie2 mediated by its membrane-proximal FNIII domains. *Proc National Acad Sci* 114, 4382–4387 (2017).

159. Khan, K. A., Wu, F. T., Cruz-Munoz, W. & Kerbel, R. S. Ang2 inhibitors and Tie2 activators: potential therapeutics in perioperative treatment of early stage cancer. *Embo Mol Med* 13, e08253 (2021).

160. Kim, M. *et al.* Opposing actions of angiopoietin-2 on Tie2 signaling and FOXO1 activation. *J Clin Invest* 126, 3511–3525 (2016).

161. Roberts, J., Hoog, L. de & Bix, G. J. Mice deficient in endothelial α5 integrin are profoundly resistant to experimental ischemic stroke. *J Cereb Blood Flow Metabolism* 37, 85–96 (2015).

162. Anderson, J. M., Li, J. & Springer, T. A. Regulation of integrin α5β1 conformational states and intrinsic affinities by metal ions and the ADMIDAS. *Mol Biol Cell* 33, ar56 (2022).

163. Hakanpaa, L. *et al.* Targeting β1-integrin inhibits vascular leakage in endotoxemia. *Proc National Acad Sci* 115, E6467–E6476 (2018).

164. Li, L., Liu, F., Welser-Alves, J. V., McCullough, L. D. & Milner, R. Upregulation of fibronectin and the α5β1 and αvβ3 integrins on blood vessels within the cerebral ischemic penumbra. *Exp Neurol* 233, 283–291 (2012).

165. Zakeri, B. *et al.* Peptide tag forming a rapid covalent bond to a protein, through engineering a bacterial adhesin. *Proc National Acad Sci* 109, E690–E697 (2012).

166. Boyken, S. E. *et al.* De novo design of protein homo-oligomers with modular hydrogen-bond network–mediated specificity. *Science* 352, 680–687 (2016).

167. Xu, C. *et al.* Computational design of transmembrane pores. *Nature* 585, 129–134 (2020).

168. Fallas, J. A. *et al.* Computational design of self-assembling cyclic protein homo-oligomers. *Nat Chem* 9, 353–360 (2017).

169. Bale, J. B. *et al.* Accurate design of megadalton-scale two-component icosahedral protein complexes. *Science* 353, 389–394 (2016).

170. Steenkiste, E. M., Berndt, J. D., Pilling, C., Simpkins, C. & Cooper, J. A. A Cas-BCAR3 co-regulatory circuit controls lamellipodia dynamics. *Elife* 10, e67078 (2021).

171. DeCicco-Skinner, K. L. *et al.* Endothelial Cell Tube Formation Assay for the In Vitro Study of Angiogenesis. *J Vis Exp* e51312 (2014) doi:10.3791/51312.

172. Liang, C.-C., Park, A. Y. & Guan, J.-L. In vitro scratch assay: a convenient and inexpensive method for analysis of cell migration in vitro. *Nat Protoc* 2, 329–333 (2007).

173. White, B. D. *et al.* β-Catenin Signaling Increases in Proliferating NG2+ Progenitors and Astrocytes during Post-Traumatic Gliogenesis in the Adult Brain. *Stem Cells* 28, 297–307 (2010).

174. Guo, Q. *et al.* Progesterone administration modulates AQP4 expression and edema after traumatic brain injury in male rats. *Exp Neurol* 198, 469–478 (2006).

175. Valable, S. *et al.* VEGF-Induced BBB Permeability is Associated with an MMP-9 Activity Increase in Cerebral ischemia: Both Effects Decreased by ANG-1. *J Cereb Blood Flow Metabolism* 25, 1491–1504 (2005).

176. Engler-Chiurazzi, E. B., Brown, C. M., Povroznik, J. M. & Simpkins, J. W. Estrogens as neuroprotectants: Estrogenic actions in the context of cognitive aging and brain injury. *Prog Neurobiol* 157, 188–211 (2017).

177. Beutel, O., Maraspini, R., Pombo-García, K., Martin-Lemaitre, C. & Honigmann, A. Phase Separation of Zonula Occludens Proteins Drives Formation of Tight Junctions. *Cell* 179, 923-936.e11 (2019).

178. Jo, G. *et al.* Structural insights into the clustering and activation of Tie2 receptor mediated by Tie2 agonistic antibody. *Nat Commun* 12, 6287 (2021).

179. Divine, R. *et al.* Designed proteins assemble antibodies into modular nanocages. *Science* 372, (2021).

180. Brunet, A. *et al.* Akt Promotes Cell Survival by Phosphorylating and Inhibiting a Forkhead Transcription Factor. *Cell* 96, 857–868 (1999).

181. Kim, I. *et al.* Angiopoietin-1 Regulates Endothelial Cell Survival Through the Phosphatidylinositol 3′-Kinase/Akt Signal Transduction Pathway. *Circ Res* 86, 24–29 (2000).

182. Daly, C. *et al.* Angiopoietin-1 modulates endothelial cell function and gene expression via the transcription factor FKHR (FOXO1). *Gene Dev* 18, 1060–1071 (2004).

183. Finn, T. E., Nunez, A. C., Sunde, M. & Easterbrook-Smith, S. B. Serum Albumin Prevents Protein Aggregation and Amyloid Formation and Retains Chaperone-like Activity in the Presence of Physiological Ligands. *J Biol Chem* 287, 21530–21540 (2012).

184. Mazurek, R. *et al.* Chapter Eight Vascular Cells in Blood Vessel Wall Development and Disease. in *Advances in Pharmacology* vol. 78 323–350 (Academic Press Inc., 2017).

185. Fukuhara, S. *et al.* Differential function of Tie2 at cell–cell contacts and cell–substratum contacts regulated by angiopoietin-1. *Nat Cell Biol* 10, 513–526 (2008).

186. Saharinen, P. *et al.* Angiopoietins assemble distinct Tie2 signalling complexes in endothelial cell–cell and cell–matrix contacts. *Nat Cell Biol* 10, 527–537 (2008).

187. Xue, G. & Hemmings, B. A. PKB/Akt–Dependent Regulation of Cell Motility. *Jnci J National Cancer Inst* 105, 393–404 (2013).

188. Koblizek, T. I., Weiss, C., Yancopoulos, G. D., Deutsch, U. & Risau, W. Angiopoietin-1 induces sprouting angiogenesis in vitro. *Curr Biol* 8, 529–532 (1998).

189. Kim, I. *et al.* Angiopoietin-1 Induces Endothelial Cell Sprouting Through the Activation of Focal Adhesion Kinase and Plasmin Secretion. *Circ Res* 86, 952–959 (2000).

190. Lee, J. *et al.* Angiopoietin-1 Guides Directional Angiogenesis Through Integrin αvβ5 Signaling for Recovery of Ischemic Retinopathy. *Sci Transl Med* 5, 203ra127 (2013).

191. Ge, X.-T. *et al.* miR-21 improves the neurological outcome after traumatic brain injury in rats. *Sci Rep-uk* 4, 6718 (2014).

192. Han, Z. *et al.* miR-21 alleviated apoptosis of cortical neurons through promoting PTEN-Akt signaling pathway in vitro after experimental traumatic brain injury. *Brain Res* 1582, 12–20 (2014).

193. Brickler, T. R. *et al.* Angiopoietin/Tie2 Axis Regulates the Age-at-Injury Cerebrovascular Response to Traumatic Brain Injury. *J Neurosci* 38, 9618–9634 (2018).

194. Liu, D. *et al.* Blood–brain barrier breakdown and repair by Src after thrombin-induced injury. *Ann Neurol.* 67, 526–533 (2010).

195. Allen, C. L. & Bayraktutan, U. Oxidative Stress and Its Role in the Pathogenesis of Ischaemic Stroke. *Int J Stroke* 4, 461–470 (2009).

196. Glushakova, O. Y., Johnson, D. & Hayes, R. L. Delayed Increases in Microvascular Pathology after Experimental Traumatic Brain Injury Are Associated with Prolonged Inflammation, Blood–Brain Barrier Disruption, and Progressive White Matter Damage. *J Neurotraum* 31, 1180–1193 (2014).

197. Wang, Y. *et al.* Rhein and rhubarb similarly protect the blood-brain barrier after experimental traumatic brain injury via gp91phox subunit of NADPH oxidase/ROS/ERK/MMP-9 signaling pathway. *Sci Rep-uk* 6, 37098 (2016).

198. Salehi, A., Zhang, J. H. & Obenaus, A. Response of the cerebral vasculature following traumatic brain injury. *J Cereb Blood Flow Metabolism* 37, 2320–2339 (2017).

199. Zhao, Y. T. *et al.* F-domain valency determines outcome of signaling through the angiopoietin pathway. *Embo Rep* 22, e53471 (2021).

200. Shen, L. & Turner, J. R. Actin Depolymerization Disrupts Tight Junctions via Caveolae-mediated Endocytosis. *Mol Biol Cell* 16, 3919–3936 (2005).

201. Bensaude, O. Inhibiting eukaryotic transcription. Which compound to choose? How to evaluate its activity? *Biochem Soc Symp* 2, 103–108 (2011).

202. Leppänen, V.-M., Saharinen, P. & Alitalo, K. Structural basis of Tie2 activation and Tie2/Tie1 heterodimerization. *Proc National Acad Sci* 114, 4376–4381 (2017).

203. Case, L. B., Pasquale, M. D., Henry, L. & Rosen, M. K. Synergistic phase separation of two pathways promotes integrin clustering and nascent adhesion formation. *Elife* 11, e72588 (2022).

204. Defilippi, P., Stefano, P. D. & Cabodi, S. p130Cas: a versatile scaffold in signaling networks. *Trends Cell Biol* 16, 257–263 (2006).

205. Meenderink, L. M. *et al.* P130Cas Src-Binding and Substrate Domains Have Distinct Roles in Sustaining Focal Adhesion Disassembly and Promoting Cell Migration. *Plos One* 5, e13412 (2010).

206. Wang, X. *et al.* De novo design of highly specific integrin alpha5beta1 protein binders. *In preparation*.

207. Takaishi, H. *et al.* Regulation of nuclear translocation of Forkhead transcription factor AFX by protein kinase B. *Proc National Acad Sci* 96, 11836–11841 (1999).

208. Hay, N. Interplay between FOXO, TOR, and Akt. *Biochimica Et Biophysica Acta Bba - Mol Cell Res* 1813, 1965–1970 (2011).

209. Jiang, S., Li, T., Yang, Z., Hu, W. & Yang, Y. Deciphering the roles of FOXO1 in human neoplasms. *Int. J. Cancer* 143, 1560–1568 (2018).

210. Kops, G. J. P. L. *et al.* Direct control of the Forkhead transcription factor AFX by protein kinase B. *Nature* 398, 630–634 (1999).

211. Papapetropoulos, A. *et al.* Angiopoietin-1 Inhibits Endothelial Cell Apoptosis via the Akt/Survivin Pathway*. *J Biol Chem* 275, 9102–9105 (2000).

212. Xu, Y. -x *et al.* Differential Expression and Function of Survivin During the Progress of Pterygium. *Invest Ophth Vis Sci* 55, 8480–8487 (2014).

213. Kim, S. H. *et al.* Forkhead box O1 (FOXO1) controls the migratory response of Toll-like receptor (TLR3)-stimulated human mesenchymal stromal cells. *J Biol Chem* 294, 8424–8437 (2019).

214. Kremer, K. N. *et al.* CXCR4 Chemokine Receptor Signaling Induces Apoptosis in Acute Myeloid Leukemia Cells via Regulation of the Bcl-2 Family Members Bcl-XL, Noxa, and Bak*. *J Biol Chem* 288, 22899–22914 (2013).

215. Pulous, F. E., Grimsley-Myers, C. M., Kansal, S., Kowalczyk, A. P. & Petrich, B. G. Talin-Dependent Integrin Activation Regulates VE-Cadherin Localization and Endothelial Cell Barrier Function. *Circ Res* 124, 891–903 (2019).

216. Silva, R. L. e *et al.* Tyrosine kinase blocking collagen IV–derived peptide suppresses ocular neovascularization and vascular leakage. *Sci Transl Med* 9, (2017).

217. Amruta, N. & Bix, G. ATN-161 Ameliorates Ischemia/Reperfusion-induced Oxidative Stress, Fibro-inflammation, Mitochondrial damage, and Apoptosis-mediated Tight Junction Disruption in bEnd.3 Cells. *Inflammation* 44, 2377–2394 (2021).

218. Su, Y. *et al.* Relating conformation to function in integrin α5β1. *Proc National Acad Sci* 113, E3872–E3881 (2016).

219. Ayloo, S. *et al.* Pericyte-to-endothelial cell signaling via vitronectin-integrin regulates blood-CNS barrier. *Neuron* 110, 1641-1655.e6 (2022).

220. Bachman, H., Nicosia, J., Dysart, M. & Barker, T. H. Utilizing Fibronectin Integrin-Binding Specificity to Control Cellular Responses. *Adv Wound Care* 4, 501–511 (2015).

221. Massia, S. P. & Hubbell, J. A. Vascular endothelial cell adhesion and spreading promoted by the peptide REDV of the IIICS region of plasma fibronectin is mediated by integrin alpha 4 beta 1. *J Biological Chem* 267, 14019–26 (1992).

Appendix Data

Appendix 1

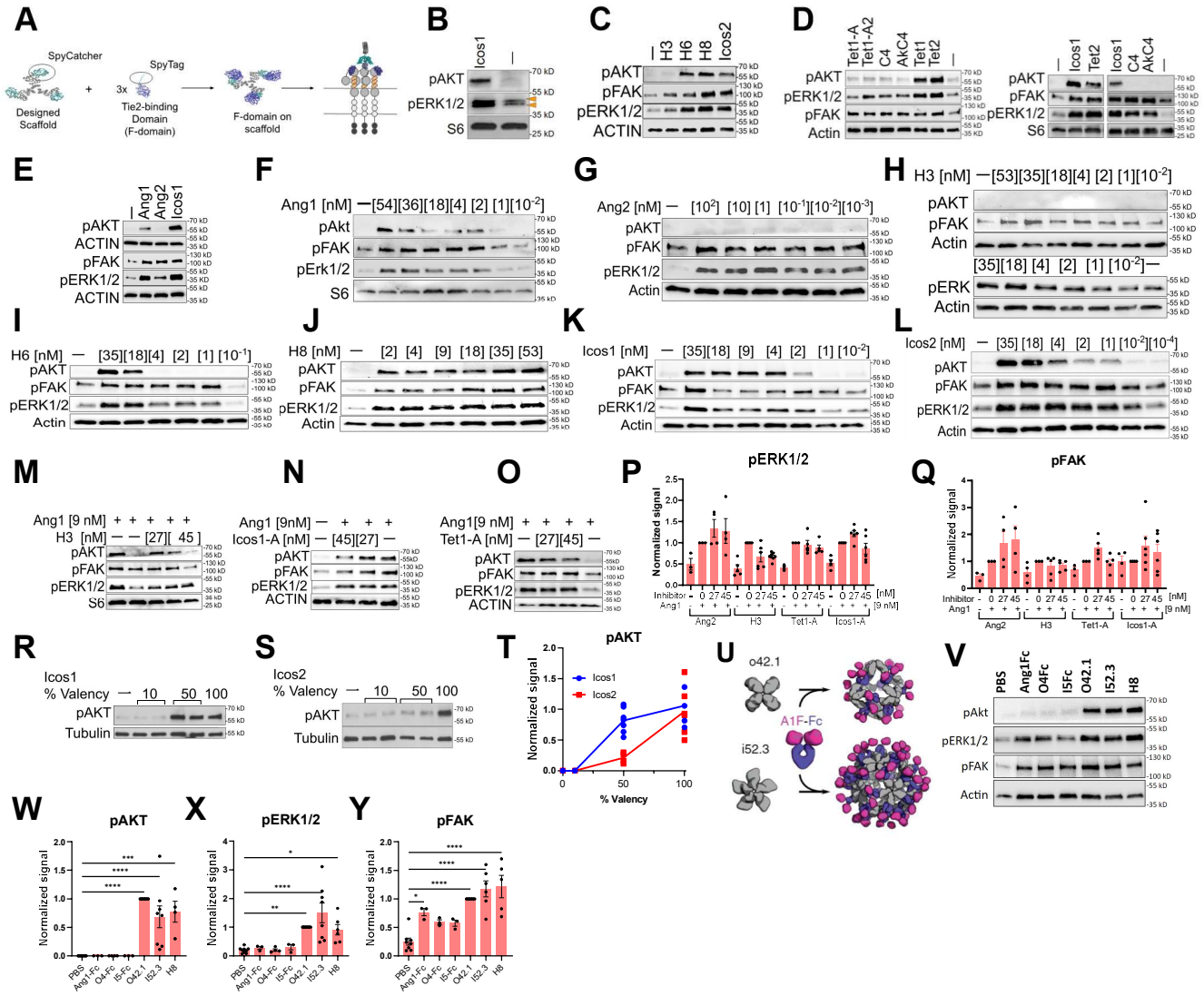

Appendix 1. The biochemical properties of designed F-domain scaffolds exhibit Ang1- or Ang2-like phenotype. A) Schematic of computationally designed protein conjugated to F-domains via SpyCatcher-SpyTag to allow Tie2 receptors binding at specific configuration and valency. **B)** Western blot showing two bands observed at expected molecular weights of pERK1/2. **C-E)** Representative immunoblots of angiopoietins and scaffolds at 18 nM F-domains showing phosphorylating Tie2 downstream targets: pAKT, pERK1/2, and pFAK. **F-L)** Representative immunoblots showing the dose-response of the Tie2 natural ligands (Ang1 and Ang2) and the designed proteins (H3, H6, H8, Icos1 and Icos2). **M-O)** Representative immunoblots of competition assay showing H3, Tet1-A, and Icos1A competition with Ang1. **P-Q)** Quantification of pFAK and pERK1/2 levels upon Ang1 stimulations with/without Ang2 or Ang2-like F-domain scaffolds. **R&S)** Immunoblots showing the phosphorylation level of AKT after treatment with 10%, 50%, 100% F-domain conjugated Icos1 and Icos2 nanocages, respectively. The pAKT level of Icos1 with 200% conjugation were also shown. Icos1-200% displays 120 copies of F-domains occupying the pentamer and trimer subunits. **T)** Quantitative representation of western blotting data illustrating the fold change of AKT phosphorylation normalized to Icos1 upon treatment with Icos1 or Icos2 at different valencies (n=3, except 10% valency of both Icos-cage in which n=2). Interestingly, Icos1 scaffolds at partial F-domain valency show pAKT activation at 50% valency presenting 30 copies of F-domains while 10% valency with 6 copies of F-domain does not. In contrast, Icos2 at 50% and 10% valency fails to activate pAKT illustrating geometry may play a role in pAKT activity. **U**) The F-domain from angiopoietin-1 was fused toFc (A1F-Fc) and assembled into octahedral (o42.1) and icosahedral (i52.3) AbCs.**V**) Representative Western blots show that A1F-Fc AbCs, but not controls, increase pAKT, pERK1/2, and pFAK signals. **W-Y**) Quantification of pAKT, pERK1/2, and pFAK quantifications are normalized to o42.1.

Appendix 2

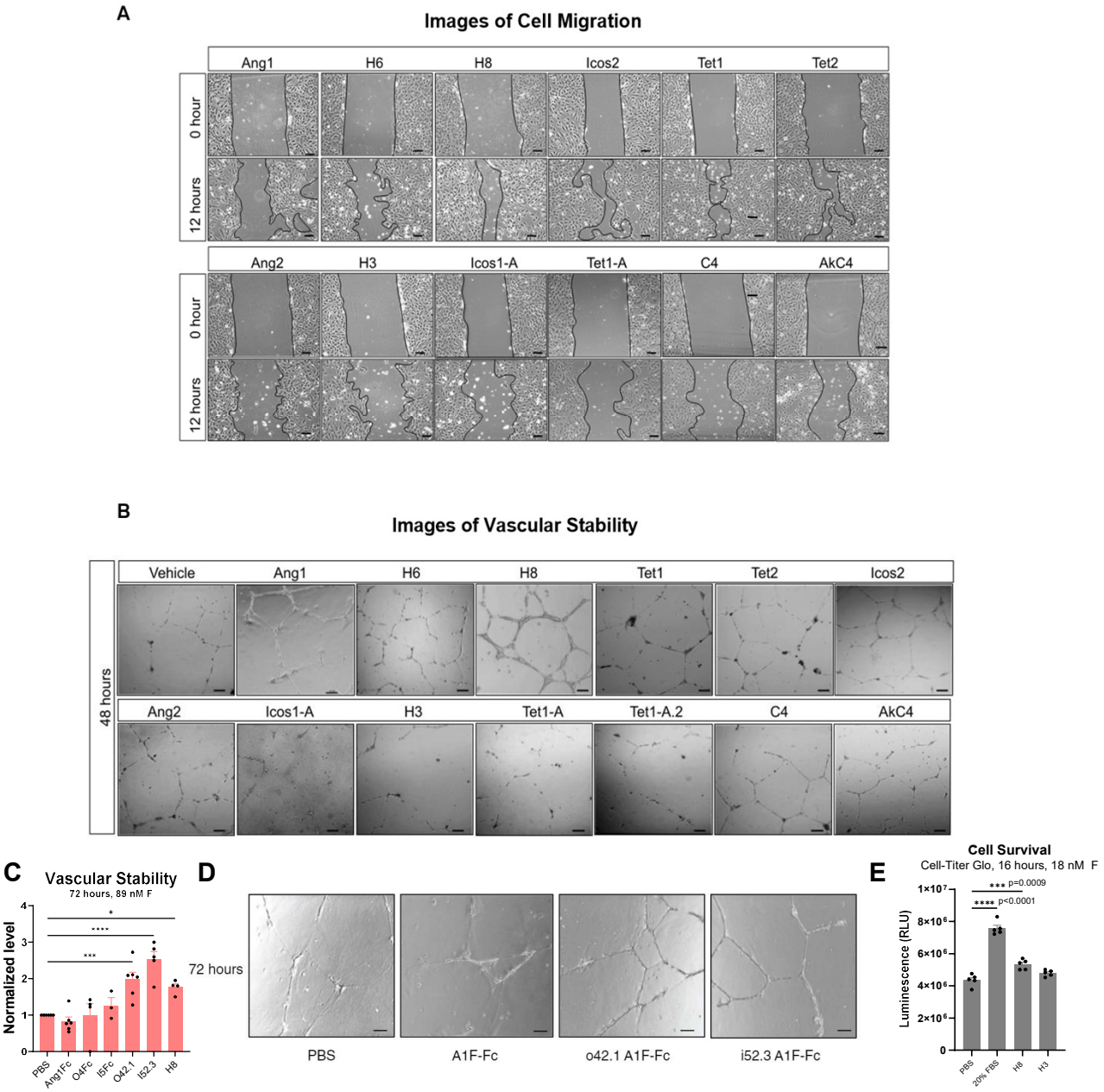

Appendix 2. High valency F-domain scaffolds enhance cell migration, vascular stability, and cell survival. A) Representative images showing *in vitro* cell migration in HUVECs after stimulation with natural ligands and designed F-domain constructs at 0- and 12-hour timepoints. **B)** Representative images demonstrating *in vitro* tube formation in HUVECs after stimulation with natural ligands or designed F-domain constructs at 48-hour timepoint. Scale bars are 100 μm. **C)** Quantification of vascular stability compared with PBS. (Right). **D**) Representative images of tubular structures after 72 hours, scale bars = 100mm. **E)** F-domain scaffolds (18 nM) were tested in 16-hour starvation cell viability assay used in previous publications (Harfouche & Hussain, 2006). Cell viability is analyzed by CellTiter-Glo and mean relative luminescence unit (RLU) ± SEM is plotted on the y-axis, n=5. Ordinary one-way ANOVA with Bonferroni's test is used to calculate the p-values. *P≤0.05; **P≤0.01; ***P≤0.001; ****P≤0.0001.

Appendix 3

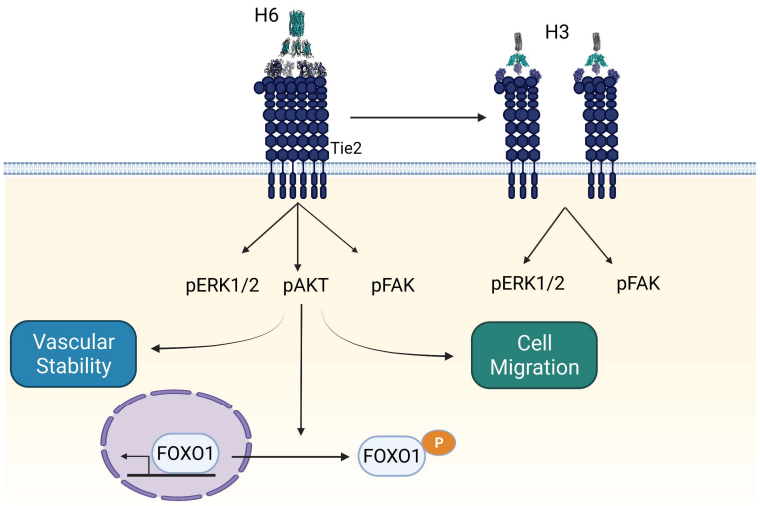

Appendix 3. Proposed molecular model illustrating the Ang/Tie2 signaling outcomes are determined by F-domain valency. Ligands that can create large clusters of Tie2 receptor can activate pAKT, pERK, pFAK, and FOXO1 nuclear exclusion. Ligands creating small clusters are not enough to activate pAKT but enough to activate pERK and pFAK. At high concentrations of low valency ligand, it can compete and break the large clusters into smaller clusters resulting in reduced pAKT level. Created with BioRender.com.

Appendix 4

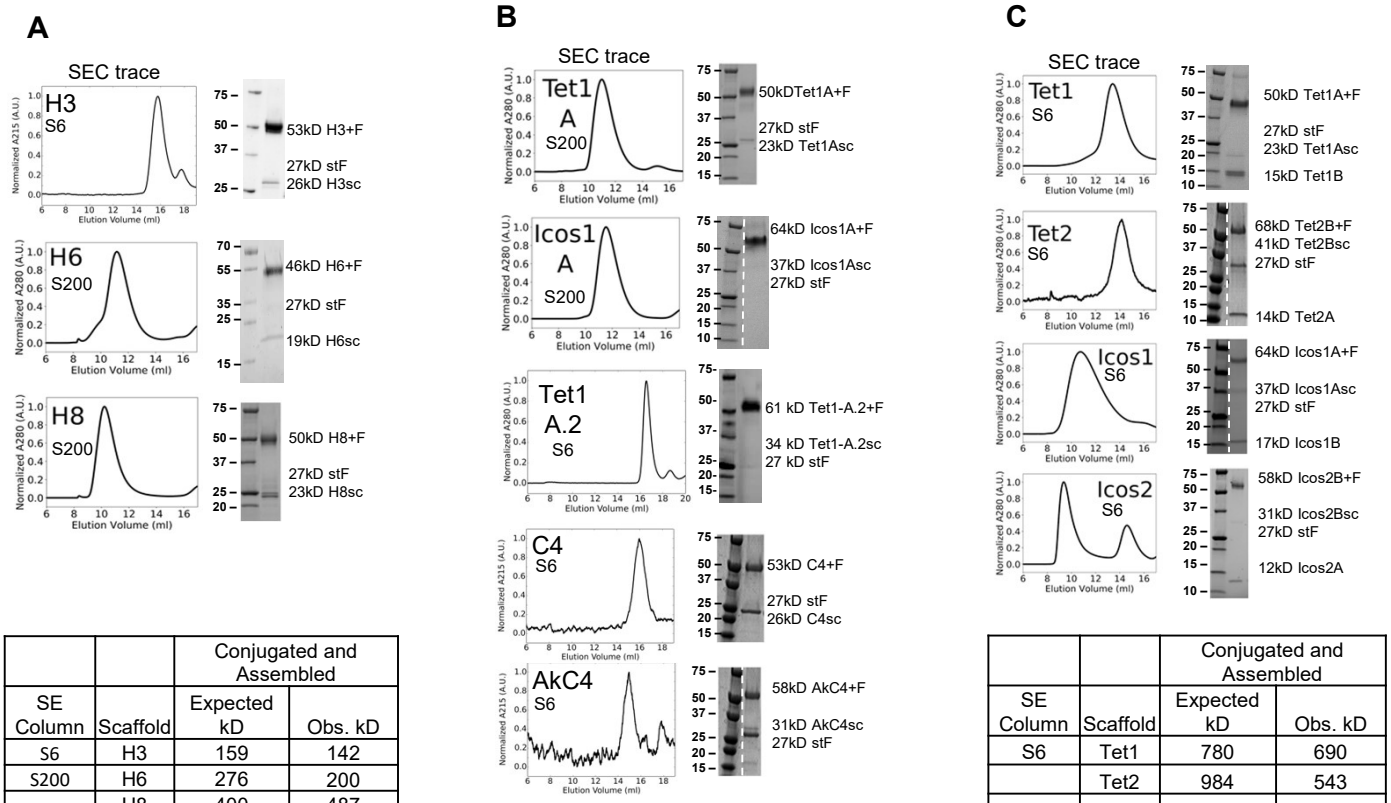

		Conjugated and Assembled	
SE Column	Scaffold	Expected kD	Obs. kD
S6	H3	159	142
S200	H6	276	200
	H8	400	487

		Conjugated and Assembled	
SE Column	Scaffold	Expected kD	Obs. kD
S200	Tet1A	162	190
	Icos1A	192	170
S6	Tet1A.2	183	172
	C4	212	278
	AkC4	232	350

	Conjugated and Assembled		
SE Column	Scaffold	Expected kD	Obs. kD
S6	Tet1	780	690
	Tet2	984	543
	Icos1	4860	1131
	Icos2	4200	1278

D

Scaffolds	X_sc (kD)	X_sc + stFd (kD)	Y (kD)
Icos1	37	64	17
Icos2	31	58	12
Tet1	24	51	15
Tet2	41	68	14
H8	23	50	-
H6	19	46	-
C4	26	53	-
AkC4	31	58	-
H3	26	53	-
Icos1A	37	64	-
Tet1A	27	54	-
Tet1A.2	34	61	-
F-domain_st	-	27	-

Appendix 4. F-domain scaffold verification. A) F-domain conjugation to helical scaffolds. **B)** F-domain conjugation to cyclic scaffolds. **C)** F-domains conjugation to 2-component nanocages. Left: size exclusion chromatography traces (predicted and observed sizes analyzed in S6 or S200 column are indicated), Right: analytical SDS-PAGE gels of subunits and conjugated product. F = F-domain, st = SpyTag, sc = SpyCatcher. Dashed line indicates the cut within the gel. The SEC-traces shown are on the conjugated samples before the last purification step; in each case the major peak at the target molecular weight was collected. **D)** Table of scaffold subunit molecular weights.

Appendix 5

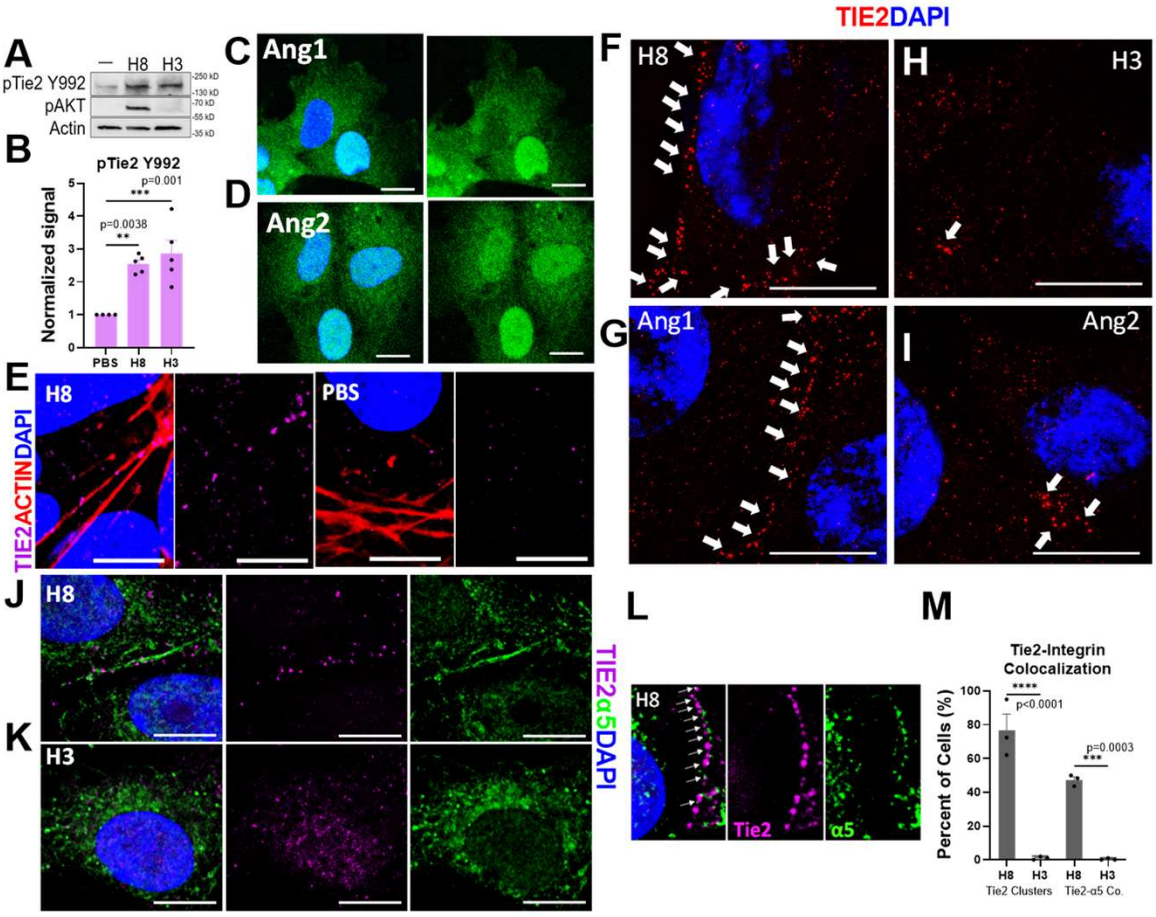

Appendix 5. H8 scaffold promotes super clustering of Tie2 receptors. Serum starved HUVECs were stimulated with H8 or H3 at 18 nM F-domains for 15 minutes before immunoblot staining for pTie2 (Y992) or 100 nM F-domain for 15 minutes before cell fixation for immunofluorescence staining to analyze Tie2 and/or α5 integrin. **A)** Representative gel of Tie2 phosphorylation at Y992 phosphorylation site. **B)** Quantification of Tie2 phosphorylation at Y992. **C-D)** Representative images of FOXO1 localization upon Ang1 or Ang2 treatment. **E)** H8 treatment or PBS control cells stained with TIE2 and ACTIN to visualize Tie2 clusters on the plasma membrane. **F-I)** Representative super resolution images of HUVECs stimulated with F-domain scaffolds or angiopoietins and stained for Tie2 cluster analysis. Representative images for colocalization of Tie2-α5 upon treatment with **I)** H8 or **J)** H3. **L)** High magnification of Tie2 clusters colocalization with integrin induces by H8. **M)** Quantification of Tie2-integrin colocalization. 100 cells were counted per sample. White scale bars are 10 µm.

Appendix 6

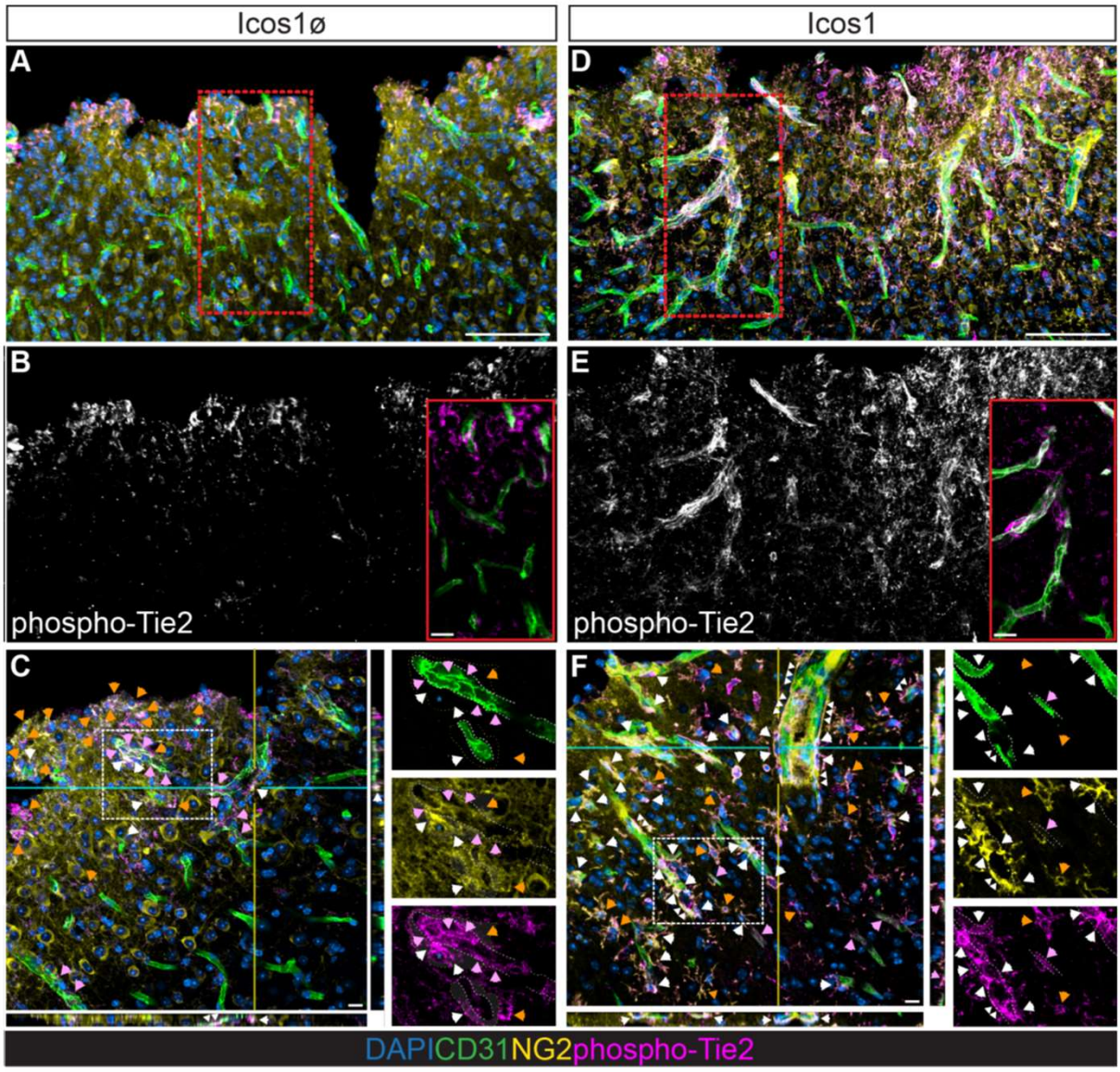

Appendix 6. Icosahedral F-domain scaffold stimulate neurovascular Tie2 activation after injury. Brain tissue from TBI-animals treated with control (Icos1ø. **A, C**) or super-agonist nanocages (Icos1. **D, F**) was stained with antibodies to visualize Tie2 receptor activation (anti-phosphoTie2: magenta), vasculature (anti-CD31: green), or neuroglia (anti-NG2: yellow) and counterstained with DAPI (nuclei, blue). Bar, 100 μm. **B**) Isolation of the phospho-Tie2 channel highlights a pattern of restricted receptor activation proximal to the TBI lesion-surface that is attenuated within deeper regions of the brain parenchyma. Isolated confocal images show Tie2 activation (magenta) proximal to CD31-vessels (green) at the lesion surface (inset from **A**, red box. Bar, 20 um) **C)** Adjacent tissue sections from Icos1ø-treated animals reveals limited Tie2 activation mostly on NG2-neuroglia (orange arrows) and along CD31-vessels (pink arrows). High resolution confocal images (insets; white box) reveal phospho-Tie2 colocalization in a pericyte (blue asterisks) within expanded perivascular space (yellow dotted-outline) along vasculature (white dotted-outline). Bar, 20 μm. **E)** In contrast, Icos1 nanocages enhanced Tie2 activation throughout the injury and reveals phospho-Tie2 activation (magenta) and along CD31-vessels (green) throughout the TBI lesion (inset from **D**, red box. Bar, 20 um). **F)** Icos1-treated tissue showed prevalent phospho-Tie2 colocalization on pericytes (white arrows) and along vasculature (pink arrows. bar, 20 μm). High resolution images (insets, white box), reveal elongated processes of NG2-pericytes with prominent phospho-Tie2 (white arrows) along CD31-vessels (white dotted-outline). Bar, 20 μm.

Appendix 7

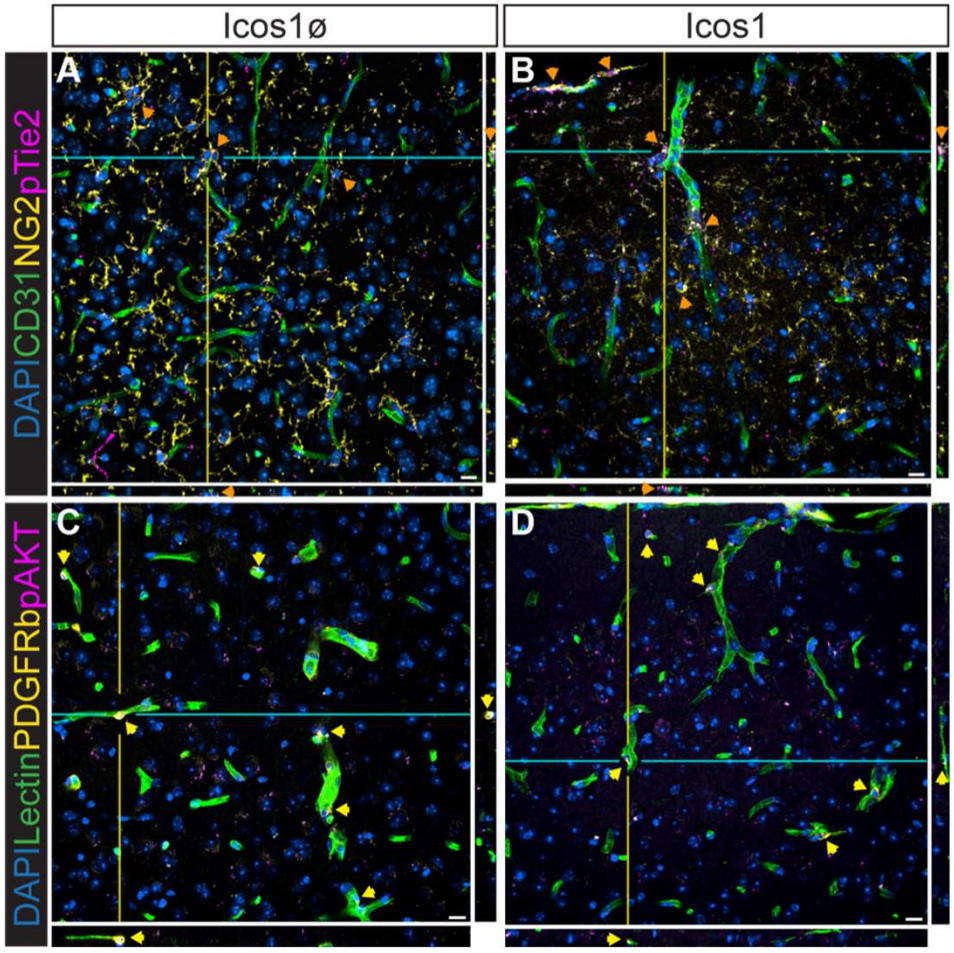

Appendix 7. No significant Icos1 dependent neurovascular Tie2/AKT activation is observed in the contralateral hemisphere of CCI-TBI mice. Brain tissue from injured animals treated with control (Icos1ø. **A** and **C**) or super-agonist nanocages (Icos1. **B** and **D**) and stained with antibodies to visualize Tie2 receptor and AKT in the contralateral hemisphere of injured mice. **A** and **B**. Confocal image of the dorsal cortex stained with antibodies to visualize Tie2 receptor activation (pTie2: magenta), vasculature (anti-CD31: green), pericytes and neuroglia (NG2: yellow). Orange arrow highlight NG2-expressing cells that colocalize with pTie2 stain. **C** and **D**. Adjacent tissue sections of contralateral hemispheres stained for activated AKT (pAKT: magenta), vasculature (lectin: green), pericytes (PDGFRb: yellow) and counterstained with DAPI (nuclei, blue). Yellow arrows highlight pericytes along CD31-vasculature. Bar, 20 μm.

Appendix 8

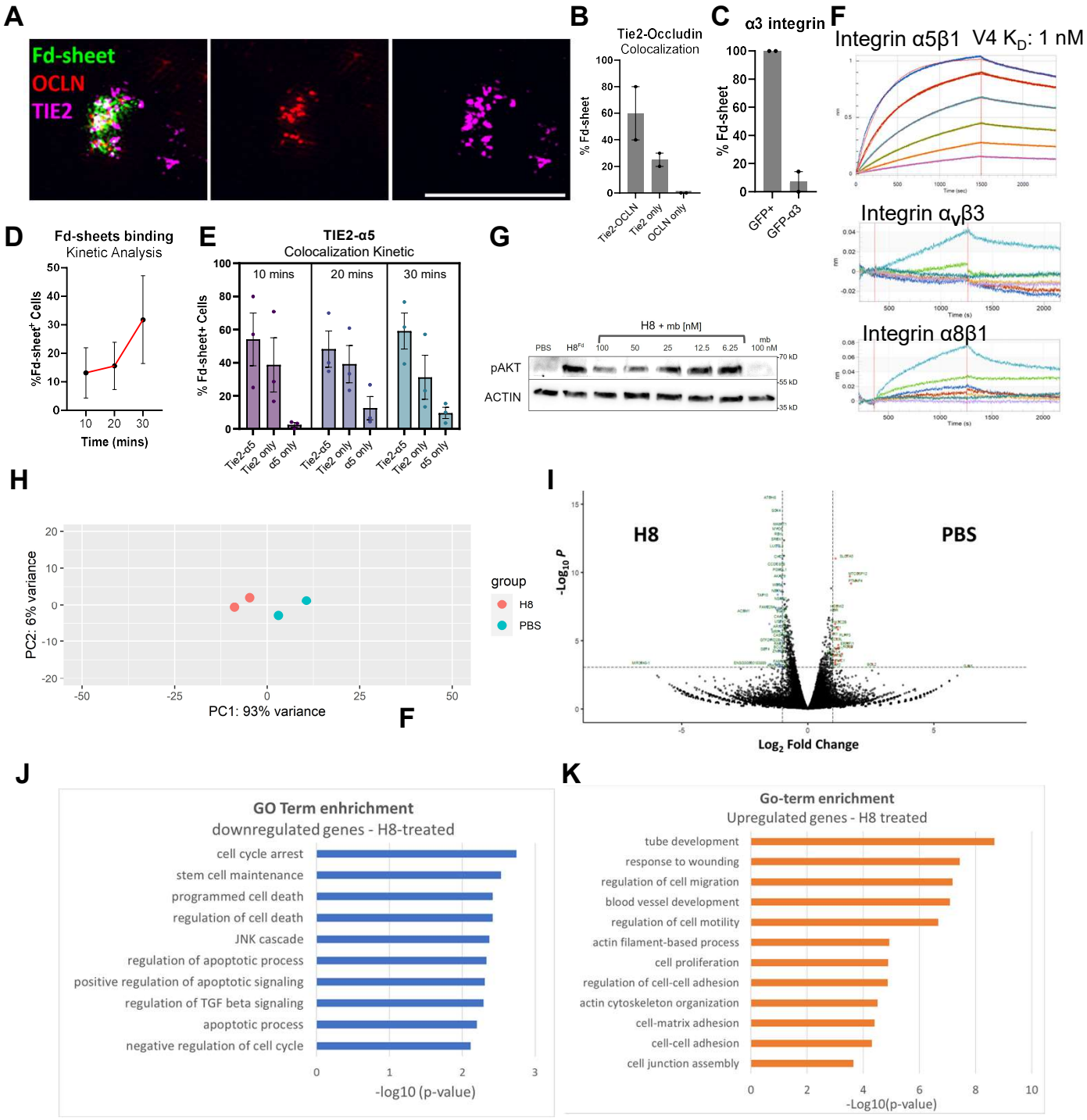

Appendix 8. Integrin-Tie2 complex regulate endothelial gene expression. A-B) Fd-sheets induced Tie2-OCLN colocalization, bar = 5μM **C)** Fd-sheets do not recruit α3 integrin. **D-E)** Kinetic analysis of Fd-sheet binding to HUVECs at 10, 20, and 30 min timepoint, more sheets bound over time. Formation of Tie2-α5β1 complexes happen at 10 mins. **F)** Bio-Layer Interferometry (BLI) measures the affinity of α5β1-mb (V4) binding to soluble biotinylated ectodomain of α5β1 (but not $\alpha_V\beta3$ and α8β1) immobilized on streptavidin-A optical tips. **G)** Western blot stain showing α5β1 mini binder (mb) did not activate pAKT but inhibited H8-dependent pAKT signal in dose-dependent manner. **H)** Principal component analysis of bulk RNA sequencing data of 6-hour serum starved HUVECs treated with H8 or PBS for 2 hours that demonstrated differential gene expression. **I)** Volcano plot shows the differentially expressed genes with p <0.05 significance cutoff. **J-K)** Go-term analysis of upregulated and downregulated genes in H8-treated samples. Lists of FOXO1 target genes in Appendix Table 2G.

Appendix Table 1

Protein sequences of designed proteins

Protein	Sequence
H3_sc	MGSSHHHHHHSSGLVPRGSHMSGAMVDTLSGLSSEQGQSGDMTIEEDSATHIKFSKRDEDGKELAGATMELRDSSGKTISTWISDGQVKDFYL YPGKYTFVETAAPDGYEVATAITFTVNEQGQVTVNGKATKGDAHILEGLNDIFEAQKIEWHEGSGSGTKYELRRALEELEKALRELKKSLDELERS LEELEKNPSEDALVENNRLNVENNKIIVEVLRIIAEVLKIIAKSD
Tet1-A_sc	MGEEAELAYLLGELAYKLGEYRIAIRAYRIALKRDPNNAEAWYNLGNAYYKQGDYDEAIEYYQKALELDPNNAEAWYNLGNAYYKQGDYDEAIEY YQKALELDPNNAEAKQNLGNAKQKQGSVDTLSGLSSEQGQSGDMTIEEDSATHIKFSKRDIDGKELAGATMELRDSSGKTISTWISDGQVKDFY LMPGKYTFVETAAPDGYEIATAITFTVNEQGQVTVNGKATKGDLEHHHHHH
Tet1-A.2_sc	MGEEAELXYLLGELAYKLGEYRIAIRAYRIALKRDPNNAEAWYNLGNAYYKQGDYDEAIEYYQKALELDPNNAEAWYNLGNAYYKQGDYDEAIEY YQKALELDPNNAEAWYNLGNAYYKQGDYDEAIEYYQKALELDPNNAEAKQNLGNAKQKQ GSVDTLSGLSSEQGQSGDMTIEEDSATHIKFSKRDIDGKELAGATMELRDSSGKTISTWISDGQVKDFYLMPGKYTFVETAAPDGYEIATAITFTV NEQGQVTVNGKATKGDLEHHHHHH
C4_sc	MGASSWVMLGLLLSLLNRLSLAAEAYKKAIELDPNDALAWLLLGSVLEKLKRLDEAAEAYKKAIELKPNDASAWKELGKVLEKLGRLDEAAEAYKK AIELDPEDAEAWKELGKVLEKLGRLDEAAEAYKKAIELDGNDGGSGGSDSATHIKFSKRDIDGKELAGATMELRDSSGKTISTWISDGQVKDFYL MPGKYTFVETAAPDGYEIATAITFTVNEQGQVTVNGKATKGLEHHHHHH
AkC4_sc	MGEEAELXYLLGELAYKLGEYRIAIRAYRIALKRDPNNAEAWYNLGNAYYKQGDYDEAIEYYQKALELDPNNAEAWYNLGNAYYKQGDYDEAIEY YQKALELDPNNAEAWYNLGNAYYKQGDYDEAIEYYQKALELDPNNAEAKQNLGNAKQKQ GSVDTLSGLSSEQGQSGDMTIEEDSATHIKFSKRDIDGKELAGATMELRDSSGKTISTWISDGQVKDFYLMPGKYTFVETAAPDGYEIATAITFTV NEQGQVTVNGKATKGDLEHHHHHH
H6_sc	MGDSATHIKFSKRDIDGKELAGATMELRDSSGKTISTWISDGQVKDFYLMPGKYTFVETAAPDGYEIATAITFTVNEQGQVTVNGKATKGGGSG GSTEDEIRKLRKLLEEAEKKLYKLEDKTRRSEEISKTDDDPKAQSLQLIAESLMLIAESLLIIAISLLLSSRNGLEHHHHHH
H8_sc	MGDSATHIKFSKRDIDGKELAGATMELRDSSGKTISTWISDGQVKDFYLMPGKYTFVETAAPDGYEIATAITFTVNEQGQVTVNGKATKGGGSG GSSAEELLRRSREYLKKVKEEQERKAKEFQELLKELSERSEELIRELEEKGAASEAELARMKQQHMTAYLEAQLTAWEIESKSKIALLELQQNQL NLELRHILEHHHHHH
Tet2 chain A	MGEEAELAYLLGELAYKLGEYRIAIRAYRIALKRDPNNAEAWYNLGNAYYKQGDYDEAIEYYQKALELDPNNAEAWYNLGNAYYKQGDYDEAIEY YEKALELDPENLEALQNLLNAMDKQG
Tet2_sc chain B	MIEEVVAEMIDILAESSKKSIEELARAADNKTTEKAVAEAIEEIARLATAAIQLIEALAKNLASEEFMARAISAIAELAKKAIEAIYRLADNHTTDTFMAR AIAAIANLAVTAILAIAALASNHTTEEFMARAISAIAELAKKAIEAIYRLADNHTTDKFMAAAIEAIALLATLAILAIALLASNHTTEKFMARAIMAIAILAAK AIEAIYRLADNHTSPTYIEKAIEAIEKIARKAIKAIEMLAKNITTEEYKEKAKKIIDIIRKLAKMAIKKLEDNRTGGSGGSDSATHIKFSKRDIDGKELAGA TMELRDSSGKTISTWISDGQVKDFYLMPGKYTFVETAAPDGYEIATAITFTVNEQGQVTVNGKATKGLEHHHHHH
Tet1_sc chain A	MGDSATHIKFSKRDIDGKELAGATMELRDSSGKTISTWISDGQVKDFYLMPGKYTFVETAAPDGYEIATAITFTVNEQGQVTVNGKATKGGGSG GSNLAEKMYKAGNAMYRKGQYTIAIIAYTLALLKDPNNAEAWYNLGNAAYKKGEYDEAIEAYQKALELDPNNAEAWYNLGNAYYKQGDYDEAIE YYKKALRLDPRNVDAIENLIEAEEKQG
Tet1 chain B	MGEEAELAYLLGELAYKLGEYRIAIRAYRIALKRDPNNAEAWYNLGNAYYKQGDYREAIRYYLRALKLDPENAEAWYNLGNALYKQGKYDLAIIAY QAALEEDPNNAEAKQNLGNAKQKQGLEHHHHHH
Icos1_sc chain A	MHHHHHHSGAMVDTLSGLSSEQGQSGDMTIEEDSATHIKFSKRDEDGKELAGATMELRDSSGKTISTWISDGQVKDFYLYPGKYTFVETAAPD GYEVATAITFTVNEQGQVTVNGKATKGDAHIGGSGGSGGKMEELFKKHKIVAVLRANSVEEAIEKAVAVFAGGVHLIEITFTVPDADTVIKALSVLK EKGAIIGAGTVTSVEQCRKAVESGAEFIVSPHLDEEISQFCKEKGVFYMPGVMTPTELVKAMKLGHDILKLFPGEVVGPQFVKAMKGPFPNVKFV PTGGVNLDNVCEWFKAGVLAVGVGDALVKGDPDEVREKAKKFVEKIRGCTEGSLEHHHHHH
Icos1 chain B	HMNQHSHKDHETVRIAVVRARWHAEIVDACVSAFEAAMETRDIGGDRFAVDVFDVPGAYEIPLHARTLAETGRYGAVLGTAFVVNGGIYRHEFV ASAVINGMMNVQLNTGVPVLSAVLTPHNYDKSKAHTLLFLALFAVKGMEAARACVEILAAREKIAA
Icos2 chain A	MPIFTLNTNIKADDVPSDFLSLTSRLVGLILSKPGSYVAVHINTDQQLSFGGSTNPAAFGTLMSIGGIEPDKNRDHSAVLFDHLNAMLGIPKNRMYI HFVNLNGDDVGWNGTTF
Icos2_sc chain B	MNQHSHKDHETVRIAVVRARWHADIVDACVEAFEIAMAAIGGDRFAVDVFDVPGAYEIPLHARTLAETGRYGAVLGTAFVVDGGIYDHEFVASAVI DGMMNVQLDTGVPVLSAVLTPHEYEDSDEDHEFFAAHFAVKGVEAARACIEILNAREKIAAGSGGSGGSGGAMVDTLSGLSSEQGQSGDMTIE EDSATHIKFSKRDEDGKELAGATMELRDSSGKTISTWISDGQVKDFYLYPGKYTFVETAAPDGYEVATAITFTVNEQGQVTVNGKATKGDAHISG HHHHHH
Hscn_ST_ Fdomain	METDTLLLWVLLLWVPGSTGHHHHHHGGSQDSTSDLIPAPPLSKVPLQQNFQDNQFQGKWYVVGLAGNAILREDKDPQKMYATIYELKEDKSY NVTSVLFRKKKCDYWIRTFVPGSQPGEFTLGNIKSYPGLTSYLVRVVSTNYNQHAMVFFKKVSQNREYFKITLYGRTKELTSELKENFIRFSKSLG LPENHIVFPVPIDQCIDGGGSENLYFQGSMAHIVMVDAYKPTKAELASEKPFRDCADVYQAGFNKSGIYTIYINNMPEPKKVFCNMDVNGGGWTV IQHREDGSLDFQRGWKEYKMGFGNPSGEYWLGNEFIFAITSQRQYMLRIELMDWEGNRAYSQYDRFHIGNEKQNYRLYLKGHTGTAGKQSSLI LHGADFSTKDADNDNCMCKCALMLTGGWWFDACGPSNLNGMFYTAGQNHGKLNGIKWHYFKGPSYSLRSTTMMIRPLDF

Appendix Table 1. Table of protein sequences used to generate synthetic Tie2 ligands. SpyCatcher sequence highlighted in green, the SpyTag in magenta, mammalian secretion tag in blue, TEV cleavage site in red and metal affinity chromatography purification tag in yellow.

Appendix Table 2

A. pAKT		*p-value*
Ang1 vs Ang2	****	<0.0001
H3 vs H6	****	<0.0001
H3 vs H8	****	<0.0001
Tet1-A vs. Tet1	****	<0.0001
Tet1-A vs. Tet2	****	<0.0001
Icos1-A vs. Icos1	****	<0.0001
Icos1-A vs. Icos2	****	<0.0001

B. pERK1/2		*p-value*
Ang2 vs. Ang1	ns	>0.9999
H3 vs. H6	**	0.006
H3 vs. H8	**	0.0042
Tet1-A vs. Tet1	ns	0.1554
Tet1-A vs. Tet2	***	0.0009
Icos1-A vs. Icos2	****	<0.0001
Icos1-A vs. Icos1	****	<0.0001

C. pFAK		*p-value*
Vehicle vs. Ang1	ns	0.0869
Vehicle vs. Ang2	ns	0.1801
Vehicle vs. H3	**	0.007
Vehicle vs. H6	***	0.0003
Vehicle vs. H8	**	0.0017
Vehicle vs. Tet1-A	***	0.0006
Vehicle vs. Tet1-A.2	*	0.0397
Vehicle vs. C4	**	0.009
Vehicle vs. AkC4	ns	0.4504
Vehicle vs. Tet1	**	0.0087
Vehicle vs. Tet2	**	0.0018
Icos1-A vs. Icos2	****	<0.0001
Icos1-A vs. Icos1	****	<0.0001

D. Cell migration		*p-value*
Vehicle vs. Ang1	****	<0.0001
Vehicle vs. Tet2	****	<0.0001
Vehicle vs. H6	****	<0.0001
Vehicle vs. H8	****	<0.0001
Vehicle vs. Tet1	****	<0.0001
Vehicle vs. Icos1	****	<0.0001
Vehicle vs. Icos2	****	<0.0001
Ang1 vs. Icos1	**	0.006
Ang1 vs. Tet2	ns	0.5526
Ang1 vs. H6	ns	0.1083
Ang1 vs. H8	*	0.0303
Ang1 vs. Tet1	ns	>0.9999
Ang1 vs. Icos2	ns	0.6673

E. Vascular stability, 48 hours		*p-value*
Ang1 vs. H6	****	<0.0001
Ang1 vs. H8	****	<0.0001
Ang1 vs. Tet1	ns	0.3783
Ang1 vs. Tet2	****	<0.0001
Ang1 vs. Icos2	**	0.0025
Ang1 vs. Icos1	****	<0.0001

F. Vascular stability, 72 hours		*p-value*
Ang1 vs. H6	****	<0.0001
Ang1 vs. H8	ns	0.1151
Ang1 vs. Tet1	ns	0.8248
Ang1 vs. Tet2	ns	0.0862
Ang1 vs. Icos2	**	0.0056
Ang1 vs. Icos1	****	<0.0001

H8-treated HUVECs : FOXO targets	
Downregulated	Upregulated
UBXN1,PHF20,PRKCSH,CHD7,GIMAP1,CHD6,ZBTB20,HSPB1,RSF1,RBPJ,CHD2,GIMAP7,BBC3,STK11,RPS19,GUK1,RB1CC1,BBX,TMSB10,SOX4,PLEKHJ1,TPRN,UPF2,EIF5B,GPX4,ARID5A,UBALD2,PGM2L1,FOXP1,SRRM1,CCDC80,KAT6B,S100A6,MALAT1,PHIP,KMT2E,WBP4,ARL2,PBXIP1,CAPG,BAZ2B,HSPBP1,BCL2L11,PALMD,CALD1,CCDC85B,ATOH8,AP2S1,PACSIN3,SNRPB2,GTF2IRD2B,SKIL,JUND,GADD45B,POLR3GL,MIB2,ARID3A,FOXN3,FBXO32,MRPL23,GFER,ATP5F1D,RNF145,NFIA,PSMC3,NFIB,NFIC,RAB13,EIF3J,ID3,TACC1,FAU,MXD4	ERRFI1,SERPINE1,ETS2,ELK3,PIK3C2B,FAM107B,PPP1R9B,RGS2,TUBA1B,TGM2,MAP2K3,DUSP4,KLF10,SH2D3C,SOX13,EMP1,TGFBR2,DUSP7,NCOR2,NAF1,KCTD12,TRIB1,PLPP3,SGK1,TRIB2,UTP25,NID1,CXXC5,RNF4,HIF1A,NID2,ZFP36L2,RAP1B,LIMA1,MAT2A,S1PR1,JUN,PHC1,FN1,MICAL2,FLI1,PRRC2B,APLN,PTPRB,MYO1B,BHLHE40,BCL2,ATP13A3,MAMLD1,FGFR1

Appendix Table 2. Table of p-values. Statistical analysis performed and respective p-values for **A-C)** signaling assays in Figure 2, **D)** cell migration assay, and vascular stability at **E)** 48-and **F)** 72-hour timepoints in Figure 3. Ordinary one-way ANOVA with Bonferroni test is used to calculate the p-values. **G)** Lists of FOXO1 target genes that were significantly (p-value < 0.05) up- or downregulated in H8-treated cells compared to PBS control, ChEA3 analysis.

Curriculum Vitae

Yan Ting (Blair) Zhao
E-mail: ytz@uw.edu
Phone: 206-446-9034
curriculum vitae

RESEARCH INTEREST

Merging the principles of stem cell biology and differentiation to promote vascularized tissue/organoid regeneration to combat a wide range of vascular-related diseases and cancers.

EDUCATION

Doctor of Philosophy in Oral Health Sciences Sept 2017 - Dec. 2022
(Formally known as Oral Biology), University Of Washington, Seattle, WA

NIH NIDCR T90 Fellow, 2020-2022
Magnuson, Warren G. Scholar, 2020-2021
NIH NCATS ITHS TL-1 Fellow, 2019-2020

Bachelor of Science in Biochemistry Sept. 2011 -March 2016
Minor degree in Chemistry
University Of Washington, Seattle, WA
GPA of 3.5
Annual Dean's List, 2011-2012
McNair Scholar, 2014-2016

Certification in Programming for Data Science with Python Jan. 2021 - April 2021
Udacity Online

RESEARCH FUNDING

1. **T90 training grant, School of Dentistry, University of Washington**
   National Institute of Health, NIDCR T90DE021984
2. **TL1 training grant, Institute of Translational Health Sciences at University of Washington**
   National Institute of Health, NCATS TL1 TR002318
3. **Pilot Research Grant**
   Dr. Douglass L. Morell Dentistry Research Fund, School of Dentistry, University of Washington, Seattle WA
4. **McNair Undergraduate Research Funding Award, 2015**
   Ronald E. McNair Achievement Program, University of Washington, Seattle WA

AWARDS & HONORS

1. **Schultz Travel Fellowship 2022,** awarded, Biochemistry department, University of Washington, Seattle, WA
2. **ISCRM annual symposium best poster award 2021-** 3rd place awarded Institute for Stem Cells and Regenerative Medicine, University of Washington, Seattle, WA
3. **Magnuson G. Warren Scholarship 2020-2021 -** awarded, School of Dentistry, University of Washington, Seattle ,WA
4. **Burroughs Wellcome Fund Travel Award 2020** for Translational Science meeting
   Awarded 2020 but canceled due to Covid-19 travel restriction, Association for Clinical and Translational Sciences, Washington DC
5. **ITHS Travel Award** for 2020 Translational Science meeting
   Awarded 2019 but canceled due to Covid-19 travel restriction, Institute for Translational Health Sciences, University of Washington, Seattle, WA
6. **3rd China-ASEAN Excellent Young Dental Student Forum Excellence Award for Oral Presentation**
   Awarded 2018, School of Stomatology Nanning University, Nanning China
7. **ISCRM Travel Award** for 2018 ISSCR Annual Meeting,
   Awarded 2018, Institute for Stem Cells and Regenerative Medicine, University of Washington, Seattle, WA
8. **Biochemistry Undergraduate Award for Research Excellence**

Awarded 2016, University of Washington, Seattle, WA

9. **Dolores Liebmann Fellowship**
   Nominated 2017, UW Graduate School, University of Washington, Seattle, WA
10. **Ronald E. McNair Scholarship**
    Awarded 2014-2016, Ronald E. McNair Achievement Program, University of Washington, Seattle WA

RESEARCH EXPERIENCES

Ruohola-Baker Lab, Seattle WA —Graduate *Research Assistant* August 2015 - Present

1. Thesis Project: Decoding Tie2 signaling using AI-based design protein scaffolds to mitigate vascular diseases. The Tie2 pathway regulates vascular permeability, stability, and remodeling. The binding of Ang1 to Tie2 promotes vascular stability, while Ang2 induces leaky blood vessels despite having almost identical receptor-binding domains (F-domain). The goal is to design Tie2 agonists and antagonists to dissect the molecular requirements for Tie2 signaling and vascular outcomes to promote stable and functional vasculatures. A combination of AI-based AlphaFold and RossettaFold were used to design self-assembling protein scaffolds with high geometric symmetry for conjugating with Ang1 F-domain at varying valency and configuration (F-domain scaffolds). This approach will enable the correlation of ligand valency with the number of Tie2 receptors needed to produce the Ang1 vs. Ang2 phenotype. Quantitative immunoblotting, tube formation, survival assay, and wound healing assay were utilized to examine signaling and function outcomes upon F-domain scaffolds administration. Characterized Tie2 superagonist was used in the mouse traumatic brain injury model. Two-dimensional protein sheets conjugated with F-domain or *de no* designed Tie2 or integrin mini binders were utilized to probe the molecular events downstream of Tie2 activation leading to vascular stability using super-resolution microscopy.

2. Utilizing *de novo* designed high-affinity mini binder proteins to neutralize SARS-COV2 virus infection in kidney organoids or cardiomyocytes. Investigated the efficacy of *de novo* designed mini protein binders (monomeric LCB and multi-valent binders) against spike protein of SARS-COV2 virus as a therapy for COVID-19. Viruses were pre-incubated with mini binders before infecting kidney organoids or cardiomyocytes. RNA was extracted from infected samples with trizol for RT-qPCR to measure the level of viral infection.

3. Investigating ameloblast differentiation from induced pluripotent stem cells - Investigated a differentiation protocol to drive induced pluripotent stem cells (iPSCs) into human ameloblasts and regenerate enamel in vitro. iPSCs will be directed into the oral lineage using a stepwise activation of different pathways via growth factors to gradually push iPSC into ameloblast based on single cell RNAseq analysis of previously collected developing human oral tissues.

4. Characterizing dental pulp stem cells and the role of Barx1 DPSCs regulation - Characterized the regenerative capacity and metabolism of dental pulp stem cells. Isolated dental pulp from primary teeth and adult teeth to harvest stem cells. Odontogenic and adipogenic differentiation using DPSCs to analyze its differentiation capacity. RNA sequencing of DPSCs vs. MSCs was done to identify the molecular marker of DPSCs. RNA sequencing demonstrated that Barx1 is a marker for DPSCs. Investigated the role of Barx1 in DPSCs by creating a Barx1 knockout cell line using CRISPR/cas9. Performed Barx1 expression correlated with slow-aging cells. Seahorse cell metabolic analysis on multiple DPSC lines to analyze the glycolytic capacity of rapid vs. slow aging cell lines. Extracted and purified RNA, DNA, and protein from dental pulp stem cells for RT-qPCR and western blot analyses

Kaeberlein Lab, Seattle WA — *Undergraduate and post-baccalaureate Research Assistant* May 2015 - Jan 2017

1. Drug screen to find natural compounds that mimic rapamycin for mTOR inhibition - (Post-Bac Research) Investigated on finding natural supplement compounds that mimic the effect of rapamycin, which was shown to extend yeast lifespan. Aimed to understand the validity of the health benefits of common supplement drugs. Used a Bioscreen Analyzer to measure the optical density of the yeast culture in suspension to investigate the growth rate under different supplement drug treatments. This study was published in GeroScience.

2. Investigation of exceptionally long-lived single mutant yeasts - (Post-Bac Research) Aimed to search for yeast strains that lived for more than 75 divisions to target genes and metabolic pathways responsible for yeast longevity. Used R programming to analyze a massive database of past experiments to extract outstanding genes that promoted a long lifespan in yeast. Created survival curves to analyze the candidate gene

3. Yeast Replicative lifespan project - (Undergraduate Research) Used yeast cells with different genotypes to perform large-scale screens to understand how different genetic, environmental, and metabolic factors affect yeast aging. Dissected and recorded yeast cells to collect replicative lifespan data that has been genetically modified or under different drug treatments.

Swedish Neuroscience Institute, Seattle WA June 2011 - May 2014

1. Finding Correlations between MRI FA and MD data with Cognitive tests scores of Multiple Sclerosis patients - (Undergraduate Research) Investigated the correlation between MRI data (Fractional Anisotropy and Mean Diffusivity values of Multiple Sclerosis (MS) patients) with MS patients' cognitive test scores. Performed advanced statistical analysis such as t-test, multiple regression, and linear regression on collected data. Aimed to develop a standardized model to diagnose Multiple Sclerosis at an early stage before it progresses into an abject state of disease.

PUBLICATIONS

---

1. Wang, X., Guillem, J., **Zhao, Y. T.**, Kumar, S., Lee, D., Li, J., Hao, Y., Springer, T., Campell, M., Cooper, J., Ruohola-Baker, H. & Baker, D. De novo design of highly specific integrin alpha5beta1 protein binders. In preparation

2. **Zhao, Y. T.**, Devon, E., Xinru, W., Saurav, K., Patrisia, L., Cameron, H., Ashish, P., Jonathan, C., Julie, M., David, B. & Ruohola-Baker, H. Multivalent computationally derived Tie2 agonists ameliorate diabetic vascular instability through two distinct classes of Tie2 complexes. In preparation

3. Alghadeer, A., Hanson-Drury, S., Ehnes, D., **Zhao, Y.T.**, Patni, A., O'Day, D., Spurrell, C., Gogate, A., Phal, A., Zhang, H., Devi, A., Wang, Y., Starita, L., Doherty, D., Glass, I., Shendure, J., Baker, D., Regier, M., Mathieu, J. & Ruohola-Baker, H. Human iPSC Derived Enamel Organoid Guided by Single-Cell Atlas of Human Tooth Development. Biorxiv 2022.08.09.503399 (2022). doi:10.1101/2022.08.09.503399

4. Ehnes, D. D., Alghadeer, A., Hanson-Drury, S., **Zhao, Y. T.**, Tilmes, G., Mathieu, J. & Ruohola-Baker, H. Sci-Seq of Human Fetal Salivary Tissue Introduces Human Transcriptional Paradigms and a Novel Cell Population. Frontiers Dent Medicine 3, 887057 (2022).

5. Hunt, A. C., Case, J. B., Park, Y.-J., Cao, L., Wu, K., Walls, A. C., Liu, Z., Bowen, J. E., Yeh, H.-W., Saini, S., Helms, L., **Zhao, Y. T.**, Hsiang, T.-Y., Starr, T. N., Goreshnik, I., Kozodoy, L., Carter, L., Ravichandran, R., Green, L. B., Matochko, W. L., Thomson, C. A., Vögeli, B., Krüger, A., VanBlargan, L. A., Chen, R. E., Ying, B., Bailey, A. L., Kafai, N. M., Boyken, S. E., Ljubetič, A., Edman, N., Ueda, G., Chow, C. M., Johnson, M., Addetia, A., Navarro, M. J., Panpradist, N., GaleJr., M., Freedman, B. S., Bloom, J. D., Ruohola-Baker, H., Whelan, S. P. J., Stewart, L., Diamond, M. S., Veesler, D., Jewett, M. C. & Baker, D. Multivalent designed proteins neutralize SARS-CoV-2 variants of concern and confer protection against infection in mice. Sci Transl Med 14, eabn1252–eabn1252 (2022).

6. Lutz, I. D., Wang, S., Norn, C., Borst, A. J., **Zhao, Y. T.**, Dosey, A., Cao, L., Li, Z., Baek, M., King, N. P., Ruohola-Baker, H. & Baker, D. Top-down design of protein nanomaterials with reinforcement learning. Biorxiv 2022.09.25.509419 (2022). doi:10.1101/2022.09.25.509419

7. Divine, R., Dang, H. V., Ueda, G., Fallas, J. A., Vulovic, I., Sheffler, W., Saini, S., **Zhao, Y. T.**, Raj, I. X., Morawski, P. A., Jennewein, M. F., Homad, L. J., Wan, Y.-H., Tooley, M. R., Seeger, F., Etemadi, A., Fahning, M. L., Lazarovits, J., Roederer, A., Walls, A. C., Stewart, L., Mazloomi, M., King, N. P., Campbell, D. J., McGuire, A. T., Stamatatos, L., Ruohola-Baker, H., Mathieu, J., Veesler, D. & Baker, D. Designed proteins assemble antibodies into modular nanocages. Science 372, (2021).

8. Helms, L., Marchiano, S., Stanaway, I. B., Hsiang, T.-Y., Juliar, B. A., Saini, S., **Zhao, Y. T.**, Khanna, A., Menon, R., Alakwaa, F., Mikacenic, C., Morrell, E. D., Wurfel, M. M., Kretzler, M., Harder, J. L., Murry, C. E., Himmelfarb, J., Ruohola-Baker, H., Bhatraju, P. K., Jr., M. G. & Freedman, B. S. Cross-validation of SARS-CoV-2 responses in kidney organoids and clinical populations. Jci Insight 6, e154882 (2021).

9. Lee, M. B., Kiflezghi, M. G., Tsuchiya, M., Wasko, B., Carr, D. T., Uppal, P. A., Grayden, K. A., Elala, Y. C., Nguyen, T. A., Wang, J., Ragosti, P., Nguyen, S., **Zhao, Y. T.**, Kim, D., Thon, S., Sinha, I., Tang, T. T., Tran, N. H. B., Tran, T. H. B., Moore, M. D., Li, M. A. K., Rodriguez, K., Promislow, D. E. L. & Kaeberlein, M. Pterocarpus marsupium extract extends replicative lifespan in budding yeast. Geroscience 43, 2595–2609 (2021).

10. **Zhao, Y. T.**, Fallas, J. A., Saini, S., Ueda, G., Somasundaram, L., Zhou, Z., Raj, I. X., Xu, C., Carter, L., Wrenn, S., Mathieu, J., Sellers, D. L., Baker, D. & Ruohola-Baker, H. F-domain valency determines outcome of signaling through the angiopoietin pathway. Embo Rep 22, e53471 (2021).

11. Macrin, D., Alghadeer, A., **Zhao, Y. T.**, Miklas, J. W., Hussein, A. M., Detraux, D., Robitaille, A. M., Madan, A., Moon,

R. T., Wang, Y., Devi, A., Mathieu, J. & Ruohola-Baker, H. Metabolism as an early predictor of DPSCs aging. Sci Rep-uk 9, 2195 (2019).

12. Lee, M. B., Carr, D. T., Kiflezghi, M. G., **Zhao, Y. T.**, Kim, D. B., Thon, S., Moore, M. D., Li, M. A. K. & Kaeberlein, M. A system to identify inhibitors of mTOR signaling using high-resolution growth analysis in Saccharomyces cerevisiae. Geroscience 39, 419–428 (2017).

CONFERENCES & PRESENTATIONS

Oral Health Sciences Research Fall Symposium - 15-min talk — Sept 2022
School of Dentistry, University of Washington - Seattle WA
1. Investigating the Tie2 Pathway using AI-based Protein Design to Promote Vascular Stability

2022 ISSCR Annual Meeting - Poster
International Society for Stem Cell Research Annual Meeting, San Fransico CA — June 2022
1. Investigating Tie2 supercluster for endothelial tight junction formation to promote vascular stability

2022 ISCRM symposium - poster — May 2022
Institute of Stem Cell and Regenerative Medicine, University of Washington - Seattle WA
1. Investigating TIE2 supercluster for endothelial tight Junction formation to stabilize BBB after TBI

2021 ISCRM Fall Symposium - poster — Spet. 2021
Institute of Stem Cell and Regenerative Medicine, University of Washington - Seattle WA
1. Tie2 Supercluster Mediated Phase-separation for Endothelial Tight Junction Formation to Promote Vascular Stability.

2021 ISCRM symposium - 3-minute lightning talk and poster — April 2021
Institute of Stem Cell and Regenerative Medicine, University of Washington - Seattle WA
1. Correlating Ang1 F-domain Valency with Tie2 Signaling Outcome to Promote Angiogenesis for Tissue Regeneration

2021 Cell Symposia - Phase separation symposium - 5-minute lightning talk and poster — Nov. 2021
Cell virtual meeting
1. Tie2 supercluster mediated phase-separation for endothelial tight junction formation to promote vascular stability

2020 ISSCR Annual Meeting - Poster presentation — June 2020
International Society for Stem Cell Research Annual Meeting, virtual Meeting
1. Angiopoietin F-domain valency determines the outcome of Tie2 receptor engagement and accelerates angiogenesis in tissue regeneration.

2020 Translational Science meeting - poster presentation — April 2020
Association for Clinical and Translational Science, Virtual Meeting
1. Angiopoietin F-domain valency determines the outcome of Tie2 receptor engagement and accelerates angiogenesis in tissue regeneration.

Oral Health Sciences Research Retreat and Symposium - oral presentation — Sept. 2019
Oral Health Sciences Department, School of Dentistry, University of Washington
1. Computer-designed protein scaffold to investigate the Ang/Tie2 pathway for angiogenesis

Translational Science Expo - poster — May 2019
Institute of Translational Health Sciences, University of Washington - Seattle WA
1. Utilizing Novel Computer-Designed Proteins to Activate Ang1/Tie2-mediated Angiogenesis

ISCRM Stem Cell Symposium - poster — April 2019
Institute of Stem Cell and Regenerative Medicine, University of Washington - Seattle WA
1. Utilizing Novel Computer-Designed Proteins to Activate Ang1/Tie2-mediated Angiogenesis

School of Dentistry Research Day - poster — Jan. 2019
Institute of Stem Cell and Regenerative Medicine, University of Washington - Seattle WA
1. Utilizing Novel Computer-Designed Proteins to Activate Ang1/Tie2-mediated Angiogenesis

China-ASEAN Excellent Young Dental Student Forum - oral presentation — Oct. 2018
College of Stomatology, Guangxi Medical University, China
1. Metabolism as an early predictor of dental pulp stem cells aging

International Society for Stem Cell Research Annual Meeting - poster — June 2018
ISSCR - Melbourne Australia
1. Metabolism as an early predictor of dental pulp stem cells aging

ISCRM Stem Cell Symposium - poster March 2018
Institute of Stem Cell and Regenerative Medicine, University of Washington - Seattle WA
1. Metabolism as an early predictor of dental pulp stem cells aging

American Aging Association Annual National Meeting - poster June 2016
American Aging Association - Seattle WA
1. Screen for Dietary Supplements that Inhibit the mTOR Pathway.

Undergraduate Research Symposium - poster May 2016
University of Washington - Seattle WA
1. Screen for Dietary Supplements that Inhibit the mTOR Pathway.
2. Creating a Diverse Library of Dental Pulp Stem Cells.

OSU's McNair Scholar Research Symposium - poster March 2016
Oklahoma State University- Tulsa, OK
1. A Growth Rate Assay on Natural Products that Inhibit the mTOR Pathway and Mimic Rapamycin.

COMMUNITY INVOLVEMENT & TEACHING

UW ISCRM STEM Camp August 2018
W.F. West High School, Chehalis, WA
Volunteer guest lecturer to teach research ethics and promote stem cell research to high school students. Facilitated students to discuss ethics on topics such as biomedical research and research in media. Research and designed interactive games for ethical discussions

Teaching Assistant, Biology department Dec 2017 - March 2018
University Of Washington, Seattle, WA
Introduction to Biology II, Biology Department, University Of Washington Seattle, WA
Demonstrates leadership in giving mini-lectures on background science, lab safety, and bench work techniques to prepare students for the lab. Provide good guidance for the student in experimental design. Able to take on the responsibility to make sure students are learning the material and lab techniques

American Dental Education Association 2017-2018
Student Chapter at the University Of Washington, Seattle, WA
As the Vice-president of the ADEA, my objective and the mission of the chapter was to promote opportunities in academic dentistry and research to college and high school students, create an inclusive and safe space to share science, bring public awareness in oral public health, and advocate for diversity in science. Organized activities, events, and meetings to bring together a community consisting of high school, undergrad, and graduate students, research faculty, and dentists.

UW STEM Alternative Spring Break Program - UW pipeline project, Jan 2018 - March 2018
Yakama Nation Tribal High School, Yakima WA
A week-long program founded by NASA allowing college students to be guest teachers in a high school classroom. Aimed to promote science to underrepresented tribal students in Washington. Teaching students about atmospheric science, climate, and physics. Supervising students in engineering projects such as building a weather balloon and collecting and analyzing weather data.

Life Science Research Weekend May 2015
Pacific Science Center, Seattle, WA
Represented the UW Kaeberlein lab to present and educate young people about scientific research methods and aging mechanisms in model organisms. Engage young audiences in interactive genetic games to teach them about gene expression that regulates cellular aging.

RELEVANT EMPLOYMENT

NuWest Group @ Allen Institute for Cell Science, Seattle WA - Research Associate June 2017 - May 2018
Developed excellent sterile techniques in tissue culturing induced pluripotent stem cells (iPSCs): passaging and feeding. Have excellent attention to detail when making observations and data recording and imaging of culture conditions of iPSCs cell scoring: looking at 3D cell images to determine the quality of the data collected. Hone meticulous skills to organize and take inventory.

Swedish Neuroscience Institute - Radiology, Seattle, WA - Research Intern June 2011 - May 2014
Have sensitive attention to patterns when performing data analysis using advanced statistical models. Developed good

organizational skills and created massive MRI data and MS cognitive test scores into excel files. Grew enormously in writing skills when writing in a professional research article format for research publication.

Fred Hutchinson Cancer Research Center, Seattle, WA - Lab Technician Nov. 2011- Sep. 2012
Developed excellent sterile techniques in tissue staining with antibodies. Gained great knowledge of the environmental safety of chemicals. Kept track of in and out of tissue samples in a spreadsheet/ log. Attaching cover slid onto stained tissue samples.